Max-Planck-Institut für Metallforschung
Stuttgart

Phase Transformation Kinetics; the Role of Stress

Goutam Mohapatra

Dissertation
an der
Universität Stuttgart

Bericht Nr. 192
November 2006

Max-Planck-Institut für Metallforschung
Stuttgart

Phase Transformation Kinetics; the Role of Stress

Goutam Mohapatra

Dissertation
an der
Universität Stuttgart

Bericht Nr. 192
November 2006

Phase Transformation Kinetics; the Role of Stress

von der Fakultät Chemie der Universität Stuttgart
zur Erlangung der Würde eines Doktors der
Naturwissenschaften (Dr. rer. nat.) genehmigte Abhandlung

vorgelegt von

Goutam Mohapatra

aus Bhubaneswar/Indien

Hauptberichter:	Prof. Dr. Ir. E. J. Mittemeijer
Mitberichter:	Prof. Dr. Dr. h. c. mult. G. Petzow
Mitprüfer:	Prof. Dr. F. Aldinger

Tag der Einreichung:	15.09.2006
Tag der mündlichen Prüfung:	13.11.2006

INSTITUT FÜR METALLKUNDE DER UNIVERSITÄT STUTTGART
MAX-PLANCK-INSTITUT FÜR METALLFORSCHUNG STUTTGART

2006

Contents

1. Introduction

1.1. General Introduction

The properties of materials (e.g. mechanical properties) can be tailored by changing the composition and/or the microstructure. Microstructure is the most important materials parameter which can bring about drastic change in materials behaviour. Microstructure can be optimised by understanding the phase transformation behaviour. Fe-based alloys or steels are among the most studied systems, for solid-solid state phase transformation, as these form an important class of materials for variety of application in automobiles, ship building, bridges, rail tracks and several other disciplines. Each application has its own requirements for the microstructure.

Phase transformations can be brought about by application of a heat treatment or a thermo-mechanical treatment. To this end comprehensive knowledge of the transformation kinetics is needed. In particular little knowledge is available on the effect of applied stress on phase transformations. This thesis is devoted to the development of dilatometric methods for such research and subsequent investigation of the massive austenite to ferrite phase transformation in Fe-Ni alloys under compressive and tensile stress.

Investigations have been carried out before on the influence of uniaxial stress on (the kinetics of) the austenite to pearlite transformation [e.g. 1], the austenite to bainite transformation [e.g. 2] and the austenite to martensite transformation [e.g. 3] in Fe based alloys. However, according to the present authors' knowledge, no literature exists on the influence of applied uniaxial tensile stress, in the elastic range, on the massive austenite (γ) to ferrite (α) transformation. The present thesis work investigates the quantitative influence of uniaxial applied stress on the γ to α massive transformation in Fe-Ni alloys. In this massive transformation the original phase transforms into a new phase, which has the same composition as the parent phase, but different crystal structure [4]. So, long range diffusion is absent during such a transformation and the transformation is interface controlled. It is possible to study the difference in interface migration mechanism during

such a transformation with and without applied stress and thus the possible role of stress on the interface migration can be investigated. The two alloy compositions chosen to study the above phenomenon are Fe-3at.%Ni and Fe-6at.%Ni.

1.2. Dilatometry for analysis of phase transformation kinetics

Austenite (γ, f.c.c.) and ferrite (α, b.c.c.) phases of Fe and Fe based alloys have distinctly different specific volumes (difference of around 1.6% for pure Fe [5]). Hence, employing a high resolution dilatometer it is possible to differentiate the volume change (length change) due γ to α transformation from the linear thermal expansions (γ and α phases) during heating and cooling of the material. A typical result showing a length change of Fe-5.93at.%Ni during heating and cooling at 20 Kmin^{-1} is demonstrated in Fig. 1.1. The up and down arrows indicate the progress of heating and cooling cycles, respectively. The decrease and increase in length change during heating and cooling correspond to the $\alpha \rightarrow \gamma$ and $\gamma \rightarrow \alpha$ transformations, respectively.

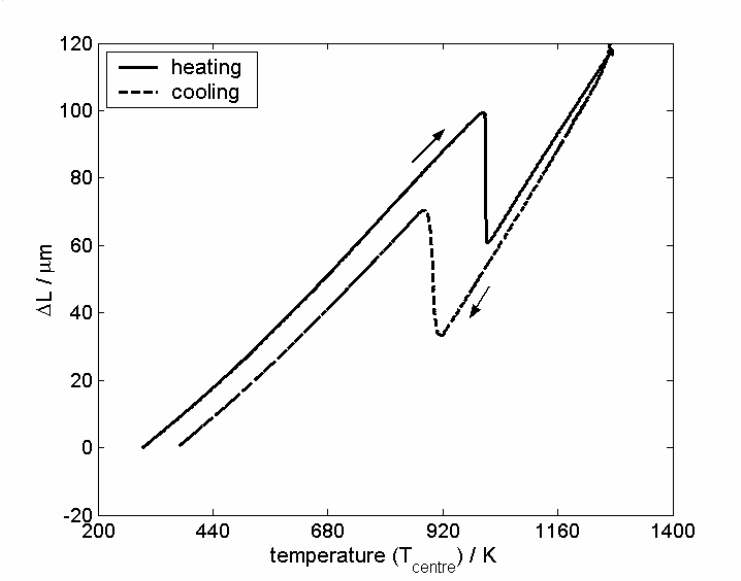

Fig. 1.1. The measured length change as a function of T_{centre} temperature (the temperature at the centre of the specimen along the longitudinal direction) for Fe-5.91at.%Ni heated from room temperature to 1273 K at 20 Kmin^{-1} isothermal heat treated for 30 minutes and subsequently cooled at 20 Kmin^{-1} to room temperature.

In the current investigation a dilatometer (DIL-805 A/D; Baehr-Thermoanalysis GmbH), employing inductive heating/cooling and capable of simultaneously applying a uniaxial force up to 5 kN was used. The applied stress was always chosen below the yield stresses of the γ and α phases of the alloys to avoid any gross plastic deformation. Thereby a possible influence of defect generation due to plastic deformation on transformation kinetics can be avoided.

1.3. Outline of the thesis

In chapter 2, a procedure has been presented for calibration of a differential dilatometer equipped with electromagnetic heating for metallic specimens both upon heating and cooling as well as under uniaxial compressive and tensile loading. The dilation signal has been calibrated on heating and cooling as well as under uniaxial load (compressive and tensile) by a platinum or iron specimen, for which recommended dilational data are available. The ferro- to paramagnetic transition (characterised by Curie temperature) of pure Fe or Fe-based alloys has been adopted to calibrate the temperature in the dilatometric measurement under different loading modes upon heating and cooling.

When a solid metallic cylindrical dilatometric specimen is heated inductively a distinct temperature gradient in the longitudinal (length) direction of the specimen exists. The heat loss is due to the conductive heat transfer from the specimen to the pushrods holding the specimen inside the induction coil. In Chapter 3 an elaborate temperature correction procedure has been proposed to correct for the above temperature inhomogeneity (gradient) that exists in the longitudinal direction of the specimen and thereby the dilation can be presented as a function of a homogeneous temperature.

Chapter 4 is dedicated to the austenite to ferrite phase transformation of Fe-2.96at.%Ni and Fe-5.93at.%Ni under the influence of constant applied uniaxial *compressive* stress within elastic limit of the material. Uniaxial compressive stresses ranging from 0.005 MPa to 7.6 MPa were applied during the $\gamma \rightarrow \alpha$ transformation. The influence of applied stress on start temperature of transformation, $\gamma \rightarrow \alpha$ transformation kinetics has been investigated in particular.

Chapter 5 is dedicated to the austenite to ferrite phase transformation of Fe-3.1at.%Ni alloys under the influence of constant applied uniaxial *tensile* stress. Uniaxial tensile stresses of 0.005, 7.6 and 12.7 MPa were applied during the $\gamma \rightarrow \alpha$ transformation. The influence of applied stress on start temperature of transformation, $\gamma \rightarrow \alpha$ transformation kinetics has been investigated and compared with the result obtained under application of compressive stresses of similar absolute value.

[1] G. Nocke, E. Jansch, P. Lenk Neue. Hutte. 1976; 21: 468.

[2] M. D. Jepson, F.C. Thompson J. Iron Steel Inst. 1949; 187: 49.

[3] J. R. Patel, M.Cohen, Acta Metall. 1962; 10: 531.

[4] M. Hillert, Met. Trans. A 1975; 6A: 5.

[5] T. A. Kop, J. Sietsma, S. Ven der Zwaag, J. Mat. Sci. 2001; 36: 519.

2. Calibration of a quenching and deformation differential dilatometer upon heating and cooling; thermal expansion of Fe and Fe-Ni alloys

G. Mohapatra, F. Sommer, E.J. Mittemeijer

Abstract

Dilatometry is a technique for precise measurement of thermal dilatation of materials during heating or cooling. A procedure has been presented for calibration of a differential dilatometer operating with electromagnetic heating for metallic specimens both upon heating and cooling as well as under uniaxial compressive and tensile loading. The dilation signal has been calibrated for both heating and cooling and for uniaxial loading (compressive and tensile) using platinum or iron reference specimens, for which recommended dilational data are available. The ferro- to paramagnetic transition (characterised by the Curie temperature) of pure iron or iron-based alloys has been adopted to calibrate the temperature in the dilatometric measurement under different loading modes during heating and cooling. On this basis calibrated data for the thermal expansion coefficients of Fe and Fe-Ni alloys have been obtained.

2.1. Introduction

Many solid materials exhibit structural changes, e.g. phase transformations, upon changing the temperature. These phase transformations are usually accompanied by a significant change in specific volume. The change in volume of a solid material is usually measured by the corresponding change in length of a specimen (long in one dimension) of this material. Thus, measurements of the change in length of solid materials are often applied for the determination of the kinetics of phase transformation of metals and alloys (e.g. [1-6]). Length-change measurement under applied compressive or tensile load during phase transformation makes it possible to investigate the influence of applied load on the phase transformation. If, upon increasing or decreasing the temperature, a phase transformation does not occur, the length of the specimen changes by thermal dilatation only, characterised by the linear thermal expansion coefficient, i.e. the relative length-change divided by the corresponding temperature interval.

The two principal factors that limit the accuracy of determination of the length-change by differential dilatometers are: (i) the thermal dilatation behaviour of the push-rods, which support the specimen and transmit the dilation signal, and (ii) the accuracy of the temperature determination of the specimen, because of the existing temperature gradient along the specimen-length axis due to heat loss by heat conduction from the specimen through pushrods and by radiation. Recently, a calibration procedure for the dilation and temperature signals upon heating and cooling in a differential dilatometer, provided with a resistance heated furnace, was proposed by *Liu et. al.* [7]. In the present work the focus is on the use of a differential dilatometer operating with electromagnetic heating in the temperature range of about 300 to 1800 K applied to a solid, cylindrical, metallic specimen.

The construction and working principle of the dilatometer in the different modes (normal, compressive and tensile) have been briefly discussed in section 2.2. Section 2.3 is dedicated to temperature profile measurement in the dilatometer specimen subjected to a heat treatment cycle. The calibration of the length-change as well of the temperature has been discussed in section 2.4. The length-change calibrations for the normal (zero load) and compressive modes and for the tensile mode have been performed by taking

pure Pt and pure Fe as reference specimens, respectively. The Curie temperature of pure Fe or Fe-based alloys has been taken as a standard for the absolute temperature calibration during heating and cooling experiments. Finally, section 2.5 presents the linear thermal expansion coefficient (LTEC) data as determined in this work for pure Fe and Fe-Ni alloys.

2.2 Experimental

2.2.1. Dilatometer

The dilatometer used in this work (DIL-805A/D (A:quenching; D:deformation) dilatometer; Baehr-Thermoanalyse GmbH; cf. Figs. 2.1(a) to 2.1(c)) measures the specimen dilation as a function of temperature in the absence of a reference specimen. It is a differential dilatometer because two pushrods are used to measure the thermal dilation behaviour. The dilatometer can be used in normal (zero load) mode and deformation (uniaxial compressive/tensile) mode (see Figs. 2.1(a) to 2.1(c)). The electrically conductive specimen is heated inductively applying a water cooled induction Cu heating coil to generate a high frequency current. An additional inner Cu coil is perforated and thus can be used for inert gas quenching. The temperature of the specimen is controlled and measured with Pt-$Pt_{90}Rh_{10}$ thermocouples (type-s) spot welded on the specimen surface. The pushrods, used to transmit thermal dilation of the specimen and to also hold the specimen in normal (zero load) mode (c.f. Fig. 2.1(a)), are either made of fused silica or alumina. The thermal dilation is measured via a linear variable differential transformer (LVDT) positioned in the measuring head. The whole system is insensitive to mechanical vibration. The LVDT and the specimen are kept isolated from each other by a dividing wall and hence the LVDT is not influenced by heat radiation or heat conduction from the specimen. The length-change resolution achievable with this instrument is about 50 nm.

2.2.1.1. Normal mode

The normal mode of operation is schematically shown in Fig.1 (a). The pushrods 2 and 3 are connected to the LVDT. The specimen is supported by pushrods 1 and 2. Pushrod 1 is fixed at the left side of the specimen; pushrod 2 is fixed at the right side of the specimen and transmits the occurring dilation; pushrod 3 serves as reference. The specimen is a solid (or hollow) cylinder; typical specimen dimensions are length of 10 mm; diameter of 5 mm; wall thickness of 1 mm for a hollow specimen. The specimen can be heated inductively under vacuum to a defined temperature with a maximum allowable heating rate of 4000 $Kmin^{-1}$ and, for a solid specimen, can be continuously cooled applying a cooling rate of maximal 200 $Kmin^{-1}$ and, with additional Ar flow through the inner, perforated Cu coil, applying a cooling rate of maximal about 1600 $Kmin^{-1}$. Ar gas can be led addionally through a hollow specimen to achieve large cooling rates up to 2500 $Kmin^{-1}$.

2.2.1.2. Compressive mode

The compressive mode of operation is schematically shown in Fig. 2.1(b). Pushrods 1 and 2 are connected to the LVDT. The specimen is supported at both sides by deformation punches. The specimen dilation is transferred via pushrod 1; pushrod 2 serves as reference. The specimen can be deformed (elastically/plastically) during heat treatment under simultaneous recording of length-change. Deformation punches are made of fused silica or alumina and have a diameter of 12 mm and a length of 35 mm. The left punch is used to apply the uniaxial, compressive load, whereas the other punch is fixed. The load, generated by a hydraulic system, is transferred via a hydraulic cylinder. The maximum applied load is limited to 25.0 kN with a sensitivity of ±0.0005 kN. The accessible heating and cooling rates in this mode are in the range or 2500 $Kmin^{-1}$ and 200 $Kmin^{-1}$, respectively.

2.2.1.3. Tensile mode

The tensile mode of operation is schematically shown in Fig. 2.1(c). The specimen to be used in the tensile mode has a geometry different from that used in the

normal or compressive modes. The solid, cylindrical specimen has a central part of length 10 mm and of diameter 5 mm, as in the normal and compressive modes, but now incorporates two additional parts (clamps) at both sides of length 29.5 mm and of diameter 9 mm. This relatively long specimen is screwed on the wall at the right side; the uniaxial tensile load is applied at the left side. The pushrods transmitting the dilation of the specimen to the LVDT are positioned in contact with the specimen as shown in Fig. 2.1(c): pushrod 1 measures the dilation of the specimen relative to pushrod 2.

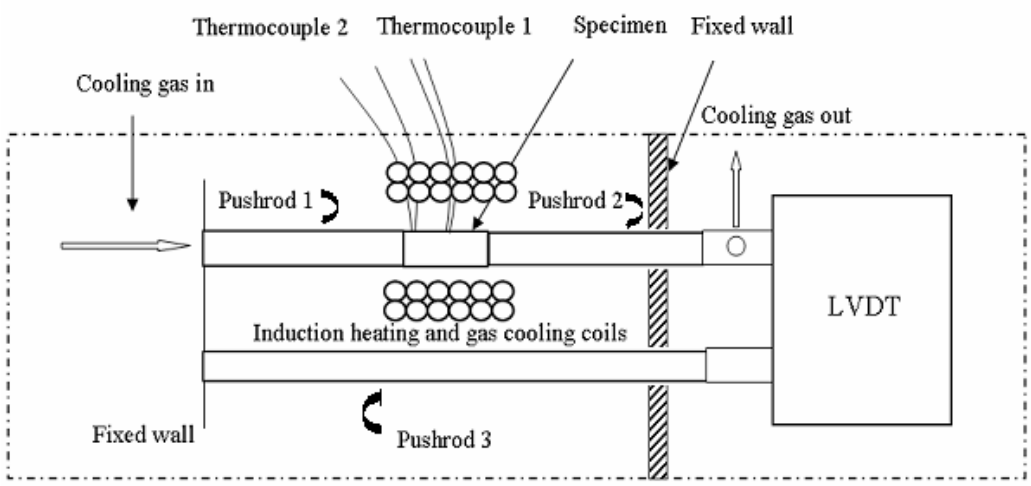

(a)

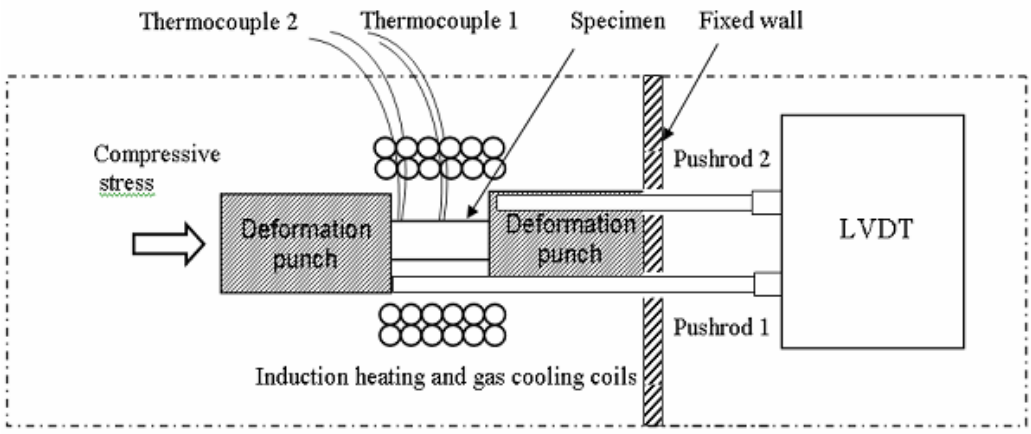

(b)

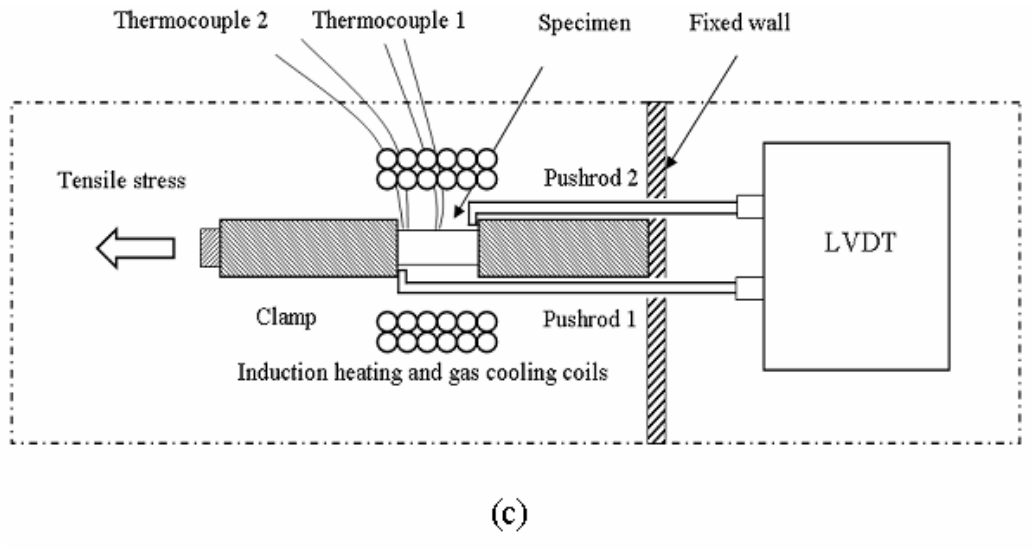

Fig. 2.1. Schematic (cross sectional top view) diagram showing the quenching and deformation differential dilatometer (from Baehr-Thermoanalyse GmbH) in different modes (a) normal mode (zero load mode), (b) compressive mode, (c) tensile mode. The length change is measured by a linear variable differential transformer (LVDT).

2.2.2. Alloy preparation

As model systems pure Fe and Fe-Ni alloys were chosen. Iron was supplied by Aldrich GmbH and nickel was supplied by Alfa Aesar GmbH; for compositions, see Table 2.1. The as-received pure Fe rods were hammered down to rods with a diameter of about 6 mm, for both normal and compressive mode specimens. Fe-Ni alloys were prepared by melting appropriate amounts of Fe and Ni in a vacuum arc melting furnace; the molten alloy was cast in a copper mould of 7 mm diameter. The as cast ingots were hammered down to rods of 6 mm diameter, for both normal and compressive mode specimens. To prepare tensile mode specimens, castings of pure Fe, of dimensions 100 mm length and 10 mm diameter, were made and subsequently hammered down to rods of 9.5 mm diameter.

In order to achieve a homogeneous microstructure, all the rods/castings were sealed in a quartz container filled with argon gas at 2×10^4 Pa. The specimens were heated from room temperature to 1423 K at 5 $Kmin^{-1}$ followed by annealing at 1423 K for 100 h and subsequently furnace cooled to room temperature. Thereafter the compositions of the Fe-Ni rods were determined by Inductive Coupled Plasma-Optical Emission

spectrometry (ICP-OES). The composition of the Fe-Ni alloys used was found to be: Fe-2.96at.%Ni and Fe-5.93at.%Ni.

Next, to prepare normal and compressive mode specimens, the rods were machined to dilatometry specimens with a diameter of 5 mm and a length of 10 mm. To prepare tensile mode specimens the rods were machined to dimensions as shown in Fig. 2.1(c) and discussed in section 2.2.1.3.

Table 2.1 Chemical composition of the iron and nickel used. Unit: ppm in mass

element	Fe	Ni
C	11	23
Si	13	0.23
Cu	1	0.18
Ti	0.6	5.3

2.3. Temperature measurement

Dilatometry specimens undergoing an inductive heating and cooling cycle experience a temperature inhomogeneity during heating and cooling. The temperature inhomogeneity is largely attributed to heat loss by heat conduction through the material (pushrods, deformation punches and clamps) holding the specimen (c.f. Figs.1a to c); heat loss by radiation is largely compensated by additional heating induced by the temperature read out by thermocouple 1 (Fig. 2.1a) controlling the inductive heating.

2.3.1. Temperature profile measurement

The temperature of the specimen during heating and cooling is controlled and measured with $Pt_{90}Rh_{10}$–Pt thermocouples (s-type) spot welded on the specimen surface.

The locations of the spot welded thermocouples to implement the programmed temperature and to measure the temperature profile during heat treatment are schematically shown in Figs. 2.1a to 2.1c. Thermocouple 1 is spot welded at the centre of the specimen to control the temperature according to the chosen temperature program. Thermocouple 2 is spot welded at the extreme end of the specimen to measure the

temperature at one end of the specimen and thus assess the temperature gradient in the specimen.

The temperatures measured with thermocouple 1 (T_{centre}) and thermocouple 2 (T_{end}) at a program temperature of 923 K for two different Fe-5.93at%Ni specimens subjected to 20 $Kmin^{-1}$ heating and cooling are shown in Table 2.2 for normal, compressive and tensile modes. The temperature gradient in both specimens is not the same for the same heating and cooling cycle which is due to the lack of reproducibility in spot welding of thermocouples or differences in the surface contacts between the pushrods (or punches) and the specimen or differences in the position of the specimen inside the induction coil. A correction procedure has been developed and has been presented elsewhere [8] that enables full correction for the temperature inhomogeneity and as a result the length-change as a function of a homogeneous temperature can be presented. This procedure has been adopted in this paper if the gradient (T_{centre}-T_{end}) in the specimen was larger than 1.0 K.

Table 2.2

Measured temperatures T_{centre} and T_{end} for a set program temperature of 923.0 K (i.e. before the start temperature of the $\gamma \rightarrow \alpha$ transformation upon cooling for Fe-5.93at.%Ni) for two different specimens each with a heating and cooling rate of 20 $Kmin^{-1}$ for normal, compressive and tensile modes.

mode	specimen	heating			cooling		
		T_{centre} (K)	T_{end} (K)	$\Delta T_{heating}$	T_{centre} (K)	T_{end} (K)	$\Delta T_{cooling}$
normal	1	923.0	919.2	3.8	923.0	915.9	7.1
	2	923.0	918.2	4.8	923.0	916.1	6.3
compressive	1	923.0	919.7	3.3	923.0	918.0	5.0
	2	923.0	920.1	2.9	923.0	916.3	4.7
tensile	1	923.0	922.2	0.8	923.0	921.9	1.1
	2	923.0	922.5	0.5	923.0	922.2	0.8

2.4. Calibration Procedures

2.4.1. Introductory remarks

Calibration of the dilation upon heating and cooling is performed, for the normal and compressive modes, by measuring the length-change of a cylindrical Pt reference specimen with diameter of 2.99 mm and length of 10.04 mm and, for the tensile mode, by measuring the length-change of a Fe reference specimen of pure Fe (large overall specimen size). The difference between the measured $\Delta L/L_0$ for the reference specimens and the recommended (reference) values for the dilatation of the platinum or iron specimen upon heating and cooling serves as a calibration (additive correction) for the relative length-change ($\Delta L/L_0$) values recorded in measurement runs performed with specimens to be investigated applying the same heat treatment procedure. The extent of the corrections depends upon temperature program employed (heating/cooling rates, see Table 2.3) and type of pushrods used (alumina or fused silica (see Fig. 2.2)), recognizing the different thermal conductivities of the different types of pushrods. To demonstrate the consequences of the choice of the type of pushrods, two heat treatment cycles were performed in normal mode, with a heating and cooling rate of 20 $Kmin^{-1}$ and an intermediate isothermal holding for 30 minutes at 1273 K, for the Pt reference specimen, the first time with the alumina pushrods and the second time with the silica pushrods. The difference in the $\Delta L/L_0$ values for the heating and cooling parts of the heat treatment cycle is much larger for using the alumina pushrods than for using the silica pushrods. This can be understood as a consequence of the fused silica having a lower thermal conductivity and lower thermal expansion than the alumina.

Table 2.3

Measured average Curie temperature (for two cycles), $T_{C,\ meas}$ characterising the ferro- to paramagnetic transition, the temperature shift (calibration correction), ΔT_C (=T_C - $T_{C,\ meas}$) (T_C=1043K [12]) as given by the difference of the reference value of the Curie temperature and the measured value.

rates, $Kmin^{-1}$	heating		cooling	
	$T_{C,\ meas}$ [K]	ΔT_C [K]	$T_{C,\ meas}$ [K]	ΔT_C [K]
10	1035.3±0.5	7.7	1034.8±0.5	8.2
*20	*1035.8±2.1	7.1	*1034.9±2.5	8.1
50	1036.4±0.5	6.6	1034.6±0.4	8.4
100	1036.2±0.6	6.9	1033.3±0.8	9.7
150	1036.4±0.5	6.6	1031.3±1.0	11.7
200	1036.6±0.5	6.4	1027.7±1.1	15.3
300	1036.2±1.2	6.8	**	**
400	1037.5±1.0	5.4	**	**
500	1037.8±1.4	5.2	**	**

** The Curie temperature could not be detected precisely from the drop in expansion coefficient (see Fig. 2.5) as a function of measured temperature, because at high cooling rates (200 $Kmin^{-1}$ and above) the drop in linear expansion coefficient is within the scatter of the measured LTEC data.

* The average Curie temperature for a repeated set of 25 experiments with a heating and cooling rate of 20 $Kmin^{-1}$.

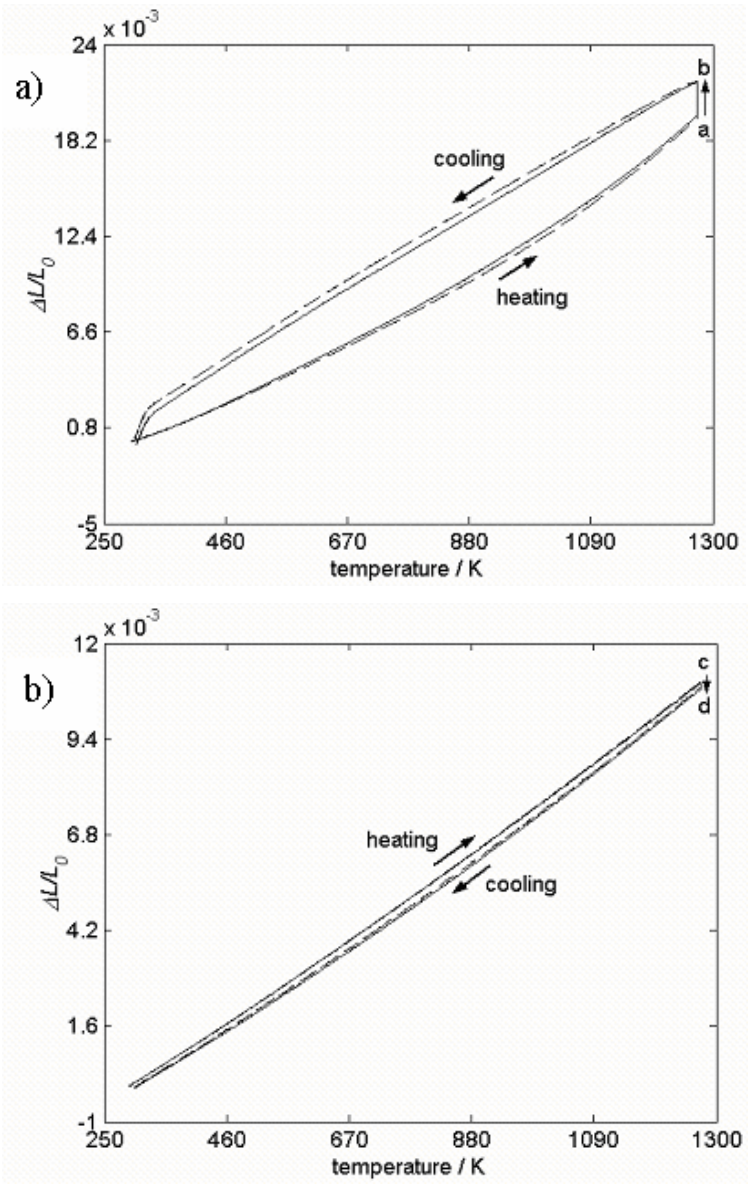

Fig. 2.2. Measured length-change in normal mode as a function of temperature of the Pt reference specimen for two successive cycles during constant heating (20 $Kmin^{-1}$) from room temperature to 1273 K and subsequent cooling (20 $Kmin^{-1}$) interrupted by an isothermal annealing at 1273 K for 30 minutes, (a) alumina pushrods, (b) fused silica pushrods.

An increase of the relative dilation of the specimen occurs during isothermal holding at 1273 K for using alumina pushrods (shown by $a \Rightarrow b$ in Fig. 2.2(a)). This can be understood as follows. The alumina pushrods have a relatively high thermal conductivity and, after heating up, upon subsequent isothermal holding at 1273 K the pushrods need time to reach thermal equilibrium. Hence, the pushrods (pushrods 1 and 2

in Fig. 2.1(a)) continue to expand at the isothermal holding temperature. This results in a *virtual* increase in relative dilation ($a \Rightarrow b$) of the specimen during the isothermal holding at 1273 K (see Fig. 2.2(a)). A reverse phenomenon, i.e. a small decrease in relative dilation upon isothermal holding at 1273 K (shown by $c \Rightarrow d$ in Fig. 2.2(b)), occurs for using fused silica pushrods. This can be understood as follows. As a consequence of radiative heat transfer from the specimen to its surroundings the reference pushrod 3 (see Fig. 2.1(a)) expands relative to pushrods 1 and 2 and this results in a small decrease in relative dilation. The temperature of the reference pushrod 3 was measured additionally during the heat treatment cycle. Indeed, the measured temperature of pushrod 3 after 30 minutes of isothermal holding at 1273 K had increased with about 24 K. If the thermal expansion coefficient of fused silica is taken as 0.5×10^{-5} K^{-1} [9] then the increase in relative length-change $(\Delta L/L_0)$ corresponding to an increase in temperature of 24 K is 12×10^{-5} which agrees well with the observed relative dilation as given by $c \Rightarrow d$ which equals 10×10^{-5}. Further, the measured relative dilation and its temperature dependences (slopes in Fig. 2.2) are larger using the alumina pushrods than using the fused silica pushrods. This is ascribed to the thermal expansion coefficient of alumina being larger than that of fused silica and to the different temperature changes for the same heat treatment cycle due to different thermal conductivity in both types of the pushrods.

Calibration of temperature depends also on the heating and cooling rate employed. Hence, to each heating and cooling rate to be used, a separate temperature calibration has to be performed, or inter- or extrapolation of calibration parameters with respect to heating/cooling rate has to be performed.

It was recently proposed to adopt the Curie temperature corresponding to the ferro- to paramagnetic phase transformation in e.g. pure iron for temperature calibration upon heating and (also) upon cooling. This idea was successfully applied to the calibration of differential thermal analysis (DTA) for determining the heat capacity in heating and cooling experiments [10] and to the differential dilatometer to measure the specific volume change on heating and cooling, respectively [7].

2.4.2. Length-change calibration

2.4.2.1. Normal and compressive modes

The correction to the measured relative length-change of the specimen under investigation is a consequence of the (undesired) thermal dilation of the pushrods/deformation punches in thermal contact with the specimen surface. To determine the true relative length-change, a correction term should be added to the measured relative length-change for each temperature for any specimen to be investigated.

A polycrystalline, platinum dilatometric specimen, of the same geometry as the specimen to be investigated, serves as the reference specimen. Then the calibration or correction term, $\left(\Delta L/L_0\right)_{cal,i}$ is given by the difference of the known true relative length-change of the reference specimen, $\left(\Delta L/L_0\right)_{ref}$ [11] and the measured length-change for the reference specimen, $\left(\Delta L/L_0\right)_{ref,\ meas,i}$:

$$\left(\frac{\Delta L}{L_0}\right)_{cal,i} = \left(\frac{\Delta L}{L_0}\right)_{ref} - \left(\frac{\Delta L}{L_0}\right)_{ref\ meas,i} \tag{2.1}$$

where i, stands for either heating or cooling. Hence, the corrected length-change of the specimen to be investigated, $\left(\Delta L/L_0\right)_i$ then is given by

$$\left(\frac{\Delta L}{L_0}\right)_{i} = \left(\frac{\Delta L}{L_0}\right)_{meas,i} + \left(\frac{\Delta L}{L_0}\right)_{cal,i} \tag{2.2}$$

where $\left(\Delta L/L_0\right)_{meas,i}$ is the measured length-change.

The measured length-change of the cylindrical platinum reference specimen upon heating and cooling is shown in Fig. 3, employing the fused-silica pushrods in normal mode (Fig. 2.3(a)) and the fused silica solid punches in compressive mode (Fig. 2.3(b)). The following isochronal heat treatment program was executed: the specimen was heated from room temperature up to 1273 K (at 20 K min^{-1}), kept at this temperature for 30 minutes, and then the specimen was cooled down continuously to 300 K (at 20 K min^{-1}). By subtracting the measured data from the known $\left(\Delta L/L_0\right)_{ref}$ values of the

platinum, the corresponding calibration data $\left(\Delta L/L_0\right)_{cal}$ are obtained for heating and cooling respectively (c.f. Eq. (2.1)). As indicated in section 2.4.1, the correction $\left(\Delta L/L_0\right)_{cal}$ is different for heating and cooling. Moreover a slight difference in correction, for both heating and cooling, occurs between the normal and compressive modes, reflecting the difference in dilatometric geometry (c.f. Figs. 2.1(a) and 2.1(b)).

2.4.2.2. Tensile mode

A polycrystalline, iron dilatometric specimen of the same geometry as the specimen to be investigated, serves as the reference specimen. The reference, relative length-change of iron as a function of temperature has been obtained using the analytical expression for LTEC of the austenite and ferrite phases, as discussed in section 2.5. The calibrated relative length-change is derived from the measured relative length-change following the same procedure as described in section 2.4.2.1. The obtained calibrations in this mode, for the heat treatment cycle described in 2.4.2.1, are shown in Fig. 2.3(c). It should be recognised that, (1) the calibrations for heating and cooling are different, for both the α and γ phases, as also observed for the normal and compressive modes, and (2) the calibrations for the α and γ phases are different, exhibiting a sharp discontinuity at the $\alpha \rightarrow \gamma$ and $\gamma \rightarrow \alpha$ phase transformations.

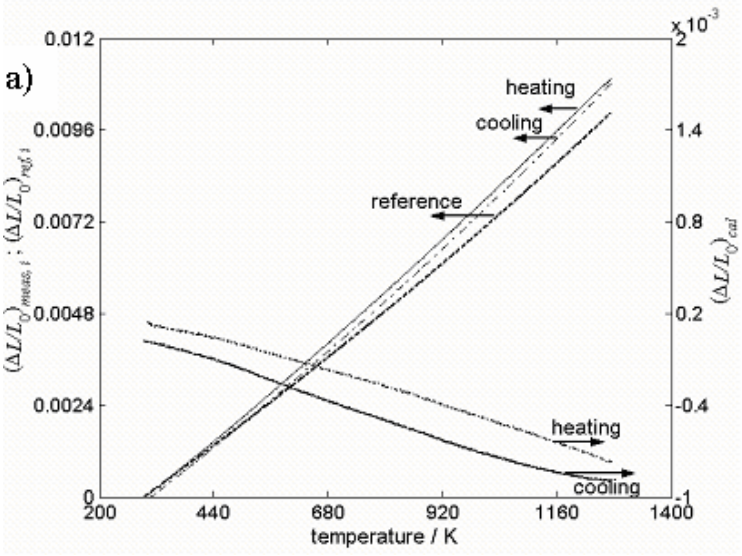
a)
heating
cooling
reference
heating
cooling
temperature / K
x10^-3

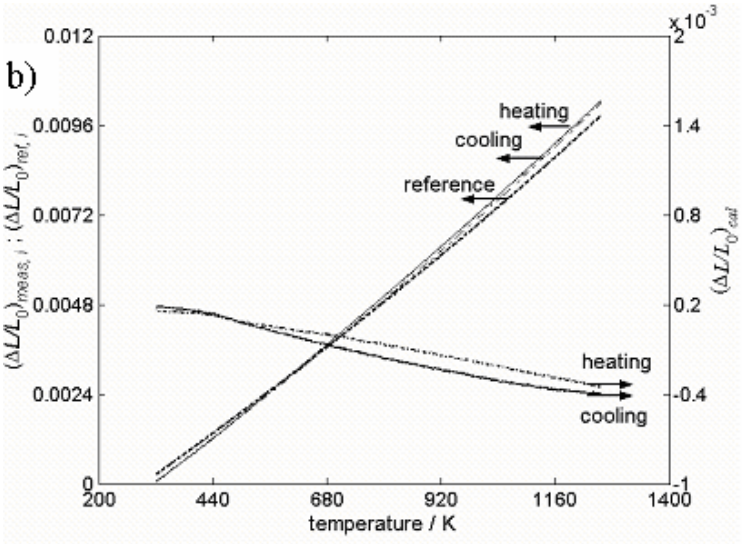
b)
heating
cooling
reference
heating
cooling
temperature / K
x10^-3

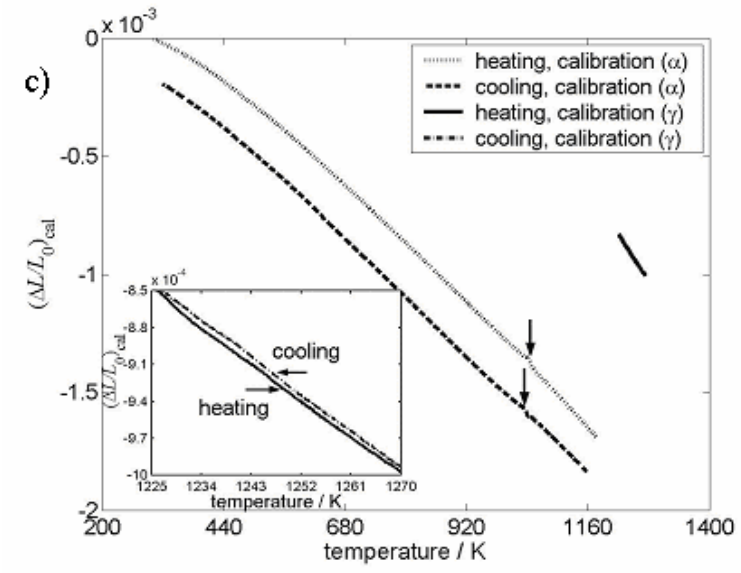

Fig. 2.3. The relative length-change, as measured for the Pt reference specimen, $\left(\Delta L/L_0\right)_{meas}$, the corresponding data according to ref [12] and the resulting relative length scale corrections, $\left(\Delta L/L_0\right)_{cal}$ (right ordinate in (a) and (b)) upon continuous heating (20 K min^{-1}) from room temperature to 1273 K and subsequent continuous cooling (20 K min^{-1}) interrupted by an isothermal annealing at 1273 K for 30 minutes, with fused silica pushrods; (a) normal mode, (b) compressive mode. (c) The obtained $\left(\Delta L/L_0\right)_{cal}$ upon heating and cooling with a pure Fe specimen subjected to the aforementioned temperature program; tensile mode; the vertical arrows indicate the measured Curie temperature upon heating and cooling in the single ferrite (α) phase region; the inserted blow up shows $\left(\Delta L/L_0\right)_{cal}$ for the single austenite (γ) phase region.

2.4.3. Temperature calibration

Execution of the temperature calibration is independent of the mode of operating the differential dilatometer. As an example the calibration procedure is discussed here for the normal mode (c.f. Fig. 2.1(a)). Several heat treatment cycles for different heating rates (10-500 Kmin^{-1}) and cooling rates (10 Kmin^{-1} to 500 Kmin^{-1}) were performed with pure iron as the specimen. The occurrence of the ferromagnetic transition was exhibited by a hump on the length-change curve [cf. Fig. 2.9 (b)] as well as by a perceivable rise/drop in HF power supply (cf. Fig. 2.4) for heating/cooling. Because of the temperature *ranges* observed for the rise/drop in HF power supply and the hump in

length-change during magnetic transition it is difficult to identify the temperature for magnetic transition.

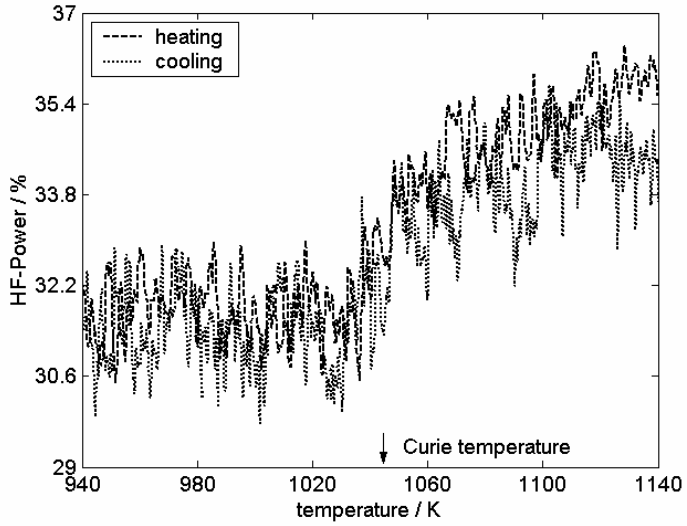

Fig. 2.4. High frequency (HF) power as a function of temperature (T_{centre}) upon heating and cooling (with 20 $Kmin^{-1}$) for pure iron in the vicinity of the true Curie temperature (=1043 K [12]). The rise of HF power upon heating and the drop of HF power upon cooling indicate the measured Curie temperature during heating and cooling, respectively.

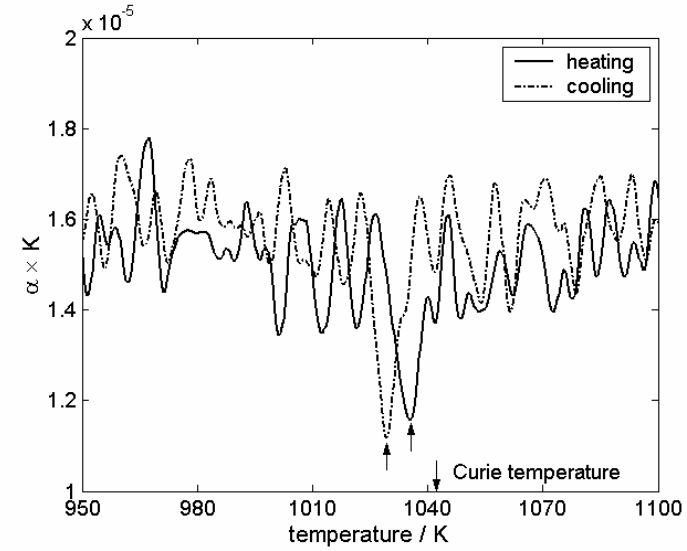

Fig. 2.5. Linear thermal expansion coefficient (α_α) of ferritic pure iron, as a function of temperature (T_{centre}), as determined from dilatometric measurements applying a heating and cooling rate of 20 K min^{-1}. The true Curie temperature [12] and the apparent Curie temperature have been indicated with arrows.

The LTEC of ferritic Fe as determined (according to Eq. (2.4) given in section 2.5) from the dilatometer measurements at a heating and cooling rate of 20 K min^{-1} is shown in Fig. 2.5. The distinct minimum in the linear thermal expansion coefficient indicated with arrows in Fig. 2.5 represents the Curie temperature for heating and cooling.

Since the dilatometric specimen exhibits a temperature gradient, during heating and cooling, which is also not constant from one experiment to another (see section 2.3.1), in principle the average of the measured temperatures T_{centre} and T_{end} (c.f. section 2.3) is used as the "measured" temperature of the specimen. However, the enthalpy consumption by the magnetic transition poses a problem here, that is dealt with as follows.

The LTEC and the temperatures T_{centre} and T_{end} have been plotted as a function of time in Fig. 2.6. The temperature T_{centre} varies linearly where as T_{end} varies nonlinearly during the magnetic transition. The temperature T_{centre} changes linearly with time because the thermocouple 1 measuring the temperature T_{centre} compensates, by controlling the induction heating, a change in temperature in the centre of the specimen due to enthalpy consumption upon magnetic transition. This is not the case for (especially) the ends of the specimen, where the temperature, T_{end}, has been measured by thermocouple 2. Hence, the temperature T_{end} does not change linearly with time during the transition: the drop observed in temperature T_{end} is due to the enthalpy change upon magnetic transition. In the ideal case, the temperature T_{end} that thermocouple 2 would have recorded, if no heat consumption due to the magnetic transition would occur (as is the case for a specimen to be investigated in this temperature range, in the absence of enthalpy change due to phase transformation), can be obtained by (linear) interpolation from the linear changes in T_{end} outside the temperature range where the minimum of the LTEC occurs; this temperature has been indicated with $T_{end,ideal}$ in Fig. 2.6. Thus, during the magnetic transition (i.e. at the Curie temperature, indicated by subscript C) the average measured temperature of the specimen is given by:

$$T_{C,meas} = \frac{T_{C,centre,meas} - T_{C,end,ideal}}{2} \qquad (2.3)$$

where $T_{C,end,ideal}$ is the interpolated temperature T_{end} at the Curie temperature. The thus measured Curie point temperatures, $T_{C,meas}\,(=T_{C,centre,meas}-T_{C,end,ideal}/2)$ and the corresponding temperature corrections (ΔT_c), adopting the true Curie temperature of pure iron as reference (1043.0 K [12]), have been listed in Table 2.3, for a number of heating and cooling rates. For all the experiments pertaining to Table 2.3 the same specimen was used without taking it out from the dilatometer, ensuring there is no change in spot welding and the location of the specimen inside the coil, which changes might otherwise have led to a different temperature gradient in the specimen.

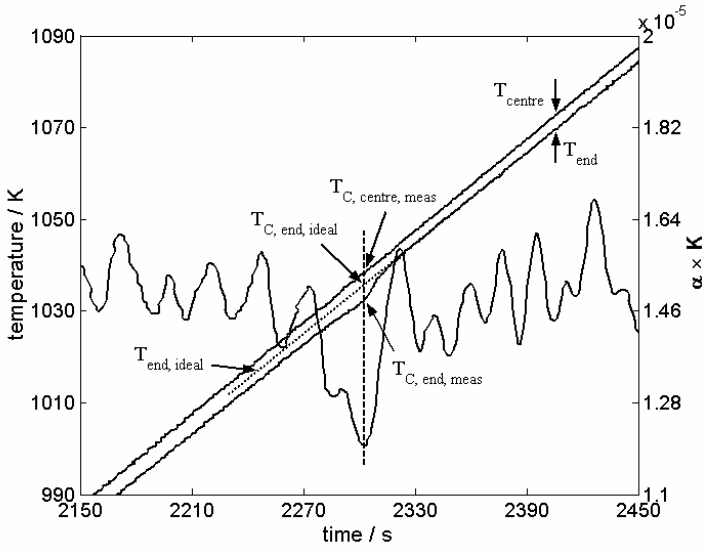

Fig. 2.6. The measured temperatures T_{centre} and T_{end} and linear thermal expansion coefficient (LTEC) (showing a hump at the magnetic transition) as a function of time. $T_{end,\ ideal}$ (dashed line) is the interpolated temperature, which would have been the *ideal* temperature T_{end} in the absence of magnetic transition. The temperatures (T_{centre} and T_{end}) corresponding to the magnetic transition, as given by the intersection of the vertical dashed line at the magnetic transition (identified by the lowest value of LTEC) with the temperature lines of T_{centre} and T_{end} are $T_{C,\ centre,\ meas}$ and $T_{C,\ end,\ meas}$, respectively. The intersection of the dashed vertical line with the temperature $T_{end,\ ideal}$ then gives the temperature $T_{C,\ end,\ ideal}$.

The obtained temperature corrections (shifts) ΔT_C, for the different heating and cooling rates, are shown in Figs. 2.7(a) and 2.7(b), respectively. In order to find out the variation in ΔT_C due to different specimen mountings in the dilatometer a set of

experiments was performed for a heating/cooling rate of 20 Kmin^{-1}. For each experiment, a fresh specimen was taken and a fresh thermocouple spot welding was done. The results are represented by the distributions shown in Fig. 2.8. The average Curie temperature was obtained as 1036.5±2.1 K and 1035.3±2.5 K upon heating (Fig. 2.8(a)) and cooling (Fig. 2.8(b)), respectively.

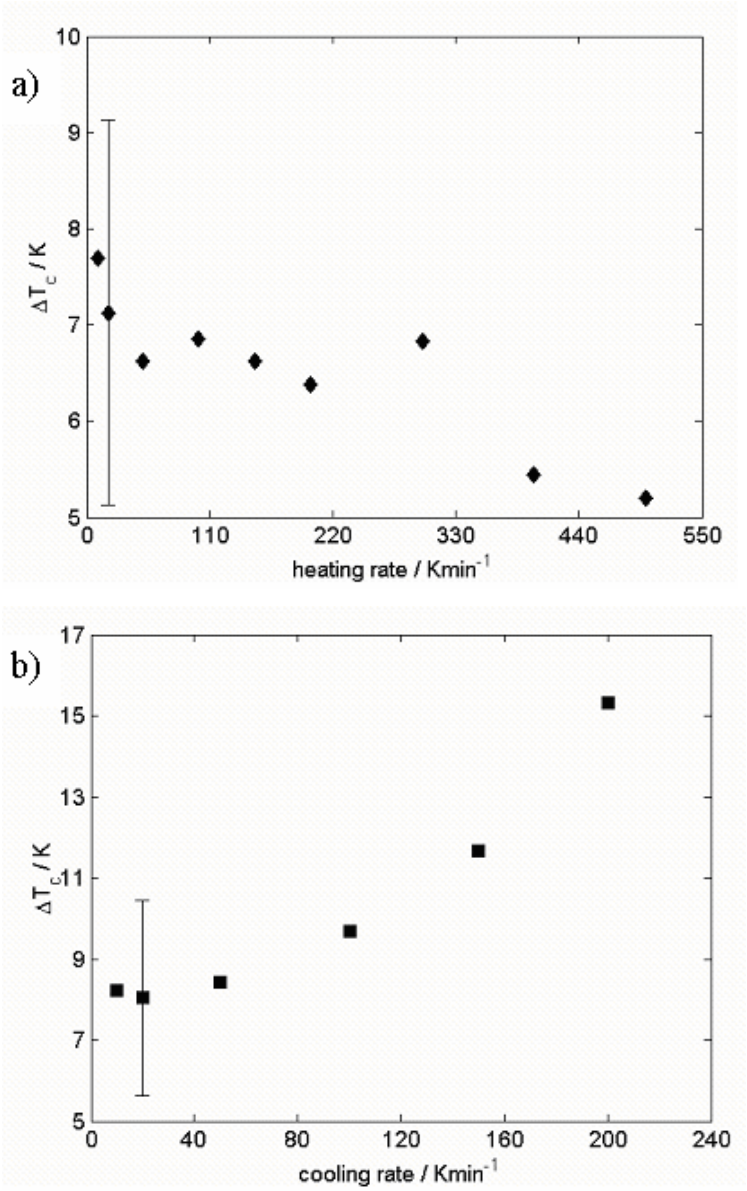

Fig. 2.7. Temperature scale correction, ΔT_C, for various heating rates (a) and cooling rates (b). A single specimen with the same pair of welded thermocouples was applied. The scatter in the temperature calibration for a repeated sets of experiments (number: 25) at 20 Kmin^{-1} heating and cooling with now for each experiment a freshly spot welded pair of thermocouples has been indicated too.

The difference in measured Curie temperature between heating and cooling is about 1 K (≈1036.5-1035.3). The standard deviations in ΔT_C for heating and cooling at 20 $Kmin^{-1}$ have also been indicated in Fig. 2.7.

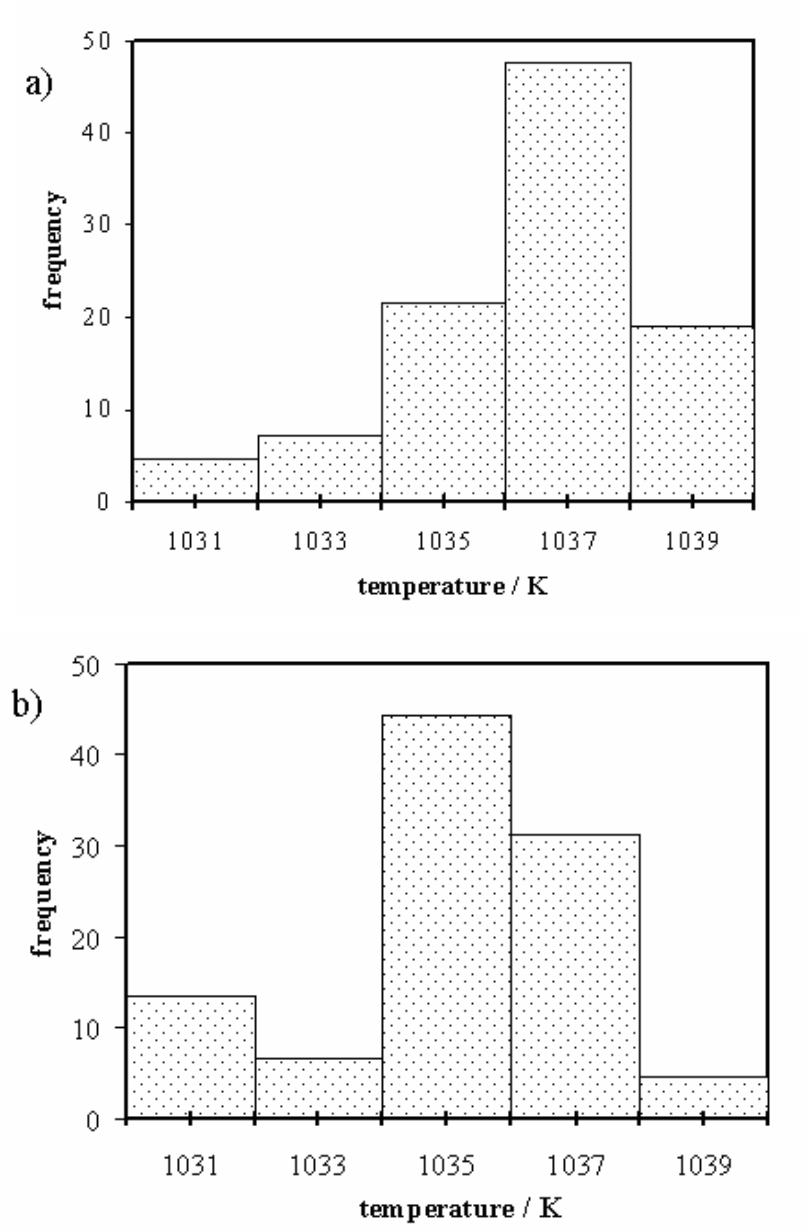

Fig. 2.8. The distribution of the values measured for the Curie temperature ($T_{C,meas}$) during heating (a) and cooling (b) for a heating and cooling rate of 20 $Kmin^{-1}$ for repeated (number: 25) sets of experiments using for each experiment a freshly spot welded pair of thermocouples.

2.5. Relative length-change calibration of pure Fe (normal, compressive and tensile modes)

The relative length change of pure iron, using the normal mode measured upon the heat treatment procedure indicated in section 2.4.2.1, is shown in Fig. 2.9(a), before and after calibration of both the temperature and the length-change scales applying the methodology developed in section 2.4. Similar relative length-change results (before and after calibration) are obtained using the compressive mode. The segment AB of the calibrated curve corresponds to the thermal expansion of the specimen upon continuous heating in the absence of a phase transformation. Part BC represents the $\alpha \rightarrow \gamma$ transformation, during which a length contraction occurs due to the formation of austenite. Parts CD and EF stand for the expansion and contraction of austenite upon heating and subsequent cooling, respectively. Part FG corresponds to the $\gamma \rightarrow \alpha$ transformation, associated with length increase. After completion of the $\gamma \rightarrow \alpha$ transformation the length of the specimen decreases continuously down to room temperature due to thermal contraction (indicated by GH).

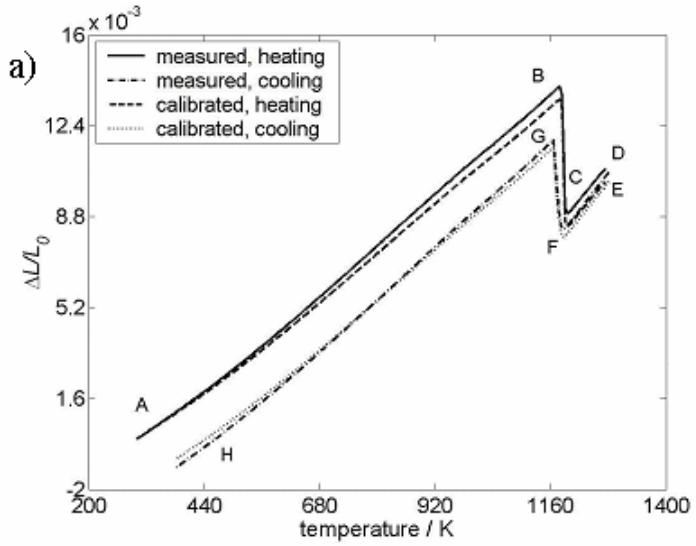

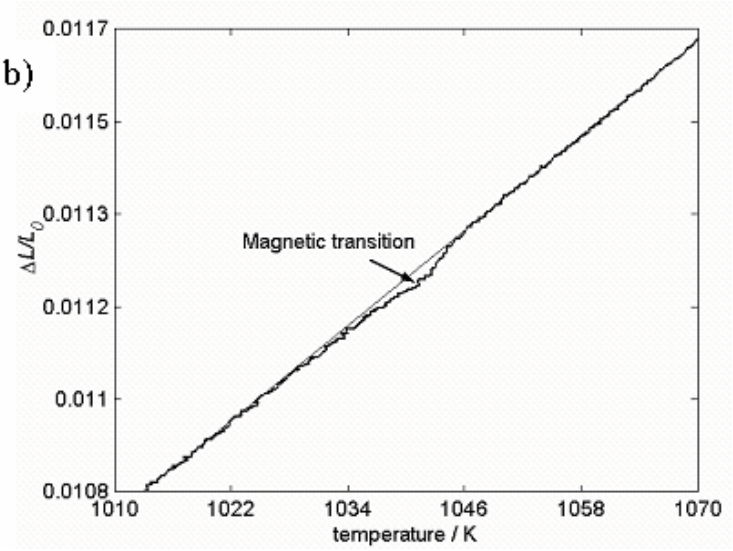

Fig. 2.9. (a) Comparison of the measured relative length-change as a function of temperature (T_{centre}) and corrected relative length-changes of pure iron (normal mode) during continuous heating (20 K min^{-1}) from room temperature to 1273 K and subsequent continuous cooling (20 K min^{-1}), interrupted by an isothermal annealing at 1227 K for 30 min. (b) Blow up of the relative length-change curve upon heating indicating the magnetic transition.

The measured relative length change of pure iron, using the tensile mode device without applying load, upon the heat treatment procedure indicated in section 2.4.2.1, is shown in Fig. 2.10(a), before and after calibration of both the temperature and the length-change scales, applying the methodology developed in section 2.4. As compared to the (linear) thermal expansion/shrinkage, a small rise in specimen length occurs at the end of $\alpha \rightarrow \gamma$ transformation and a small drop in specimen length occurs before the start of $\gamma \rightarrow \alpha$ transformation, according to the relative length-change data as a function of temperature (see Fig. 2.10 (b)). This effect is due to the prevailing temperature gradient in the specimen. The clamps are part of the entire specimen and therefore of the same material as the inner part of the specimen that is used for measuring the dilation (see section 2.2.1.3; Fig. 2.1(c)) The portions of the clamps in contact with the pushrods (see Fig. 2.1(c)) are at a lower temperature than the inner part of the specimen because large parts of the clamps are outside the heating zone (i.e. outside induction coil) (c.f. Fig. 2.1(c)). Hence, upon cooling they start to transform earlier than the inner part of the specimen. In that stage, then the pushrods 1 and 2 move *towards* each other (because of

the transformation induced volume expansion) and thereby cause an apparent decrease in relative length-change just before the start of $\gamma \rightarrow \alpha$ transformation in the inner part of the specimen. A similar reasoning can be applied for the heating run and explain the apparent increase in relative length change at the end of the $\alpha \rightarrow \gamma$ transformation due to later completion of this transformation in the outer part (clamps) of the specimen. The start temperature of the $\gamma \rightarrow \alpha$ transformation and the end temperature of the $\alpha \rightarrow \gamma$ transformation are taken as the temperatures corresponding to the minimum of relative length-change (see the vertical arrows in Fig. 2.10(b)).

2.6. Linear thermal expansion of Fe and Fe-Ni alloys

2.6.1. Linear thermal expansion coefficient (LTEC) of ferrite

The relative length-changes as a function of temperature of pure Fe and Fe-Ni alloys (Fe-2.96at.%Ni and Fe-5.93at.%Ni and) are shown in Figs. 2.9 and 2.11, respectively. The heat treatment cycles considered here (see section 2.4.2.1) were carried out in normal mode. The magnetic transition temperature of Fe-2.96at.%Ni was found to be 1033.3 K, and the temperature calibration was performed as for pure Fe (see section 2.4.3). For Fe-5.93at.%Ni a value for the magnetic transition could not be obtained, because both during heating and cooling the magnetic transition appears in the temperature range of the $\alpha \rightarrow \gamma$ and the $\gamma \rightarrow \alpha$ transformation, respectively. Thus, for this alloy the temperature calibration was done on the basis of the magnetic transition measured separately for pure Fe (see section 2.4.3).

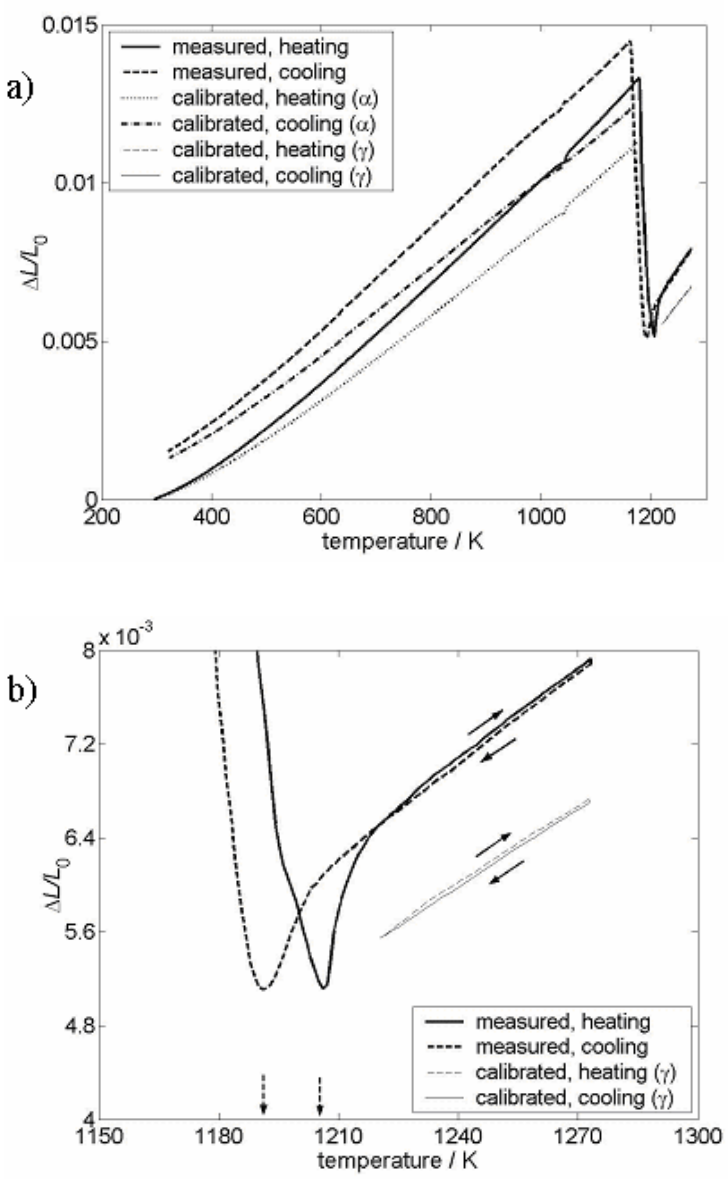

Fig. 2.10. (a) Comparison of the measured and corrected relative length-changes (without $\alpha \rightarrow \gamma$ and $\gamma \rightarrow \alpha$ length-change corrections) as a function of temperature (T_{centre}) of pure iron, using the tensile mode device without applying a load, upon continuous heating (20 K min^{-1}) from room temperature to 1273 K and subsequent continuous cooling (20 K min^{-1}), interrupted by an isothermal annealing at 1273 K for 30 minutes. (b) Enlargement of the measured length-change of the pure γ phase during heating and cooling in Fig. 2.9 (a) indicating the sudden rise (heating) and fall (cooling) in measured relative length-change. The non-vertical arrows are meant to guide the eye for the heating and cooling process. The vertical dashed arrows indicate the measured end temperature of the $\alpha \rightarrow \gamma$ transformation and start temperature of the $\gamma \rightarrow \alpha$ transformation upon heating and cooling, respectively.

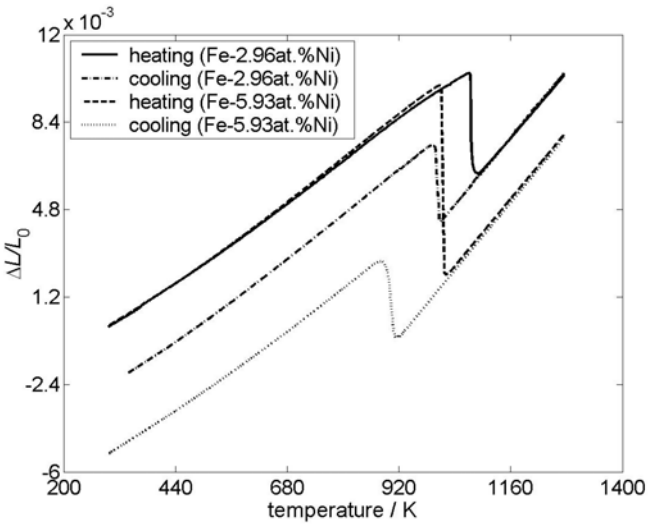

Fig. 2.11. Measured relative length-change as a function of temperature (T_{centre}), for two Fe-Ni alloys as indicated, during heating (20 $Kmin^{-1}$) from room temperature to 1273 K, with an intermediate isothermal annealing for 30 minutes, and during subsequent cooling (20 $Kmin^{-1}$) to room temperature.

Values for the linear thermal expansion, $\alpha(T)$, can be calculated from the relative length-change data according to

$$\alpha(T) = \frac{d\left(\Delta L/L_0\right)}{dT} \qquad (2.4)$$

An analytical description for the temperature dependence of the relative length-change ($\Delta L/L_0$) of pure iron, ignoring the magnetic contribution to the thermal expansion of the ferrite and austenite phases, has been given in Ref. [11]. Recently, an analytical expression for the thermal expansion coefficient of ferrite, α_α, was presented that does take into account both non-magnetic and magnetic contributions [7].

$$\alpha_\alpha = b + cT + dT^2 + f_i \exp\left(e_i T^*\right)\left(T^*\right)^{g_i} \qquad 300\ K<T<1185\ K \qquad (2.5)$$

The thermal expansion coefficient of the ferrite phase of pure Fe as obtained by applying Eq. (2.4) to the relative length-change data given in Fig. 2.9, is shown in Fig. 2.12(a), along with the result obtained by fitting Eq. (2.5) to these α_α data. The thus obtained optimised LTEC data (values of b_α, c_α.... g_α; see Table 2.4) agree with corresponding values given in Ref. [7] within experimental accuracy; the small difference is due to the larger scatter in the measured LTEC data obtained with the present

dilatometer with electromagnetic heating (DIL 805 A/D) as compared to the dilatometer with resistance heating (DIL 802).

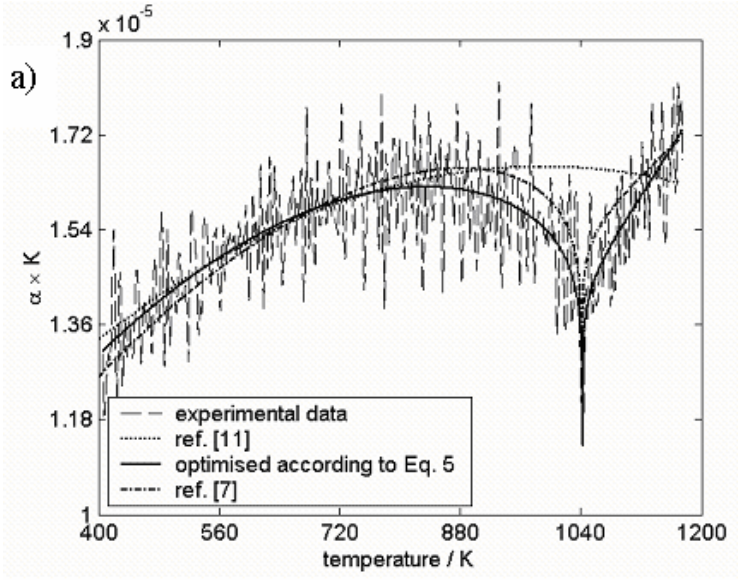

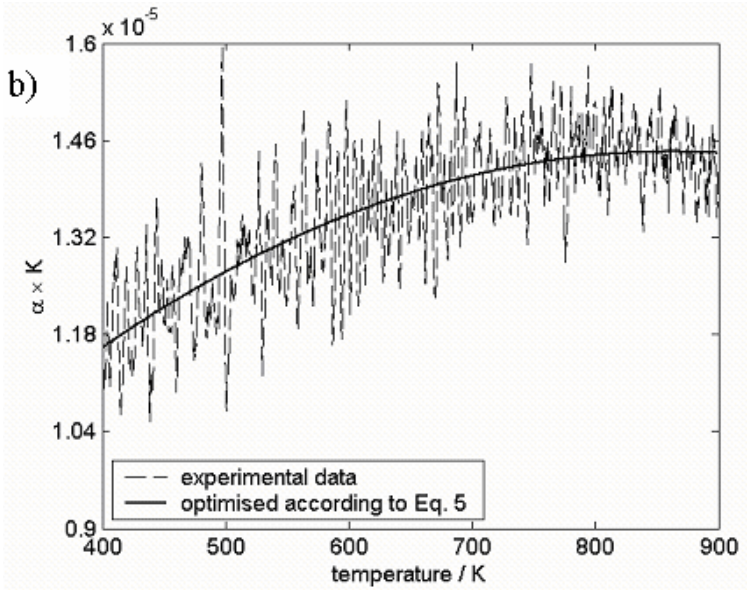

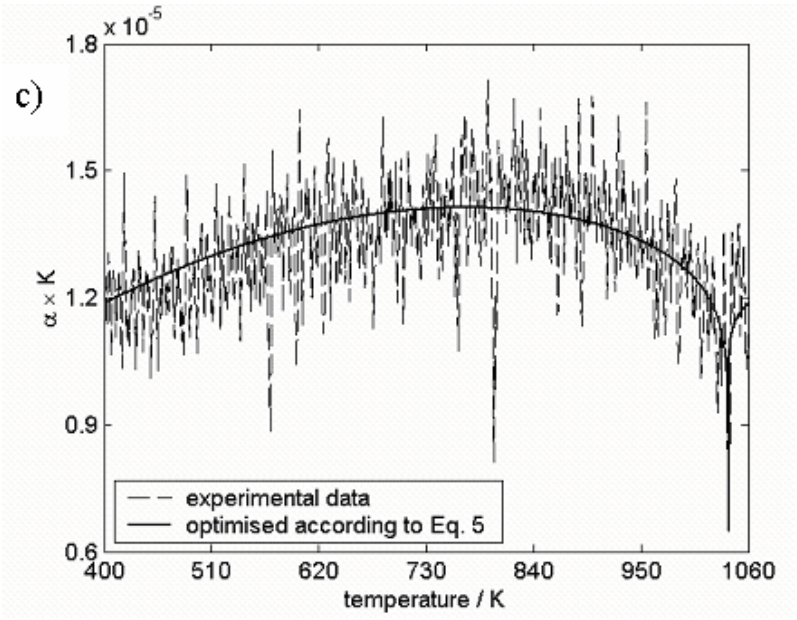

Fig. 2.12. Comparison of the measured (with a heating rate of 20 K min^{-1}), and optimized data according to Eq. (2.5) (full line) of ferritic (a) pure Fe, (b) Fe-5.93at.%Ni and (c) Fe-2.96at.%Ni.

The thermal expansion of the pure ferrite phase for Fe-5.93at.%Ni is free from a magnetic transition and therefore only the non-magnetic contribution in Eq. (2.5) is fitted to the measured LTEC data of the ferritic Fe-5.93at.%Ni. The thus obtained fit is shown in Fig. 2.12(b). For Fe-2.96at.%Ni the magnetic transition occurs within the temperature range for thermal expansion of the single ferrite phase and hence the analytical expression given by Eq. (2.5), including magnetic and non-magnetic contributions, is fitted to the measured experimental LTEC data. The result is shown in Fig. 2.12(c). The obtained fit parameters for the LTEC of the ferrite phases of both Fe-5.93at.%Ni and Fe-2.96at.%Ni have been gathered in Table 2.4 as well.

Table 2.4 Values for the parameters in the analytical description (cf. Eq. (2.5)) of the thermal expansion of the ferrite phase of pure Fe, Fe-2.96Ni and Fe-5.93at.%Ni, as obtained by fitting to the experimental data after length-change scale and temperature scale corrections as developed in this work.

alloys	parameters	parameter values
pure Fe	b (K^{-1})	-4.61e-9
	c (K^{-1})	2.35e-8
	d (K^{-1})	-2.11e-11
	e1	-1.30
	e2	2.56
	f1(K^{-1})	1.57e-5
	f2(K^{-2})	1.45e-5
	g1	0.04
	g2	0.03
Fe-2.96at.%Ni	b (K^{-1})	-4.22e-9
	c (K^{-1})	1.92e-8
	d (K^{-1})	-1.68e-11
	e1	-1.15
	e2	1.92
	f1(K^{-1})	1.39e-5
	f2(K^{-2})	1.19e-5
	g1	0.07
	g2	0.03
Fe-5.93at.%Ni	b	1.08e-5
	c (K^{-1})	5.35e-9
	d (K^{-2})	2.25e-12

2.6.2. Linear thermal expansion coefficient (LTEC) of austenite

An analytical description of the temperature dependence of the relative length-change of austenite by thermal expansion/shrinkage is given by the linear terms (first two terms : $b + cT$) of Eq. (2.5). By fitting this expression for LTEC of austenite upon cooling for both the pure Fe and Fe-Ni alloys, the linear thermal expansion coefficient of austenite has been obtained as:

Fe:	$1.8\times10^{-5}+4.6\times10^{-9}T$	1190 K<T<1260 K	(2.6)
Fe-2.96at.%Ni:	$2.1\times10^{-5}+11.0\times10^{-10}T$	1085 K<T<1260 K	(2.7)
Fe-5.93at.%Ni:	$2.1\times10^{-5}+8.0\times10^{-10}T$	1085 K<T<1260 K	(2.8)

The LTEC for the austenite phase of pure Fe obtained in the present work agrees well with the data given in Ref. [11] (see Fig. 2.13). The corresponding data presented in Ref. [7] slightly deviate (see Fig. 2.13), which may be due to the small temperature range applied in Ref. [7].

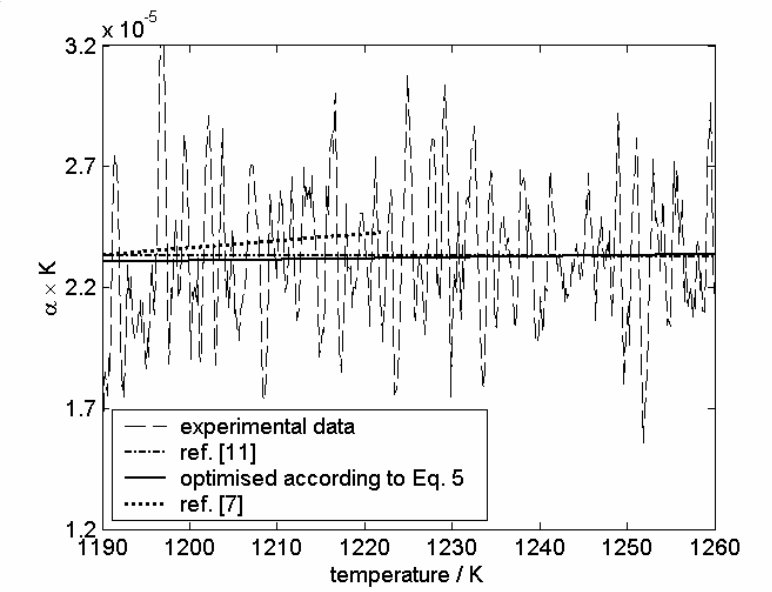

Fig. 2.13. Comparison of the measured and optimized data according to the linear terms in Eq. (2.5) (full line) of austenitic pure Fe.

2.7. Conclusions

1. Calibration of the temperature and length-change scales of a differential dilatometer is a prerequisite to accurately determine the (linear) thermal dilation as well the dilation associated with phase transitions. Corresponding corrections for a quenching and deformation differential dilatometer with an electromagnetic heating device have been developed for the normal, compressive and tensile loading modes.

2. The length-change calibration has to be performed for heating and cooling separately. The length-change calibration for the normal and compressive modes is possible applying a Pt reference specimen with known thermal dilation data and for the tensile mode applying pure iron as reference material.

3. The temperature calibration for both heating and cooling and for all modes can be performed utilizing the hysteresis-free Curie temperature of pure Fe.

4. Temperature calibration can be performed in situ if the investigated alloy exhibits a ferro-magnetic transition.

5. Although a quenching and deformation differential dilatometer with electromagnetic heating is naturally less accurate than a "normal" differential dilatometer with resistive heating, the LTEC obtained for the ferrite phase in the present work with the quenching and deformation dilatometer agrees well with the data obtained in ref. 7 with a more accurate differential dilatometer.

6. The calibration correction methods developed in this work were applied successfully to determine the LTEC for both the ferrite phase and the austenite phase of Fe-2.96at.%Ni and Fe-5.93at.%Ni.

References

[1] E. J. Mittemeijer, J. Mater. Sci. 1992; 27: 3977.

[2] C. Capdevila, F. G. Caballero and C. Gracia de Andres. Metall. Mater. Trans. A 2001; 32: 66

[3] C. M. Li, F. Sommer and E. J. Mittemeijer. Mater. Sci. Eng. A 2002; 325: 307.

[4] Y. C. Liu, F. Sommer and E. J. Mittemeijer. Acta Mater. 2003; 51: 507.

[5] H. K. D. H. Bhadeshia. Mater. Sci. Technol. 1999; 15: 22.

[6] G. H. Prior. Mater. Forum 1994; 18: 265.

[7] Y. C. Liu, F. Sommer, E. J. Mittemeijer, Thermochimica Acta 2004; 413: 215.

[8] G. Mohapatra, F. Sommer, E. J. Mittemeijer, submitted for publication.

[9] Handbook of Thermophysical properties of Solid Materials, Volume. 3, Ceramics, Pergamon Press, Oxford, 1961.

[10] A. T. W. Kempen, F. Sommer and E. J. Mittemeijer. Thermochim. Acta 2002; 383: 21.

[11] Y. S. Touloukian, Thermal Expansion: Metallic Elements and Alloys, Plenum Press, New York, 1975

[12] A. T. Dinsdale, CALPHAD 1991; 15: 317.

3. A temperature correction procedure for temperature inhomogeneity in dilatometer specimens

G. Mohapatra, F. Sommer, E.J. Mittemeijer

Abstract

Dilatometry is a thermo-analytical technique used to measure the expansion or shrinkage of materials during heating or cooling, whether or not in association with a phase transformation. A temperature correction procedure has been developed to correct for the temperature inhomogeneity that exists in an inductively heated specimen during the heating/cooling process and to represent the dilation as a function of a homogeneous temperature. As an example, taking a Fe-5.91at.%Ni specimen and subjecting it to two different cooling rates, the temperature correction has been performed for the temperature range where the austenite to ferrite phase transformation takes place as well as for the pure austenite and ferrite phases close to the temperature range of the transformation.

3.1. Introduction

Dilatometry is a technique used to precisely measure the thermal dilation as well as the dilation due to a phase transformation associated with a change of specific volume of the material. It is important to determine precisely both the dilation due to the transformation and the corresponding temperature during the heating/cooling, in order to analyse accurately the phase transformation kinetics.

Relative dilatometers, in which the length change of a specimen is measured relative to the length change of another, reference material, e.g. push-rod dilatometers, are widely used. For small heating and cooling rates (up to 20 $Kmin^{-1}$) a resistance heated furnace can provide the desired change of specimen temperature [1]. To achieve high heating and cooling rates a metallic specimen can be heated directly by inductive heating. With this type of heating the dilatation due to phase transformation can also be measured under applied uniaxial compressive or tensile load. A schematic diagram of such a dilatometer is shown in Fig. 3.1. The temperature of the specimen is controlled by spot welded thermocouples on the specimen. A dilatometer specimen undergoing heat treatment cycles in an inductively heated/cooled environment experiences a temperature inhomogeneity (temperature gradient) in the longitudinal direction [e.g. 2] due to heat loss through the pushrods holding the specimen at its ends in the longitudinal direction. The resulting temperature gradient depends upon the position of the specimen inside the induction coil (the specimen during heat treatment should be positioned in the centre of the induction coil), the quality of spot welding of the thermocouples and the applied heating/cooling rates. Furthermore, the temperature gradient may change during phase transformation due to heat release (recalescence) which depends on the rate of transformation.

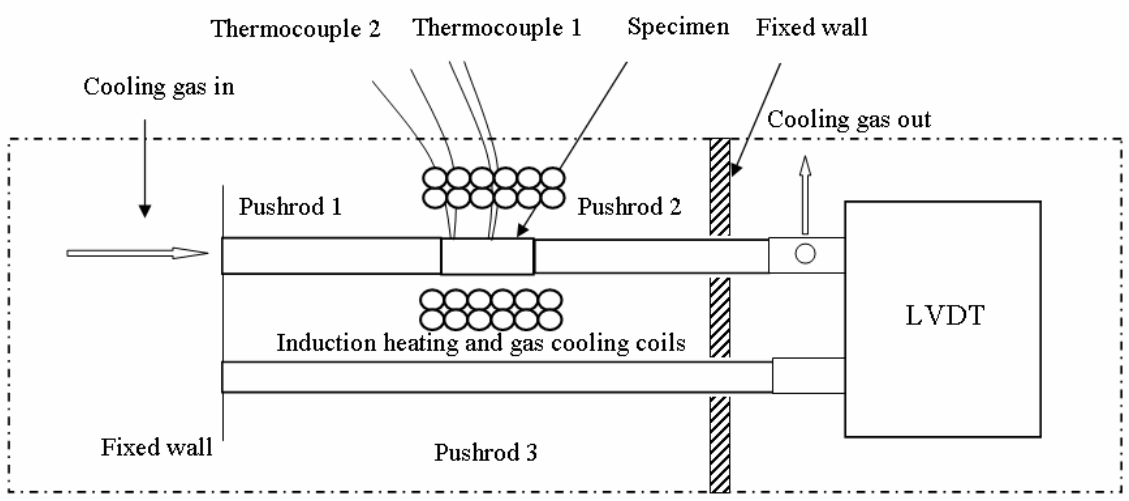

Fig. 3.1. Schematic diagram showing the spot welded thermocouples on the metallic specimen. Thermocouple 1 controls the imposed heat treatment cycle and thermocouple 2 measures the temperature at the end of the specimen. The length change is measured by a linear variable differential transformer (LVDT).

The current practice is to represent the dilation for inductively heated specimens as function of the temperature measured by the thermocouple which controls the applied temperature program. However, such information is biased because the temperature in the specimen is inhomogeneous and the recorded dilation signal cannot be interpreted straightforwardly. In this work an original temperature correction procedure has been developed which allows to extract the specimen dilation as function of a homogeneous temperature.

3.2. Experimental

3.2.1. Specimen preparation

Bulk high purity Fe (99.98 wt. %) and Ni (99.99 wt. %) were used for the preparation of the alloy. The purity of both Fe and Ni has been indicated by the composition data (determined by Inductive Coupled Plasma-Optical Emission Spectrometry (ICP-OES)) in Table 3.1. The melting process was carried out in a vacuum-melting furnace, and the molten alloy was cast in a copper mould. The as-cast ingots of 7 mm in diameter were hammered down to rods of 6 mm diameter. In order to achieve a homogeneous distribution of the alloying element all rods were sealed in a quartz container

filled with argon gas at 3×10^4 Pa, annealed at 1423 K for 100 h and cooled down to the ambient temperature within the furnace. The compositions of the rods were determined by Inductive Coupled Plasma-Optical Emission spectrometry (ICP-OES). The composition of the alloy was found to be Fe-5.91 at.%Ni. The rods were machined into cylindrical shaped, solid specimens with a length of 10 mm and a diameter of 5 mm.

Table 3.1 Chemical composition of the iron and nickel used. Unit: ppm in mass

element	Fe	Ni
C	11	23
Si	13	0.23
Cu	1	0.18
Ti	0.6	5.3

3.2.2. Dilatometry

A dilatometer DIL-805 A/D (Baehr-Thermoanalysis GmbH) (see Fig. 3.1), employing inductive heating/cooling was used to measure the thermal dilation of Fe-5.91 at.%Ni specimens upon cooling from the austenite- phase field. The experiments were performed under vacuum (6×10^{-6} mbar) to avoid oxidation of the specimen. The specimens were subjected to a heating rate of 20 $Kmin^{-1}$ from room temperature to 1273 K followed by isothermal holding at 1273 K for 30 minutes and subsequently cooled down to room temperature at 20 $Kmin^{-1}$ or 140 $Kmin^{-1}$.

The pushrods applied were made of polycrystalline Al_2O_3 or quartz (see Fig.1). The thermocouple1 which controls the applied temperature program was fixed at the surface at half height of the cylindrically shaped specimen. The longitudinal temperature gradient was measured by spot welding two further thermocouples, one at each end (L and R) of the specimen. The corresponding temperatures measured by these thermocouples are T_{centre} and $T_{end(L)}$ and $T_{end(R)}$. Pt-$Pt_{90}Rh_{10}$ thermocouples were used. It was verified that the same temperature gradient holds for both halves of the specimen (i.e. the temperature profile is symmetric with respect to the central cross-sectional plane of the specimen). $T_{end(L)}$ and $T_{end(R)}$, differ only about 0.5 K, whereas the difference of T_{centre} and $T_{end(L)}$ or $T_{end(R)}$ amounts to almost 5 K (see Fig. 3.2).

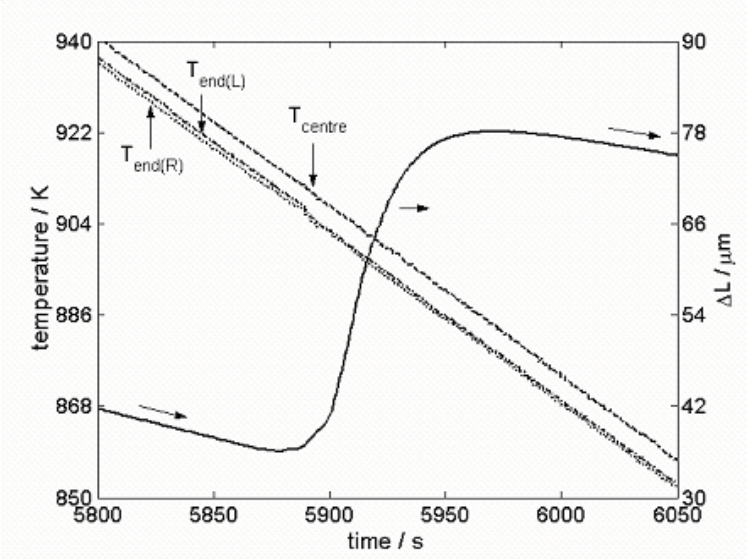

Fig. 3.2. The measured temperatures, T_{centre}, $T_{end(L)}$, $T_{end(R)}$, and the length change, ΔL, as a function of temperature during the $\gamma \rightarrow \alpha$ transformation of Fe-5.91 at.%Ni cooled at 20 $Kmin^{-1}$. $T_{end(L)}$, $T_{end(R)}$ are the temperatures measured by thermocouples spot welded on the left and right ends of the specimen, respectively.

For reproducible temperature measurements for different specimens, involving different spot weldings, a reproducible spot welding procedure had to be applied. The oxide free surface of the specimens should exhibit the same surface finish (roughness) and the spot welding should provide a mechanically stable connection. The thermocouple wires were spot welded separately parallel to each other. This procedure needed only a small electric current and short time for the spot welding. Thus the dissolution of elements of the specimen in the thermocouple wire could be minimized.

3.3. Experimental results

The measured values for the length change, ΔL and for the temperatures, T_{centre} and T_{end}, have been plotted as function of cooling time, *t*, during the $\gamma \rightarrow \alpha$ transformation for the two applied cooling rates in Figs. 3.3(a) and 3.3(b). The difference between T_{centre} and T_{end} reveals that a temperature gradient occurs in the specimen during cooling. The small fluctuations in the $T_{centre}(t)$ and $T_{end}(t)$ data (measured locally at the surface for both cooling rates), which are in the range of ±0.5 K inside the transformation range and ±0.2 K outside the transformation range, do not represent the temperature in the specimen: Temperature

fluctuations of T_{end} in the transformation range are, at least partially, due to a locally changing heat release due to successions of periods of acceleration and retardation in the prevailing interface-controlled ($\gamma \rightarrow \alpha$) transformation process, in correspondence with observations by in-situ transmission electron microscopy analysis [3] and dilatometry [4]. The fluctuations of T_{centre} are smaller because thermocouple1 (Fig. 3.1; measures the temperature, T_{centre}) controls the applied temperature program; however, the program cannot compensate local temperature fluctuations in the range of ±0.2 K. Against this background the temperatures T_{centre} (t) and T_{end} (t) have been smoothened by applying a moving weighted-average filter [5] (see Fig. 3.4).

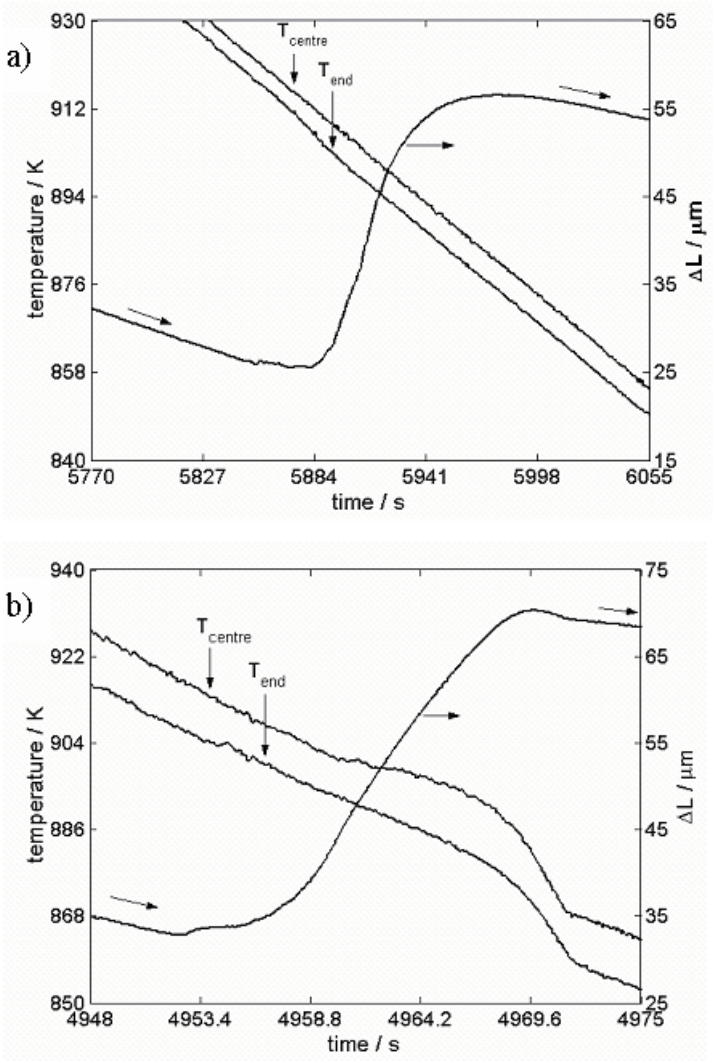

Fig. 3.3. The length change, ΔL and the temperatures, T_{centre} and T_{end}, as a function of time during the $\gamma \rightarrow \alpha$ transformation of Fe-5.91 at.%Ni for the two applied cooling rates, (a) 20 $Kmin^{-1}$, (b) 140 $Kmin^{-1}$.

The smoothed T_{centre} and T_{end} values decrease about linearly with time/temperature. The temperature difference (T_{centre}-T_{end}) is practically constant until the onset of the $\gamma \rightarrow \alpha$ transformation, but different for both applied cooling rates ((T_{centre}-T_{end}) is larger for the cooling rate of 140 Kmin^{-1}; Fig. 3.4). During the phase transformation T_{end}, for the cooling rate of 20 Kmin^{-1}, and both T_{centre} and T_{end}, for the cooling rate of 140 Kmin^{-1}, decrease nonlinearly with temperature, which is ascribed to heat release during the phase transformation (recalescence).

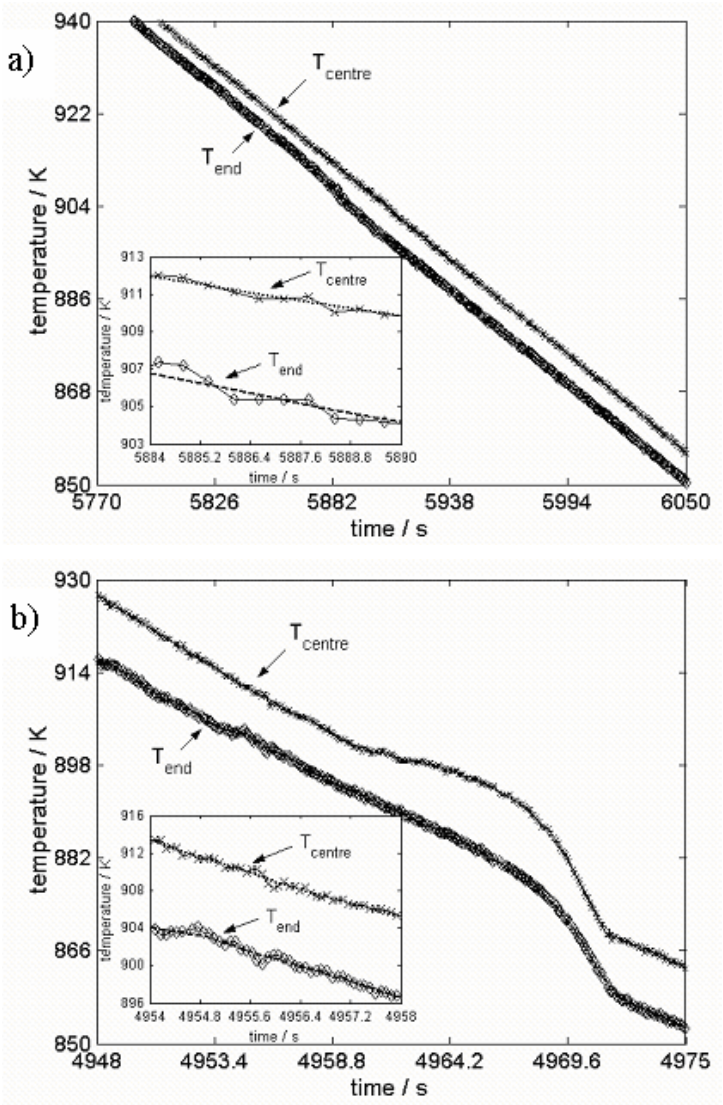

Fig. 3.4. The measured (data points) and smoothened (dashed and dotted lines) temperatures, T_{centre} and T_{end} as a function of time during the $\gamma \rightarrow \alpha$ transformation of Fe-5.91 at.%Ni for the two applied cooling rates, (a) 20 Kmin^{-1}, (b) 140 Kmin^{-1}.

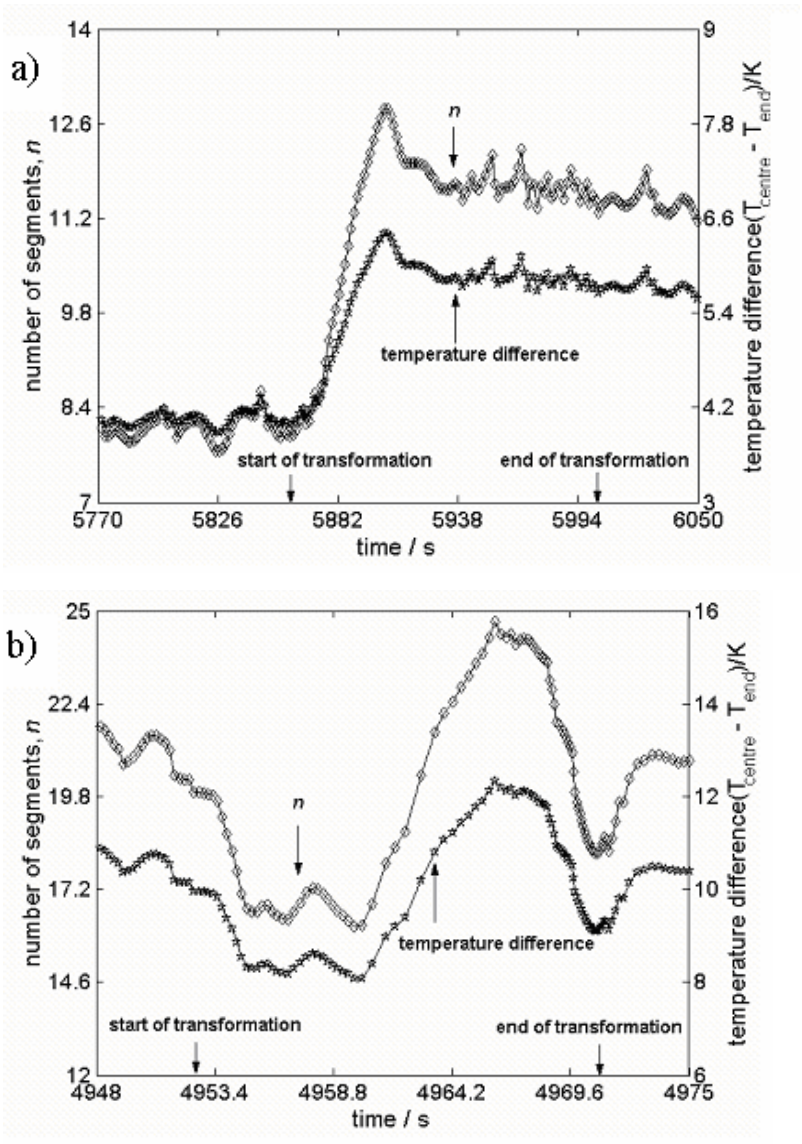

Fig. 3.5. The temperature difference, (T_{centre} - T_{end}), and the corresponding number of segments, n, (for a temperature difference of two adjacent segments, ΔT, equal to 0.5 K; cf. Eq. (3.1)) as function of time during the $\gamma \rightarrow \alpha$ transformation of Fe-5.91 at.%Ni for two applied cooling rates, (a) 20 $Kmin^{-1}$, (b) 140 $Kmin^{-1}$.

The temperature difference (T_{centre}-T_{end}) as function of T_{centre}, at 0.5 K intervals, during the $\gamma \rightarrow \alpha$ transformation, is shown in Fig. 3.5. The temperature difference (T_{centre}-T_{end}) increases during the first part of the transformation for the cooling rate of 20 $Kmin^{-1}$ and remains nearly constant for the largest part of the transformation, whereas for the cooling rate of 140 $Kmin^{-1}$ the temperature difference oscillates between the temperature

difference at the start of about 10 K and at the end of transformation of about 9 K (cf. Figs. 3.5(a) and 3.5(b))

3.4. Correction procedure for temperature inhomogeneity

3.4.1. Transformation dilation correction

A temperature gradient exists in the longitudinal direction of the dilatometry specimen undergoing induction heating/cooling. In order to calculate the dilation of the specimen as a function of a homogeneous temperature, the entire specimen in the longitudinal direction is hypothetically divided (cut perpendicular to the length axis) into a number of small specimens, which will be called *segments*. Each segment is assigned a homogeneous temperature. If the length change contribution by a segment can be calculated at each homogeneous temperature then the length change for the entire specimen at the same homogeneous temperature follows from a simple addition of the contributions of all segments.

The temperature profile can be assumed to be linear from the centre (= half height) of the specimen, where the temperature is identical to the measured value of T_{centre}, to the end of the specimen, where the temperature is identical to the measured value of T_{end} (see Figs. 3.1 and 3.4). Further, the temperature profile is taken symmetrical with respect to centre, where T_{centre} is measured (this symmetry has been verified; Fig. 3.2 and see section 3.2). The number of segments of one half of the specimen is given by the chosen temperature difference, ΔT of two adjacent segments as

$$n = \frac{T_{centre} - T_{end}}{\Delta T} \tag{3.1}$$

where n is a real number $(n = j + \eta,\ j = 1, 2..\ (\text{i.e. integer}), 0 \le \eta < 1)$ and $\Delta T \ll T_{centre} - T_{end}$. Thus there are j full segments and one fractional segment (fraction is η) in one half of the specimen. The entire specimen is composed of 2n segments along the longitudinal direction; n from the centre of the specimen to each of both ends.

The obtained numbers of segments along with the temperature differences (T_{centre}-T_{end}) are shown for $\Delta T = 0.5$ K and two different applied cooling rates in Fig. 3.5. The temperature difference (T_{centre}-T_{end}) for the applied cooling rate of 20 $Kmin^{-1}$ increases

from about 4 K to about 6 K during the first part of the transformation (see section 3.3) and hence the obtained number of segments, n, increases from about 8 to about 12 (see Fig. 3.5(a)). With the cooling rate of 140 $Kmin^{-1}$ the temperature difference varies from about 9 K to about 10 K during the transformation and thus the obtained number of segments, n varies from about 18 to about 20 (see Fig. 3.5(b)).

The length of a full segment, l, in the specimen at a particular time during cooling/heating is

$$l = \frac{\left(L/2\right)}{n} \tag{3.2}$$

where L is the length of the specimen at the time considered and $n = j + \eta$. There are j full segments with length l and one fractional segment with a length $l_\eta = \eta l$. The above described segmentation is performed during the cooling/heating at different times dictated by T_{centre} where the difference between the successive values of T_{centre}, ΔT_{step}, is taken equal to the constant, chosen temperature difference ΔT governing the segmentation (cf. Eq. (3.1)). It is important to note that as the transformation proceeds the number of segments and hence the segment length changes.

From the experimentally determined length changes, due to thermal expansion/shrinkage and transformation, first the length change due to the transformation as function of an operative temperature, either T_{centre} or T_{end} (cf. Fig. 3.6(a)), has to be determined. To this end the tangents AB and CD have been drawn in Fig. 3.6(a) as a function of time. They represent the (extrapolated) length change of the austenitic specimen upon cooling (AB) and the (extrapolated) length change of the (fully transformed) ferritic specimen upon cooling (DC). The first deviations from the tangents AB and CD, for decreasing temperature and increasing temperature, respectively, determine the value of the start and end temperatures of the transformation. The length change ΔL due to the transformation is here given as a function of T_{end}:

$$\Delta L\left(T_{end}\right)_i = L\left(T_{end}\right)_i - L_\gamma\left(T_{end}\right)_i \tag{3.3}$$

where $\left(T_{end}\right)_i$ denotes the temperature at the end of the specimen (in the longitudinal direction) at (time/) temperature step i during transformation, $L\left(T_{end}\right)_i$ is the length of

the transforming specimen at $(T_{end})_i$ and $L_\gamma(T_{end})_i$ is the (extrapolated) length of the pure austenitic specimen at $(T_{end})_i$ as obtained by extrapolation according to AB.

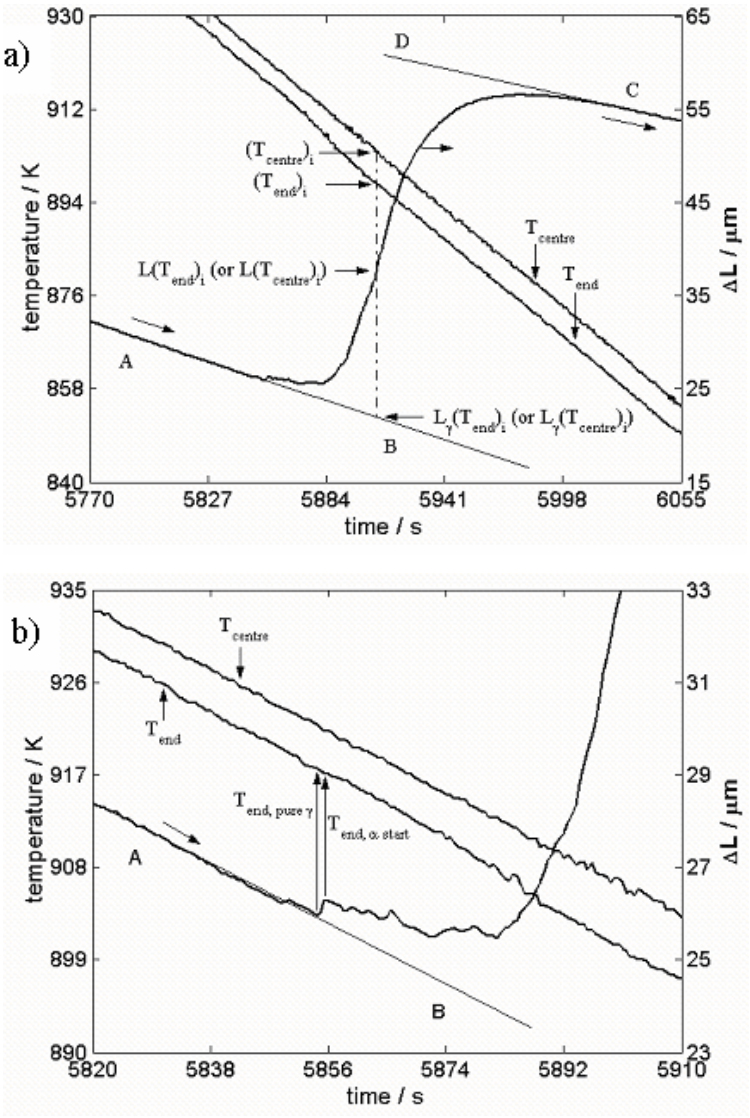

Fig. 3.6. (a) The measured length change, ΔL as a function of time during the $\gamma \rightarrow \alpha$ transformation of Fe-5.91 at.%Ni for the cooling rate of 20 $Kmin^{-1}$. AB and CD represent the (extrapolated) thermal shrinkage of the γ phase and the (extrapolated) thermal expansion of the α phase and (b) enlarged portion of (a) around the start of the transformation where $T_{end,\ pure\ \gamma}$ and $T_{end,\ \alpha\ start}$ correspond to the temperatures at the end of the stability of the pure γ phase and at the first observable deviation of length change from the linear shrinkage of the pure γ phase.

Recognizing that the lowest temperature in the specimen of inhomogeneous temperature is T_{end}, the length change for the entire specimen during transformation can be discussed as follows. For the temperature-step $i = 1$, i.e. at the onset of the transformation, the number of *transforming* (fractional) segments, n_{start}, can be determined from the value measured for T_{end} at the end of the stability of pure γ phase (just before the first deviation from linear part AB), $T_{end,\ pure\ \gamma}$, and the value measured for T_{end} corresponding to the first observable deviation from the linear part AB pertaining to the pure γ phase, $T_{end,\ \alpha\ start}$, according to (cf. Eq. (3.1)):

$$n_{start} = \frac{T_{end,\ pure\ \gamma} - T_{end,\ \alpha\ start}}{\Delta T} \tag{3.4}$$

$T_{end,\ \alpha\ start}$ is measured for the moment where the first deviation of T_{end} (larger than the scatter of the data) from the linear thermal dilation (shrinkage) behaviour of the pure γ phase is recorded as a value of T_{end} (see Fig. 3.6(b)). The (fractional) segment transforming in the first temperature step is shown as a shaded segment in Fig. 3.7(a) (one at each end of the specimen). The observed length change, $\Delta L\left(T_{end}\right)_{i=1}$ (see Fig. 3.6(b)) corresponds to transformation in the above two fractional segments. Because the difference in temperature between adjacent segments, ΔT, is taken equal to $\Delta T_{step} = \text{constant}$ (cf. below Eq. (3.2)), for the next temperature step ($i = 2$) the observed length change, $\Delta L\left(T_{end}\right)_{i=2}$ is due to transformation in the last two segments at both ends of the specimen (shown in shades). Thus, the total length change due to the transformation in temperature steps 1 and 2 is given by the sum of (a) the length change contribution by the shaded (fractional) segment in temperature step $i = 1$, $\Delta L\left(T_{end}\right)_{i=1}$ (segments in Fig. 3.7 connected by the arrow have the same temperature) and (b) the *excess* segments contributing to the length changes $\Delta L\left(T_{end}\right)_{i=2}$ in temperature step $i = 2$: the (fractional) end segment plus part of the segment adjacent to it (if in temperature step $i = 1$ the end segment was fractional). The *excess* segments, shown in part A in Fig. 3.7(a), are responsible for the increase in length $\left(\Delta L\left(T_{end}\right)_{i=2} - \Delta L\left(T_{end}\right)_{i=1}\right)$, in

temperature step $i = 2$ as compared to temperature step $i = 1$. As the transformation proceeds, further segments contribute to the length change due to transformation.

Consider two successive intermediate temperature steps $i-1$ and i. At both temperature steps all the segments are transforming. The top box in Fig. 3.7(b) represents the segments in the specimen at temperature step $i-1$ and the box underneath represents the segments in the specimen at temperature step i of the transformation. If the temperature gradient is constant (T_{centre}-T_{end} = constant), the temperatures of those segment pairs of temperature steps, $i-1$ and i connected by arrows in Fig. 3.7(b) are equal, and hence their contributions to specimen length change are equal. Then upon increasing i (i=1, 2, 3…), the length change contribution of the end segments at each step i follows from the measured values of $\Delta L\left(T_{end}\right)_i$ by subtracting the length change contributions of the other segments, which can be derived from the determined values for the length change contributions of T_{end} (i) values occurring at the previous temperature steps.

Now consider the case of a change in temperature gradient (change in T_{centre}-T_{end}) for two successive intermediate temperature steps when all the segments are transforming. If the change in T_{centre}-T_{end} for two successive temperature steps is sufficiently small, the number of full segments of two successive temperature steps is the same and also their lengths are practically the same: only the length of the fractional end segments changes significantly (cf. Eq. (3.1)). This is shown in Fig. 3.7(c) for a case corresponding to a slight increase in temperature gradient.

The temperatures and the length change contributions from pairs of segments connected by the arrows are identical (Fig. 3.7(b)) or practically identical (Fig. 3.7(c)). So, the resulting increase in length in temperature step i as compared to temperature step $i-1$ originates from (a) the excess segments (as defined above), indicated by part A in Figs. 3.7(b) and 3.7(c), and (b) segment B adjacent to the centre of the specimen (note: for the case shown in Fig. 3.7(a) segment B has not been considered because at the onset of transformation it does not contribute to any length change). Now in all the cases (Figs. 3.7(a), 3.7(b) and 3.7(c)) the two fractional (excess) end segments, contained in part A, can be treated as one segment with the same length but of homogeneous temperature T_{end} (i) provided ΔT is sufficiently small. The contribution of the uncancelled (see the arrows

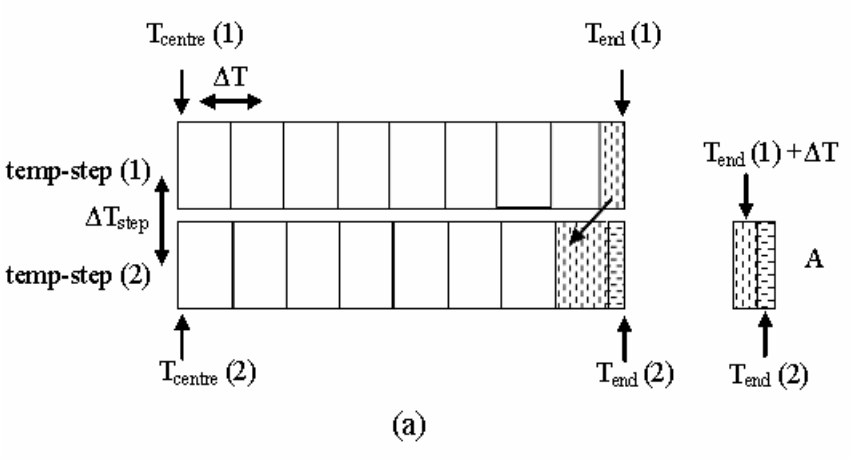
T_{centre} (1)
T_{end} (1)
ΔT
temp-step (1)
ΔT_{step}
temp-step (2)
T_{end} (1) +ΔT
A
T_{centre} (2)
T_{end} (2)
T_{end} (2)

(a)

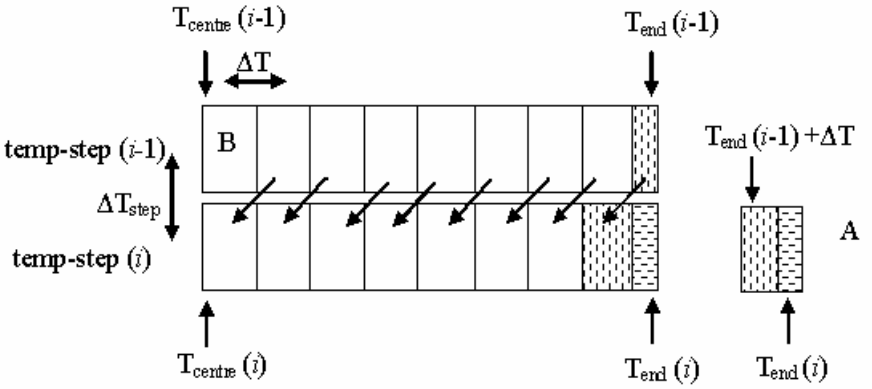
T_{centre} (*i*-1)
T_{end} (*i*-1)
ΔT
B
temp-step (*i*-1)
ΔT_{step}
temp-step (*i*)
T_{end} (*i*-1) +ΔT
A
T_{centre} (*i*)
T_{end} (*i*)
T_{end} (*i*)

(b)

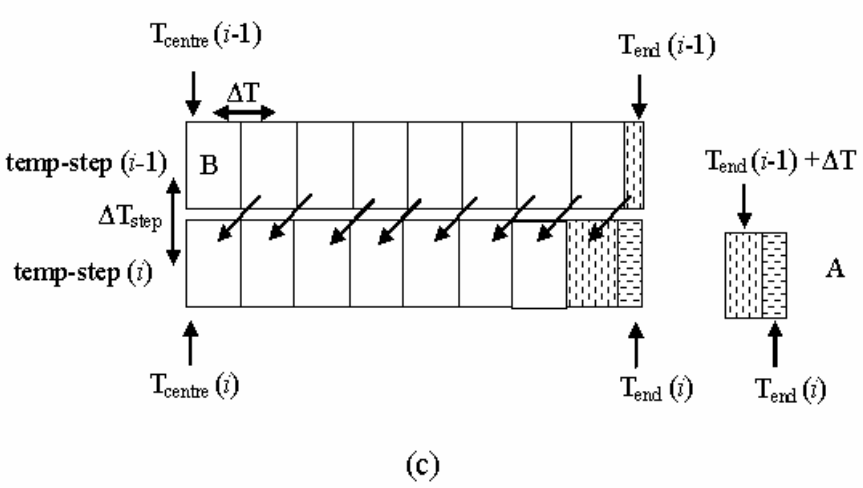

Fig. 3.7. A hypothetical schematic presentation of segmentation of the specimen experiencing a ($\gamma \rightarrow \alpha$) transformation. In each case (a, b, c) the segmentation shown in the upper box belongs to temperature step $i-1$ and the one shown in the bottom box belongs to temperature step i. The arrows connect pairs of segments with the same temperature in two successive temperature steps. (a) Initial two temperature steps ($i=1$ and $i=2$) where only the shaded segments transform, (b) Two consecutive, intermediate temperature steps where all segments transform. T_{centre}-T_{end} = constant and hence the numbers of segments (both full and fractional) in temperature steps $i-1$ and i are the same. (c) Two consecutive, intermediate temperature steps where all segments transform. T_{centre}-$T_{end} \neq$ constant and hence the number of segments in temperature steps $i-1$ and i are unequal: the number of full segments is the same but a significant length increase of the fractional end segments has occurred in temperature step i compared to temperature step $i-1$. Part A shown at the right in (a), (b), (c) shows the so-called excess segments (see text); which, together with segment B, are responsible for the change of specimen length occurring upon proceeding from temperature step $i-1$ to temperature step i: $\Delta L\ (T_{end})_i - \Delta L\ (T_{end})_{i-1}$ (see text and Eq. (3.5)).

in Figs. 3.7(b), 3.7(c) and text above) segment B in Figs. 3.7(b) and 3.7(c) in temperature step $i-1$ is known because a segment of temperature B has already occurred as an end segment (called here B') at some temperature step before. Although the temperature of both these segments (B in temperature step $i-1$ and B' in some previous temperature step) are the same, the corresponding segment lengths need not be necessarily equal: the segment length l, depends on L and n (see Eq. (3.2)) which both change during the transformation (cf. above discussion and Fig. 3.5). Hence, a multiplication factor, μ, is introduced, which accounts for the fractional increase or decrease in length of a full

segment B in temperature step $i-1$ as compared to the length of the corresponding segment B' of the same temperature in a temperature step $i-k$.

On the basis of entire discussion above the length change of the entire specimen in temperature step i, as compared to temperature step $i-1$, is then directly related to the difference in length change contribution from part ("segment") A and segment B. Recognizing that segment B' occurred as end "segment" A (=part A) in temperature step $i-k$, one can now write:

$$\Delta L\ (T_{end})_i - \Delta L\ (T_{end})_{i-1} = 2\ \left[\Delta L_{A,\,i}(T_{end})_i - \mu\ \Delta L_{A,\,i-k}(T_{end})_{i-k}\right] \qquad (3.5)$$

where $\Delta L_{A,\,i}(T_{end})_i$ and $\Delta L_{A,\,i-k}(T_{end})_{i-k}$ are the length change contributions from the end "segment" A (part A) in temperature step i and in temperature step $i-k$, respectively. The factor 2 recognises that the segments part A and B occur twice at temperature steps i and $i-1$, respectively.

The difference (length change), $\Delta L\ (T_{end})_i - \Delta L\ (T_{end})_{i-1}$, is shown in Fig. 3.8 for the cooling rate of 20 $Kmin^{-1}$. The difference upon cooling initially increases reaches a maximum and subsequently decreases. From these data, and because μ and $\Delta L_{A,\,i-k}(T_{end})_{i-k}$ are known, the unknown value of $\Delta L_{A,\,i}(T_{end})_i$ can be determined for all i in a recursive way (Eq. (3.5)).

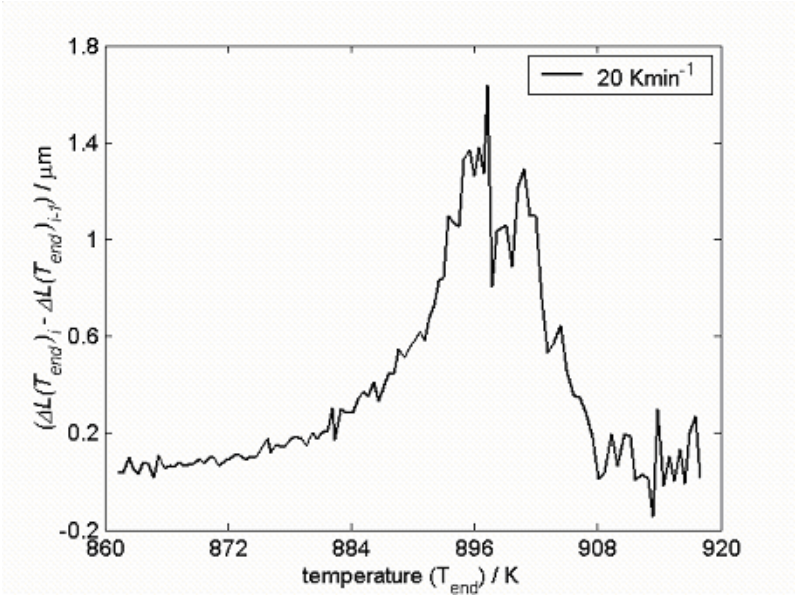

Fig. 3.8. Calculated length change, $\Delta L\left(T_{end}\right)_i - \Delta L\left(T_{end}\right)_{i-1}$, as function of temperature T_{end} during the $\gamma \rightarrow \alpha$ transformation for the indicated cooling rate.

Hence, the above treatment leads to the determination of the change of length of the end "segment" (part A) for all values of $(T_{end})_i$. Because the absolute length of the end "segment" A at all temperature steps i is also known, the relative change of length of the "segment" A at the temperature $\left(T_{end}\right)_i$ is known and thus the absolute length change of a hypothetical full segment at $\left(T_{end}\right)_i$ is known as well. On this basis the length change of the entire specimen at a homogeneous temperature $\left(T_{end}\right)_i$ as compared to the specimen length at $\left(T_{end}\right)_{i-1}$ is given by:

$$\Delta L_{\gamma\rightarrow\alpha}\left(T_H\right) = {}^{L}\!/\!_{l}\, \Delta L_{end}\left(T_H\right) \tag{3.6}$$

where ΔL_{end} denotes the length change at $T_H\,(\equiv (T_{end})_i)$ for a (hypothetical) full end segment, L is the length of the specimen at the time considered, l is the length of a full segment.

The thus obtained length change $\Delta L_{\gamma\rightarrow\alpha}\left(T_H\right)$, from Eq. (3.6), for the cooling rate of 20 $Kmin^{-1}$ is shown in Fig. 3.9. A considerable fluctuation is imposed on the resulting curve. Obviously, the difference term, $\Delta L\ \left(T_{end}\right)_i - \Delta L\ \left(T_{end}\right)_{i-1}$, is very sensitive to the

experimental fluctuation in $\Delta L(T_{end})$, in particular near the end of transformation where the change of length $\Delta L(T_{end})$ eventually becomes of the order of the experimental fluctuation.

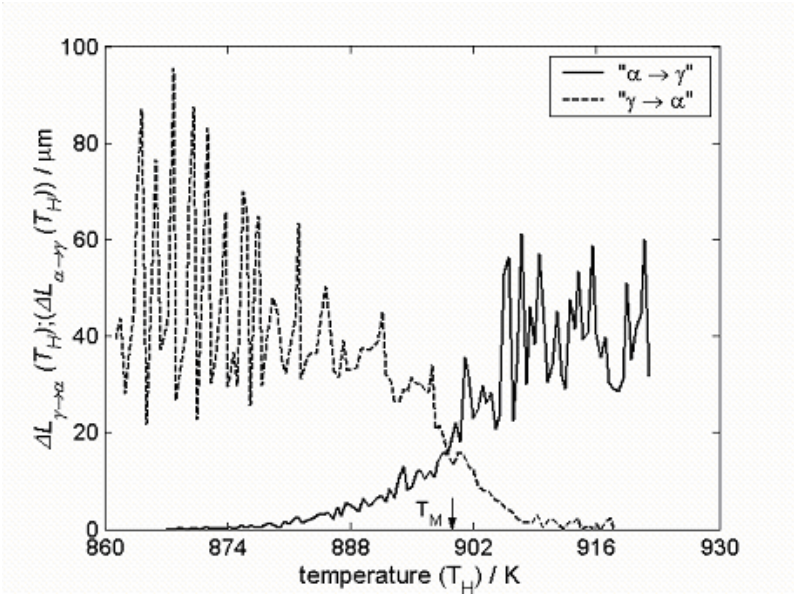

Fig. 3.9. The length change, $\Delta L_{\gamma\to\alpha}(T_H)$ and $\Delta L_{\alpha\to\gamma}(T_H)$ as function of homogeneous temperature, T_H, during the $\gamma \to \alpha$ transformation starting from untransformed prior γ phase to end with fully transformed α phase and the (hypothetical; see text) $\alpha \to \gamma$ transformation using the dilatational data measured upon cooling ($\gamma \to \alpha$) starting at the fully transformed α phase to end with untransformed prior γ phase. Cooling (hypothetical heating) rate: 20 $Kmin^{-1}$.

The dilation correction procedure was executed also using the same dilatational data but starting at the fully transformed α phase to end with untransformed prior γ phase *. The resulting hypothetical $\Delta L_{\alpha\to\gamma}(T_H)$ in Fig. 3.9 shows a similar behaviour as $\Delta L_{\gamma\to\alpha}(T_H)$ with fluctuations of increasing amplitude towards the end of the (hypothetical) transformation.

* The highest temperature of the specimen is T_{centre} at any temperature step. Then, upon virtual heating the first segment to transform is given by temperature, T_{centre}. So, the homogeneous temperature in this case is given by $T_H = T_{centre}$ (c.f. discussion of the procedure given for cooling)

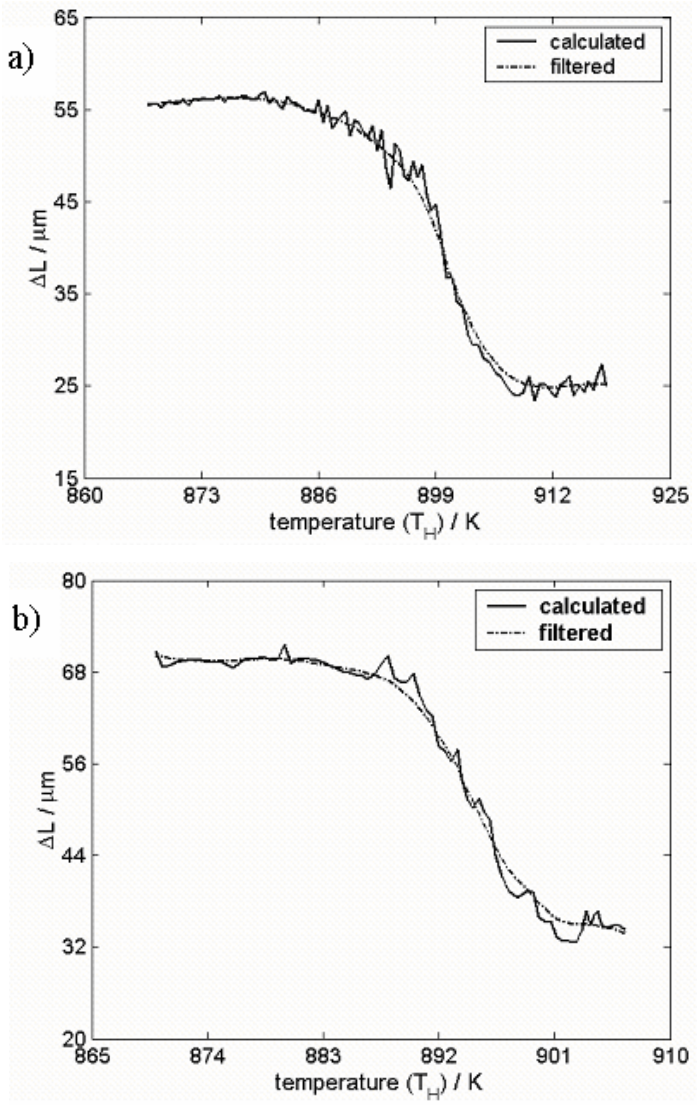

Fig. 3.10. The calculated (corrected for temperature inhomogeneity) and filtered (using a moving weighted-average filter) length change, ΔL, as function of homogeneous temperature, T_H, pertaining to the $\gamma \rightarrow \alpha$ transformation for two applied cooling rates, (a) 20 $Kmin^{-1}$, (b) 140 $Kmin^{-1}$.

To remedy the occurrence of these fluctuations the following procedure was adopted. First a suitable intermediate temperature, T_M, in the temperature range of the transformation was chosen beyond which the fluctuations become large (see the temperature T_M indicated with the arrow in Fig. 3.9). Secondly, (i) the length changes, $\Delta L_{\gamma\rightarrow\alpha}(T_H)$ and $\Delta L_{\alpha\rightarrow\gamma}(T_H)$ were calculated starting from the parent γ phase and starting from the product α phase, respectively, until temperature T_M; (ii) the resulting length change, $\Delta L_{\gamma\rightarrow\alpha}(T_H)$ until T_M was added to the extrapolated linear shrinkage of the

parent γ phase (after the correction as described in section 3.4.2) and the resulting length change $\Delta L_{\alpha\to\gamma}(T_H)$ until T_M was subtracted from the extrapolated linear expansion of the product α phase (after the correction as described in section 3.4.2). The thus obtained final results for two applied cooling rates are shown in Fig. 3.10. Indeed, by this procedure the scatter on the dilatation curve has been decreased substantially.

3.4.2. Thermal dilation correction for a not transforming phase.

The *measured* (*extrapolated*) lengths for both the parent and the product phases, $L_\gamma(T_{centre})$ and $L_\alpha(T_{centre})$ for pure γ and α, have to be corrected as well for the inhomogeneous temperature of the specimen; i.e. the lengths of the pure parent specimen and the pure product specimen have to be calculated for a hypothetical specimen of homogeneous temperature, T_H.

Taking T_H as T_{centre}, the length of all the segments with temperature different from T_{centre} (i.e. lower than T_{centre}) have to be extended with contributions proportional to $l_s\alpha(T_{centre}-T_s)$ where l_s denotes the length of the segment (i.e. for a full segment $l_s = l$ and for a fractional segment $l_s = l_\eta$ (see discussion of Eq. (3.2)), T_s is the segment temperature and α is the thermal expansion coefficient. Hence the length of the specimen with homogeneous temperature T_H (=T_{centre}) is given by

for pure austenite:

$$L_\gamma(T_H) = L_\gamma(T_{centre}) + \frac{(L/2)}{n}\left[2\left(\alpha_\gamma\left(\sum_{i=1}^{j} i\Delta T\right) + \alpha_\gamma(\eta\Delta T)\right)\right] \tag{3.7}$$

for pure ferrite:

$$L_\alpha(T_H) = L_\alpha(T_{centre}) + \frac{(L/2)}{n}\left[2\left(\alpha_\alpha\left(\sum_{i=1}^{j} i\Delta T\right) + \alpha_\alpha(\eta\Delta T)\right)\right] \tag{3.8}$$

where α_γ and α_α are the linear thermal expansion coefficients of austenite and ferrite, respectively. Note that, in contrast with the treatment in section 3.4.1, for cooling/heating of a pure phase which is not undergoing a phase transformation, T_{centre}-T_{end} and thus n is

practically constant. The segment length, l_s (for full and fractional segments) can then also be considered to be practically constant.

On the basis of Eqs. (7) and (8) and using the appropriate values of L, n, α_γ and α_α [in preparation] and ΔT, the dilation corrections for pure γ and pure α phases, $L_\gamma(T_H) - L_\gamma(T_{centre})$ and $L_\alpha(T_H) - L_\alpha(T_{centre})$, can be determined straightforwardly. Results are shown in Table 3.2. The thus determined dilation corrections for the two phases have to be applied to the measured linear dilations of the respective phases (AB and CD in Fig. 3.6(a)) as a function of the temperature T_{centre}.

Table 3.2 The applied cooling rates, number of segments at the onset of the $\gamma \rightarrow \alpha$ transformation, n_γ, the number of segments at the end of the $\gamma \rightarrow \alpha$ transformation, n_α and the length change correction for the pure γ phase, $L_\gamma(T_H) - L_\gamma(T_{centre})$ and the pure α phase, $L_\alpha(T_H) - L_\alpha(T_{centre})$.

cooling rate ($Kmin^{-1}$)	n_γ	n_α	$L_\gamma(T_H) - L_\gamma(T_{centre})$, μm	$L_\alpha(T_H) - L_\alpha(T_{centre})$, μm
20	4.2	5.6	0.6	0.6
140	10.0	8.5	1.3	0.8

3.4.3. Full dilatation correction

Finally, the length of the specimen as a function of homogeneous temperature T_H in the transformation range of the $\gamma \rightarrow \alpha$ transformation is obtained by adding the corrected dilation, $\Delta L_{\gamma\rightarrow\alpha}(T_H)$, pertaining to the $\gamma \rightarrow \alpha$ transformation (see section 3.4.1) to the corrected thermal dilation of the pure γ phase, $L_\gamma(T_H)$ (see section 3.4.2), as a function of homogeneous temperature, T_H. The resulting length change as function of T_H is shown in Fig. 3.10 for both applied cooling rates of 20 $Kmin^{-1}$ and 140 $Kmin^{-1}$ for the Fe-5.91 at.%Ni specimens. The as measured dilations as function of T_{centre} and the corrected dilations as a function of T_H can be compared for applied cooling rates of 20 $Kmin^{-1}$ and 140 $Kmin^{-1}$ in Figs. 3.11 and 3.12. Evidently, the correction is larger for 140 $Kmin^{-1}$ than for 20 $Kmin^{-1}$, because the specimen subjected to higher cooling rate experiences a larger temperature gradient. The dilation corrections for the pure phases (γ and α) and for the specimen that transforms are independent of each other. Then it is

satisfying to observe (see the enlargement of parts of Figs. 3.11(a) and 3.12(a) in Figs. 3.11(b), 3.11(c), 3.12(b), 3.12(c), respectively, for the applied cooling rates of 20 $Kmin^{-1}$ and 140 $Kmin^{-1}$) that the corrected length change due to the $\gamma \rightarrow \alpha$ transformation matches well with both the thermal shrinkage of the pure γ phase at the start of the transformation and with the thermal shrinkage of the pure α phase at the end of the transformation. So the correction procedures proposed in sections 3.4.1 and 3.4.2 are compatible with each other.

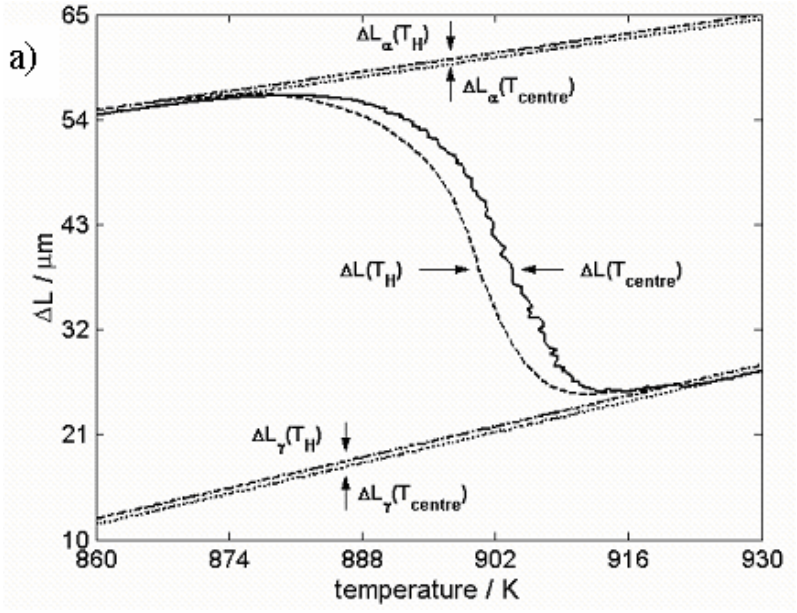

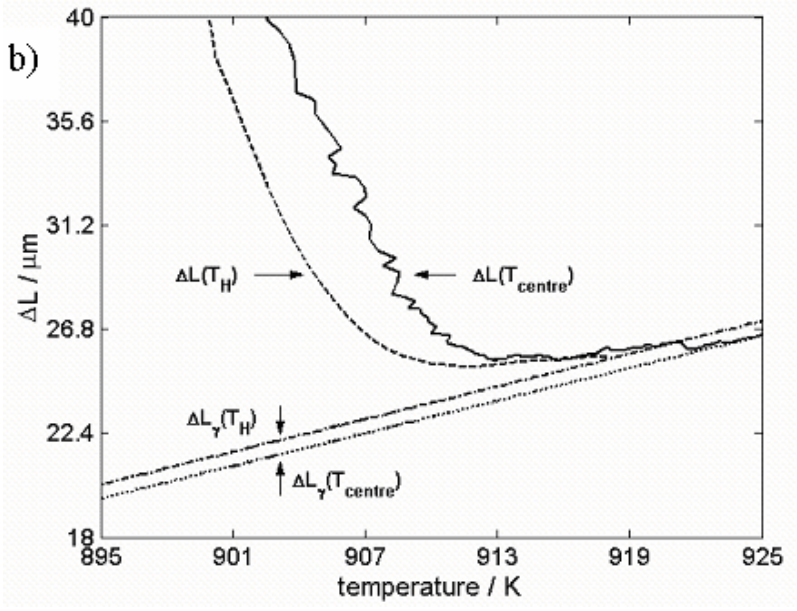

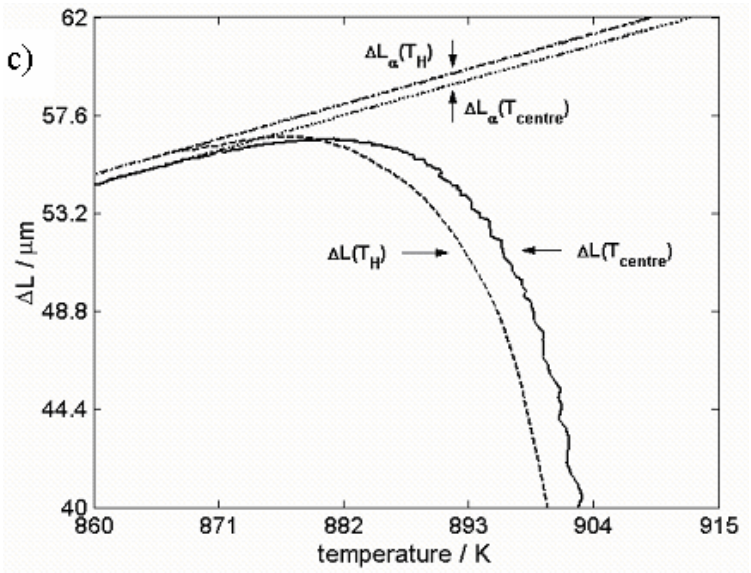

Fig. 3.11. (a) The measured, $\Delta L\left(T_{centre}\right)$, and corrected, $\Delta L\left(T_H\right)$, dilations of the transforming specimen ($\gamma \rightarrow \alpha$ transformation of Fe-5.91at.%Ni for the applied cooling rate of 20 $Kmin^{-1}$) along with the measured and corrected dilations of the pure austenite phase and the pure ferrite phase, ΔL_γ and ΔL_α, as a function of temperature. (b) and (c): enlargements of parts of (a) (see text for discussion).

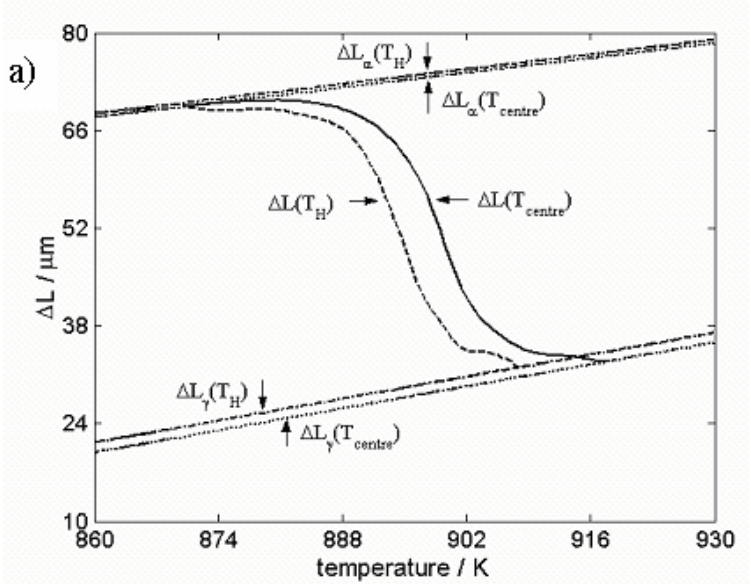

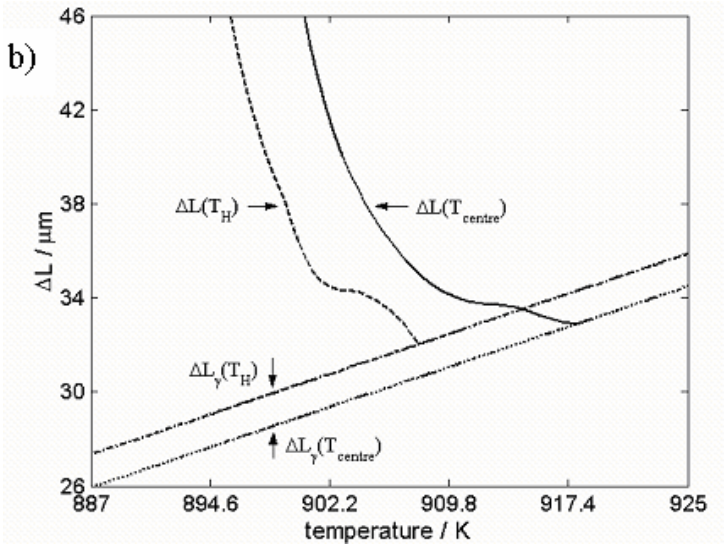

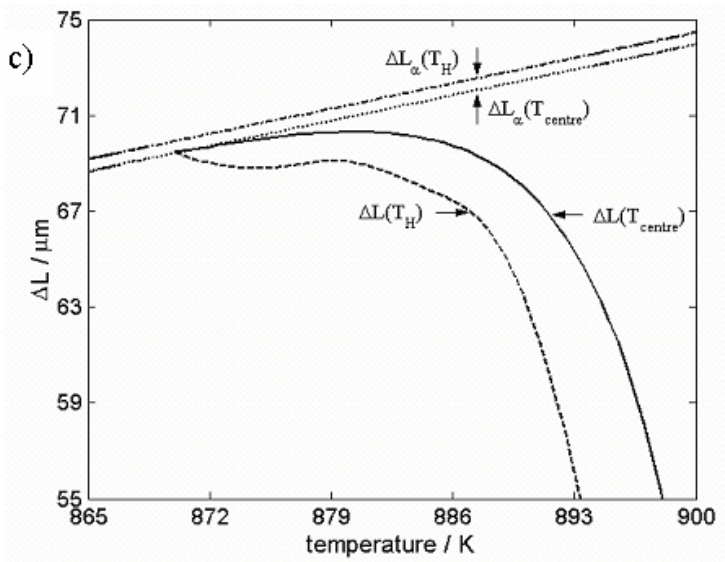

Fig. 3.12. (a) The measured, $\Delta L\left(T_{centre}\right)$, and corrected, $\Delta L\left(T_H\right)$, dilation of the transforming specimen ($\gamma \rightarrow \alpha$ transformation of Fe-5.91at.%Ni for the applied cooling rate of 140 $Kmin^{-1}$) along with the measured and corrected dilations of the pure austenite phase and the pure ferrite phase, ΔL_γ and ΔL_α, as a function of temperature. (b) and (c): enlargements of parts of (a) (see text for discussion).

3.5. Conclusions

1. A distinct temperature gradient occurs along the longitudinal direction of an inductively heated dilatometer specimen during heating and/or cooling, which increases with increasing heating/cooling rate. Thus the measured dilation cannot be interpreted directly in terms of transformation kinetics.
2. For the first time a temperature correction procedure was developed to obtain the dilation as a function of a homogeneous temperature. The method is based on hypothetical segmentation of the specimen into a number of small segments in the longitudinal direction so that each segment can be supposed to have a homogeneous temperature and such that the temperature difference between adjacent segments in a particular temperature step and the temperature difference of successive temperature steps are identical. The dilation contribution from one segment, during transformation, is calculated from the difference in dilation for the whole specimen between two successive temperature steps. This leads to a recursive procedure to calculate the relative change of length during the transformation. The obtained dilation for one segment can then be used to calculate the dilation for the full specimen.
3. Combining the *independent* dilation corrections for (i) temperature inhomogeneity in the not transforming parent and product phases and for (ii) the temperature inhomogeneity during the transformation leads to length changes for the specimen which are compatible.

References

[1] Y. C. Liu, F. Sommer, E. J. Mittemeijer, Thermochim. Acta 2004; 413: 215.

[2] T. A. Kop, Y. V. Leeuwen, J. Sietsma, S. Van Der Zwaag, ISIJ International 2000; 40: 713.

[3] M. Onink, F. D. Tichelaar, C. M. Brakman, E. J. Mittemeijer, S. Van Der Zwaag, J. Mater. Sci. 1995; 30: 6223.

[4] Y. C. Liu, F. Sommer, E. J. Mittemeijer, Acta Materialia 2004; 52: 2549.

[5] W. H. Press, S. A. Teukolsky, W. T. Vetterling, B. P. Flannery, Numerical Recipes in C, Cambridge University Press, NY, 1997.

4. Observations on the influence of uniaxial applied compressive stress on the austenite-ferrite transformation in Fe-Ni alloys

G. Mohapatra, F. Sommer, E.J. Mittemeijer

Abstract

Differential dilatometry has been employed to study the kinetics of the austenite (γ)-ferrite (α) massive phase transformation upon cooling of Fe-Ni alloys subjected to an applied constant uniaxial compressive stress. The imposed stress level is below the yield stress of the alloys. An increase in compressive stress results in a slight but significant increase of the start temperature of $\gamma \rightarrow \alpha$ transformation. A phase transformation model, involving site saturation, interface-controlled continuous growth and incorporating an appropriate impingement correction, has been employed to extract the interface velocity of the γ/α interface. The obtained interface velocity is independent of the applied stress (in the elastic regime), within experimental accuracy.

4.1. Introduction

Understanding of the γ(austenite)$\rightarrow\alpha$(ferrite) transformation behaviour in iron-based alloys is essential to control the final microstructure of the α phase, recognizing that the microstructure of a material is one of the most important parameters governing its (e.g. mechanical) properties (e.g. Ref. [1]). Materials used in practice are often subjected to pronounced applied or residual stresses. Thus, both from a fundamental and practical point of view, it is of interest to investigate the influence of an applied stress on the kinetics of the $\gamma \rightarrow \alpha$ transformation.

This paper reports the first quantitative investigation of the influence of an applied uniaxial compressive stress on the massive $\gamma \rightarrow \alpha$ transformation kinetics in terms of, start temperature, length change evolution and transformation interface velocity. The massive transformation of the γ (austenite) phase to the α (ferrite) phase upon cooling of Fe-Ni alloys has been studied over a wide compositional range in the absence of applied stress [e.g.2-5]. As model systems Fe-2.96at.%Ni and Fe-5.93at.%Ni alloys were chosen, which were subjected to applied uniaxial compressive stresses below the yield stresses of the alloys considered.

4.2. Phase transformation kinetics

The Fe-Ni partial equilibrium phase diagram relevant to the present study is shown in Fig. 4.1 [5]. This phase diagram was determined employing very long annealing times (days) in order to assure that equilibrium was reached [e.g. 6]. The investigated Fe-2.96at.%Ni alloy reaches the single phase region upon cooling at about 960 K (see the dashed line in Fig. 4.1). The $\gamma \rightarrow \alpha$ phase transformation occurring upon cooling of the Fe-5.93at.%Ni alloy cannot be completed, in practical time-spans, according to this equilibrium phase diagram (see the dotted line in Fig. 4.1). The T_0 curve, indicating the temperature where the Gibbs energies of the product (α) and parent (γ) phases of the same composition are equal, has been shown as function of Ni content in Fig. 4.1 as well.

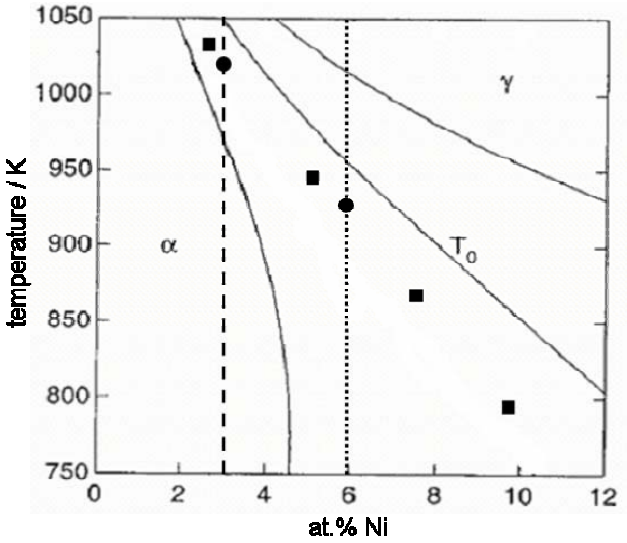

Fig. 4.1. Partial equilibrium phase diagram for Fe-Ni showing the T_0 line (temperature corresponding to equal Gibbs free energy of the product and the parent phase), the temperature corresponding to the 10% transformation at a cooling rate of 10Kmin^{-1} [7] (square data points). The dashed lines and the dotted lines represent the present alloy compositions (Fe-2.96at.%Ni and Fe-5.93at.%Ni). The measured start temperatures of transformation of $\gamma \rightarrow \alpha$ transformation at a cooling rate of 20 Kmin^{-1} for the respective alloys (with a very small applied stress of 0.005 MPa) have been indicated by the circular data points.

4.2.1. Transformation model

A general procedure for the simulation of phase transformation kinetics on the basis of nucleation, growth and impingement mechanisms has been given in Refs. [8, 9]. The first step of this procedure involves the calculation of the volume of all growing particles, assuming that the grains never stop growing and that new grains hypothetically nucleate also in the transformed material (i.e. at this stage, 'hard impingement' is ignored). This volume is called the extended volume (V_e), and the extended volume divided by the total specimen volume (V_0) is called the extended transformed fraction x_e. V_e is given by

$$V_e = g\left(\int v(T,f)\,dt\right)^3 \tag{4.1}$$

where g is a geometrical factor (which is 1 for cubical growth and $4\pi/3$ for spherical growth), v is the interface velocity which depends on the temperature, T, and the transformed fraction, f.

The interface velocity is considered to be proportional with the product of the interface mobility (M) and the driving force ($-\Delta G_{\alpha\gamma}$) [10]:

$$v_\alpha = M(T)\left[-\Delta G_{\alpha\gamma}(T,f)\right] \tag{4.2a}$$

The interface mobility exhibits an Arrhenius-like temperature dependence

$$M(T) = M_0 exp(-Q/RT) \tag{4.2b}$$

where M_0 is the pre-exponential factor, Q is the activation energy.

Data for the interface mobility are experimentally hardly available. With known driving forces, the interface mobility can be calculated from the observed interface migration velocity. In this work experimental mobility data on the recrystallization of pure iron ferrite have been used as reported in Ref [4] with M_0=4.9×10^3 ms^{-1}molJ^{-1}, and Q=1.47×10^5 Jmol^{-1} [4]. $\Delta G_{\alpha\gamma}$ in Eq. (4.2a) is given by

$$\Delta G_{\alpha\gamma}(T,f_\alpha) = \Delta G_{\alpha\gamma}^{chem}(T) + \left[\Delta G_{\alpha\gamma}^{def}(f_\alpha) + \Delta G_{\alpha\gamma}^{int}(f_\alpha)\right] \tag{4.3}$$

where $\Delta G_{\alpha\gamma}^{chem}$ is the molar chemical Gibbs energy difference between ferrite and austenite which depends on temperature, T. $\Delta G_{\alpha\gamma}^{int}$ is the molar free energy of the γ/α interface, and $\Delta G_{\alpha\gamma}^{def}$ is the summation of elastic and plastic molar accommodation energies resulting from misfit strains between ferrite and austenite phases. The driving force, $\Delta G_{\alpha\gamma}$, consists of a negative term, $\Delta G_{\alpha\gamma}^{chem}$, which favours the transformation, and two positive terms ($\Delta G_{\alpha\gamma}^{def}$ and $\Delta G_{\alpha\gamma}^{int}$) which obstruct the transformation. The chemical driving force depends on temperature, and not on the fraction transformed, because the transformation is partitionless. Both $\Delta G_{\alpha\gamma}^{int}$ and $\Delta G_{\alpha\gamma}^{def}$ depend primarily on the fraction transformed, f_α (and not directly on temperature).

In a next step, the extended transformed fraction is corrected for 'hard impingement' of the growing particles. Here an intermediate case of ideally periodic and ideally random dispersion of growing particles is considered, which is described by [8]:

$$f = tanh\left(x_e\right) \tag{4.4}$$

with $x_e = V_e/V_0$ as the extended fraction.

In view of the applied (low) cooling rate of 20 Kmin^{-1} it can be supposed that all nuclei (i.e. particles larger than the critical size) are already present at the very start of growth, i.e. 'site saturation' can be adopted. Since the transformation is partitionless, interface controlled growth prevails. Then, straightforward application of the model discussed leads the following expression relating to the rate of transformation, df_α/dt, to the interface velocity, v_α, and the mean grain size radius, $\overline{r}_\alpha$, of the product ferrite phase:

$$df_\alpha/dt = 3(1 - f_\alpha^2)arctanh^{\frac{2}{3}}(f_\alpha)\overline{r}_\alpha^{-1}v_\alpha(T, f_\alpha) \tag{4.5}$$

4.3. Experimental details

4.3.1. Specimen preparation

Bulk high purity Fe (99.98 wt. %) and Ni (99.99 wt. %) were used for the preparation of alloys. The purity of both Fe and Ni has been indicated by the composition data (determined by Inductive Coupled Plasma-Optical Emission Spectrometry (ICP-OES)) in Table 4.1. Melting of appropriate amounts of Fe and Ni was carried out in a vacuum-melting furnace, and the molten alloy was cast in a copper mould. The as-cast ingots of 7 mm in diameter were hammered down to rods of 6 mm diameter. In order to achieve a homogeneous microstructure, the rods/castings were sealed in a quartz container filled with argon gas at 2×10^4 Pa. The specimens were heated from room temperature to 1423 K at 5 Kmin^{-1} followed by annealing at 1423 K for 100 h and subsequently furnace cooled to room temperature. The compositions of the Fe-Ni rods were found to be Fe-2.96at.%Ni and Fe-5.93at.%Ni (determined by Inductive Coupled Plasma-Optical Emission spectrometry (ICP-OES)). Thereafter, the rods were machined into dilatometric specimens with a diameter of 5 mm and a length of 10 mm.

Table 4.1 Chemical composition of the iron and nickel used. Unit: ppm in mass

element	Fe	Ni
C	8	16
Si	10	0.23
Cu	1	0.17
Ti	0.6	1.3

4.3.2. Dilatometry measurements and temperature program

A dilatometer, employing inductive heating/cooling (DIL-805 A/D; Baehr-Thermoanalysis GmbH; see Fig. 4.2) was used to measure the thermal dilation of the alloys as a function of temperature/time during applied heat treatment cycles. Two thermocouples were spot welded on the surface of the dilatometric specimen, as shown in Fig. 4.2, to measure the temperature difference between the centre and the end of the specimen in its longitudinal direction.

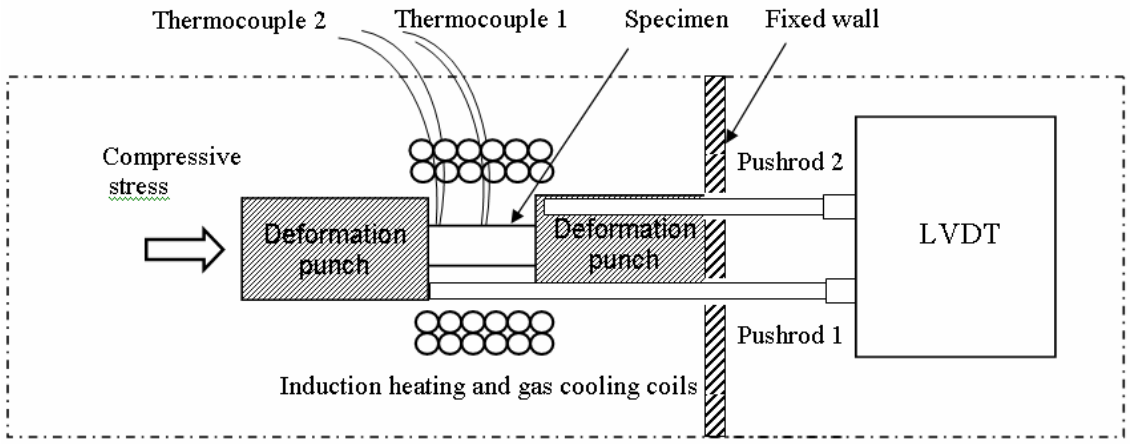

Fig. 4.2. Schematic (cross sectional top view) diagram showing the arrangement for the dilatometer DIL-805 A/D in compressive mode. The length change is measured by a linear variable differential transformer (LVDT).

The experiments were performed under vacuum (6×10^{-6} mbar) to avoid oxidation of the specimen. The applied thermal treatment cycle was as follows: the as received machined specimens of Fe-2.96at.%Ni and Fe-5.93at.%Ni (exhibiting average grain diameters of 65.7±3 μm and 49±3 μm, respectively) were heated from room temperature up to 1273 K at a rate of 20 $Kmin^{-1}$ and kept at this temperature for thirty minutes [11]. Then all the specimens were cooled down to room temperature at 20 $Kmin^{-1}$ and simultaneously subjected to various uniaxial constant compressive stresses of 0.005, 2.6, 5.1 and 7.6 MPa during the $\gamma \rightarrow \alpha$ transformation.

4.3.3. Austenite yield stress measurement

The yield stress of the alloys was measured in order to determine the elastic limit at temperatures above the start temperature of the $\gamma \rightarrow \alpha$ transformation. To this end specimens of Fe-2.96at.%Ni and Fe-5.93 at.%Ni were heated from room temperature to 1273 K and subsequently cooled to 1073 K and 973 K, respectively, and isothermally held there for 3 minutes. At these temperatures the alloy compositions of the specimens are within the two-phase region (see Fig. 4.1) and the temperatures are above the respective T_0 temperatures. The specimens remain fully austenitic for the short holding time of 3 minutes (the diffusion lengths of Ni at 1073 K and 973 K for 3 minutes are about 28 nm and 7 nm, respectively [12]). For yield stress measurement at these temperatures (1073 K and 973 K) the specimens were subjected to a continuously increasing uniaxial compressive stress (during the short holding time of 3 minutes) and the corresponding strain was monitored.

4.3.4. Temperature and length change calibration

The temperature calibration for Fe-5.93at.%Ni was performed by measurement of the Curie temperature, T_C, (ferro- to paramagnetic transition) of pure Fe during the heating and cooling parts of the same heat treatment cycle as applied to the Fe-5.93at.%Ni alloy (for details, see Ref. [13]). For the Fe-2.96at.% Ni alloy an *in situ* self calibration on this basis was possible from the observed Curie temperature during heating. The observed hysteresis of the Curie temperature for heating and cooling of pure Fe [13] is only 1 K and the calibration for Fe-2.96at.%Ni for cooling part of the heat treatment was corrected

accordingly. In all other cases the T_C falls within the temperature range for the $\alpha \rightarrow \gamma$ transformation (heating) and $\gamma \rightarrow \alpha$ transformation (cooling).

The length change calibration was performed according to the procedure described in Ref. [13].

4.3.5. Grain size determination

The fully transformed ($\gamma \rightarrow \alpha$) dilatometric specimens were sectioned along the longitudinal direction. The grain boundaries were exposed by etching with a 2.5 vol.% Nital solution and subsequently analyzed by light optical microscopy. The line intercept method [14] was employed in three different directions in order to determine the grain size. The line-intercept method results in a grain size value, which underestimates the true grain size. The true average of all grain diameters of the ferrite, $2\bar{r}_\alpha$ was thus assessed by multiplying the obtained intercept length by a factor of 1.5 [14]. The grain-size distribution was obtained by dividing the number of grains in a certain range of values for the true average grain diameter by the total number of measured grains.

4.4. Results and discussion

4.4.1. Austenite yield stress

The obtained stress as a function of strain is shown in Figs. 4.3 and 4.4 for the Fe-2.96at.%Ni alloy and the Fe-5.93at.%Ni alloy at 1073 K and 973 K, respectively. The elastic limit (yield stress) was determined by drawing a tangent, OA, to the measured linear portion of the stress-strain curve. The thus obtained yield point (A) is around 23 MPa for Fe-2.96at.%Ni at 1073 and 28 MPa for Fe-5.93at.%Ni at 973 K. In order to avoid plastic deformation during the $\gamma \rightarrow \alpha$ transformation in these alloys, the maximum stress applied was 7.6 MPa, which is well within the elastic limit of both alloys.

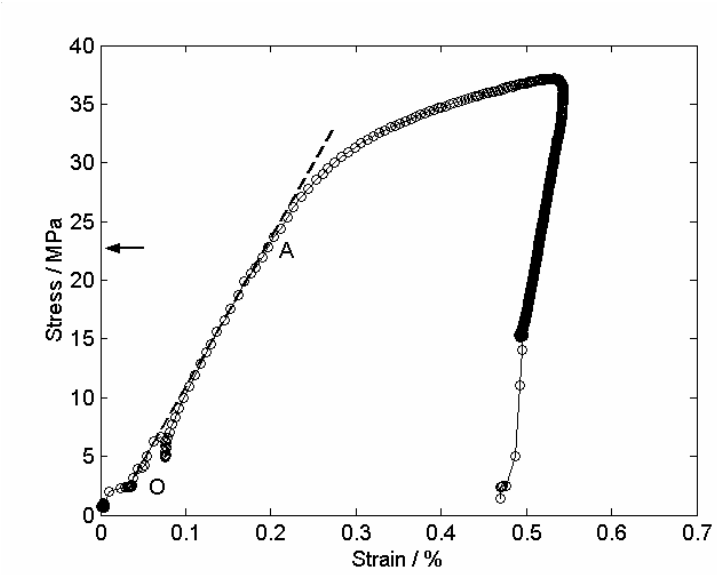

Fig. 4.3. The compressive stress-strain curve for Fe-2.96at.%Ni at 1073 K. OA indicates the region of linear elastic deformation, with point A representing the transition from the elastic to the plastic regime.

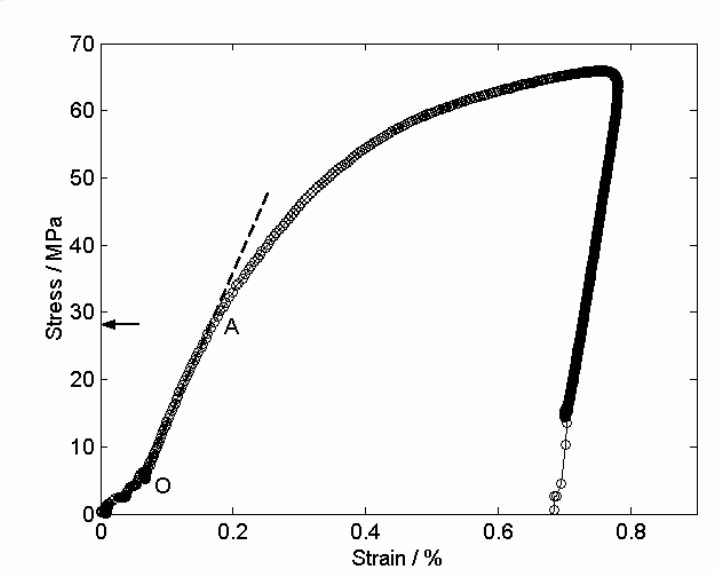

Fig. 4.4. The compressive stress-strain curve for Fe-5.93at.%Ni at 973 K. OA indicates the region of linear elastic deformation, with point A representing the transition from the elastic to the plastic regime.

4.4.2. Length change due to $\gamma \rightarrow \alpha$ transformation

The measured length change during heating and cooling of Fe-2.96at.%Ni and Fe-5.93at.%Ni for various values of applied compressive stress is shown in Figs. 4.5 and 4.6, respectively. The "up"-arrows indicate the heating part of the heat treatment cycle and the "down"-arrows indicate the cooling part of the heat treatment cycle. The small drop in length change before the start of the transformation (most clearly seen in the enlarged portions of the dilatometric curves for the $\gamma \rightarrow \alpha$ transformation upon cooling shown in Figs. 4.5(b) and 4.6(b)) corresponds to the application of stress and the small rise in length change after the completion of the transformation corresponds to the release of stress.

The total length change pertaining to the $\gamma \rightarrow \alpha$ transformation for a repeated sets of experiments (see Table 4.4) is shown in Figs. 4.7(a) and 4.7(b) as function of applied stress for Fe-2.96at.%Ni and Fe-5.93at.%Ni, respectively. The measured total length change is practically constant with increasing applied stress up to 5.1 MPa and decreases slightly for higher values of applied stress for both alloys.

The average total length change of Fe-5.93at.%Ni is larger than for Fe-2.96at.%Ni. This can be explained as a consequence of the difference in the transformation temperature (range): If the transformation would be completely isotropic the total length change due to transformation is influenced by the difference between the slopes (i.e. thermal expansion coefficients) of the γ and α phases. The slope (thermal expansion coefficient) of the γ phase is larger than that of the α phase. So a decrease in the $\gamma \rightarrow \alpha$ transformation temperature range results in an increase in length change due to transformation (provided the intrinsic volume change due to the transformation is about the same for the two alloys; here around 1.6 % [15]). Thus one can expect for Fe-5.93at.%Ni, as compared to Fe-2.96at%Ni, an increase in total $\gamma \rightarrow \alpha$ length change of about $8\ \mu m$, due to the difference in $\gamma \rightarrow \alpha$ transformation temperature: about 1011 K for Fe-2.96at.%Ni and about 922 K for Fe-5.93at.%Ni. This agrees qualitatively with the observed difference in average total length pertaining to the $\gamma \rightarrow \alpha$ transformation.

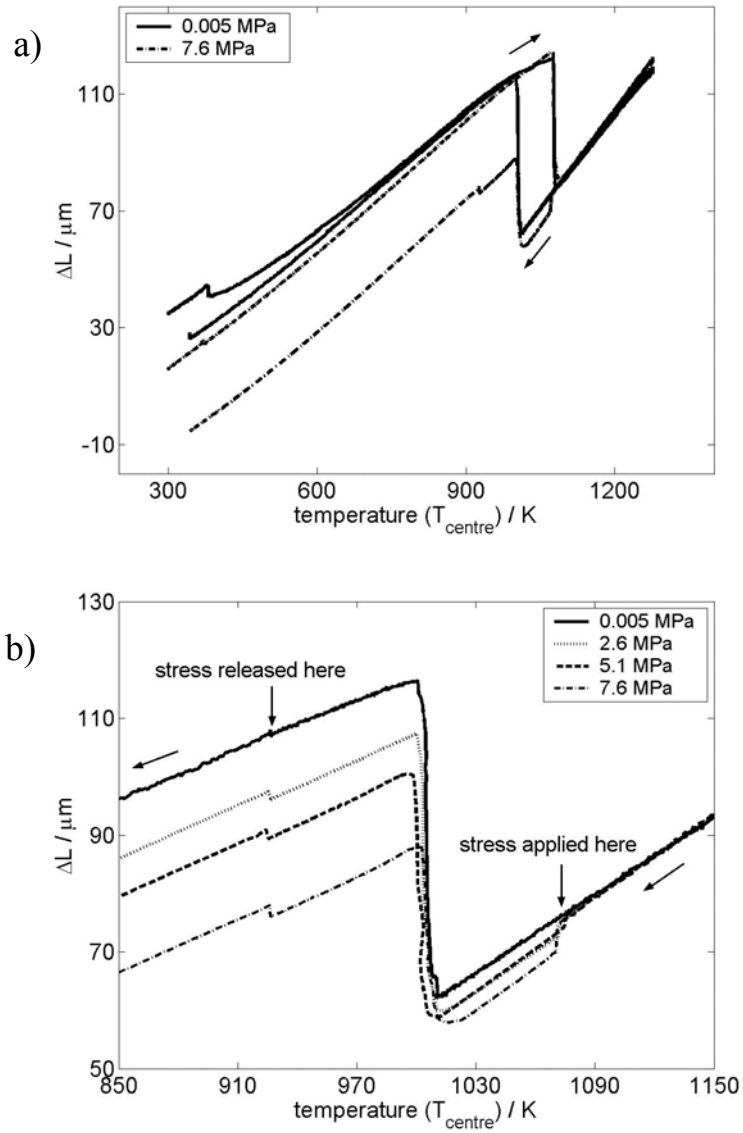

Fig. 4.5. (a) The measured length change (for minimum:0.005 MPa and maximum:7.6 MPa applied uniaxial compressive stresses) as a function of temperature, T_{centre}, with a heating and cooling rate of 20 $Kmin^{-1}$ of Fe-2.96at.%Ni. The up-arrow and down-arrow indicate the heating and cooling parts of the heat treatment cycle, respectively. The up-arrow and down-arrow indicate the heating and cooling cycle respectively. (b) enlargements of parts of (a) (see text for discussion) showing $\gamma \rightarrow \alpha$ transformation (the length change pertaining to the pure austenite phase is superimposed for all the experiments).

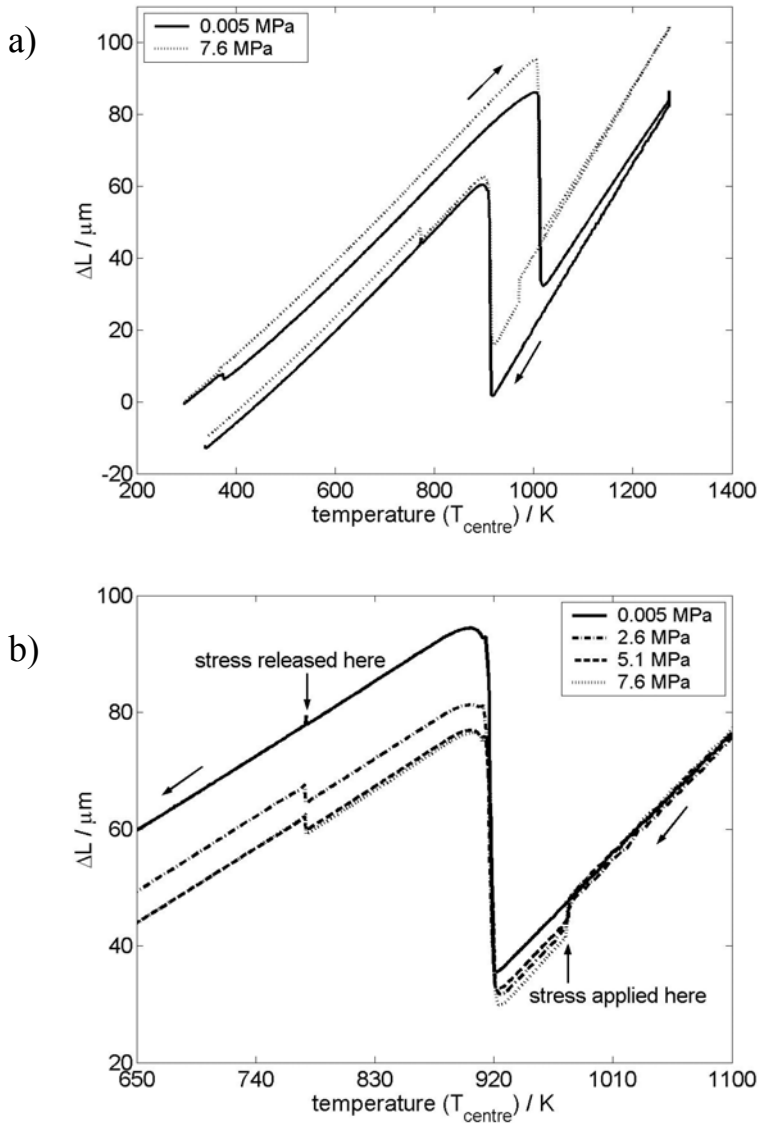

Fig. 4.6. (a) The measured length change (for one minimum:0.005 MPa and one maximum:7.6 MPa applied uniaxial compressive stress) as a function of temperature, T_{centre}, with a heating and cooling rate of 20 $Kmin^{-1}$ of Fe-5.93at.%Ni. The up-arrow and down-arrow indicate the heating and cooling parts of the heat treatment cycle, respectively. (b) enlargements of parts of (a) (see text for discussion) showing $\gamma \rightarrow \alpha$ transformation (the length change pertaining to the pure austenite phase is superimposed for all the experiments).

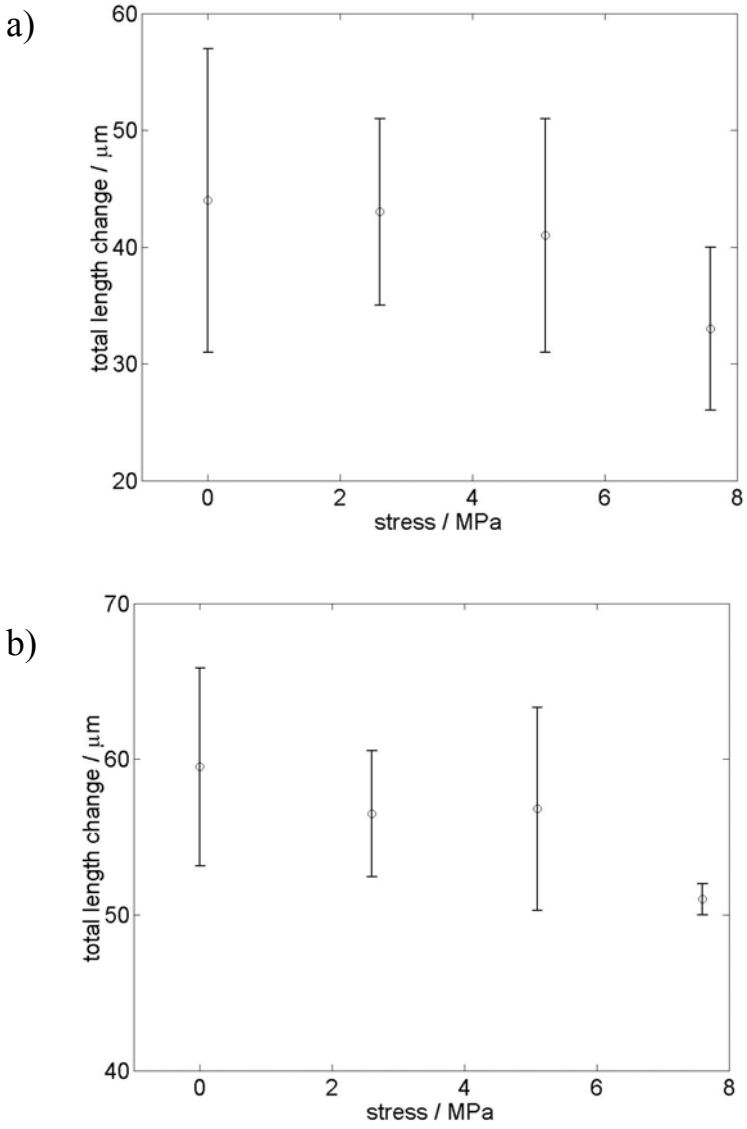

Fig. 4.7. The total length change pertaining to the $\gamma \rightarrow \alpha$ transformation as a function of applied compressive stress for (a) Fe-2.96at.%Ni and for (b) Fe-5.93at.%Ni. The error bars correspond to the standard deviations for repeated sets of experiments.

The diameter of the specimens was measured before and after one complete heat treatment cycle for various applied stresses. The results are shown in Fig. 4.8. It follows that the diameter of the specimen increases with increasing applied compressive stress.

It should be recognized that the volume expansion upon $\gamma \rightarrow \alpha$ transformation, as determined by both the specimen-length change and specimen-diameter change, is

constant, irrespective of the value of applied stress; see the results in Fig. 4.9: the small difference in volume before and after transformation is within the experimental uncertainty of the measurement. Slip bands were not observed in SEM micrographs taken from the surface of the dilatometic specimen after completed $\gamma \rightarrow \alpha$ transformation upon cooling under an applied stress of 7.6 MPa (the highest applied stress). Thus, a possible role of local plastic deformation induced by transformation plasticity influencing the specimen dimension (decrease in length and increase in diameter with applied stress) is unlikely. It can be concluded that with increase in applied compressive stress the volume change due to the transformation preferentially occurs in the radial directions and thereby a reduced (as compared to isotropic dilation) total length change due to the $\gamma \rightarrow \alpha$ transformation occurs.

4.4.3. Length change as a function of homogeneous temperature

The temperatures measured by the two thermocouples 1 (centre of the specimen and 2 (end of specimen) (see section 4.3.2) revealed the presence of a temperature gradient during heating and cooling. The temperature correction procedure as described in Ref. [16] has been applied to derive, from the measured length change, the specimen dilation as function of a *homogeneous* temperature during cooling in the vicinity of the $\gamma \rightarrow \alpha$ transformation. As an example the thus determined length change as a function of homogeneous temperature, $\Delta L\ (T_H)$, and the as measured length change, $\Delta L\ (T_{centre})$, are shown in Fig. 4.10 for Fe-2.96at.%Ni with an applied stress of 0.005 MPa. Evidently, the correction is significant.

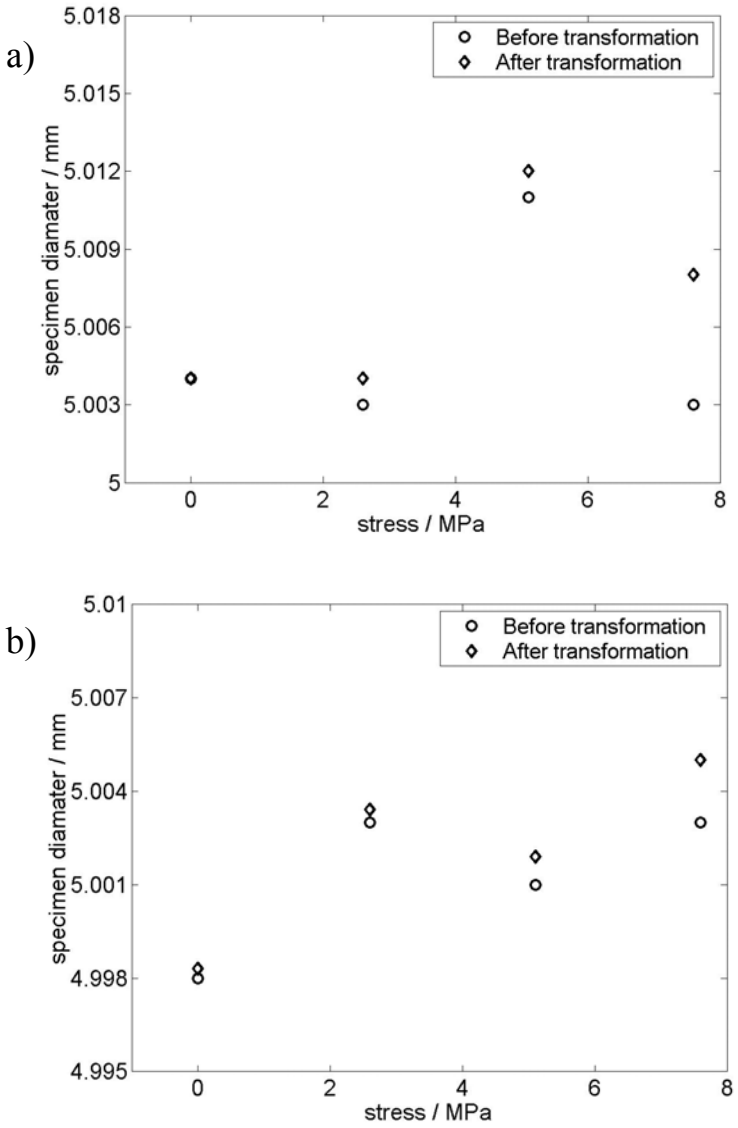

Fig. 4.8. The measured average (measured at various locations of the specimen) specimen diameter before and after one complete heat treatment cycle as a function of applied compressive stress for (a) Fe-2.96at.%Ni and for (b) Fe-5.93at.%Ni.

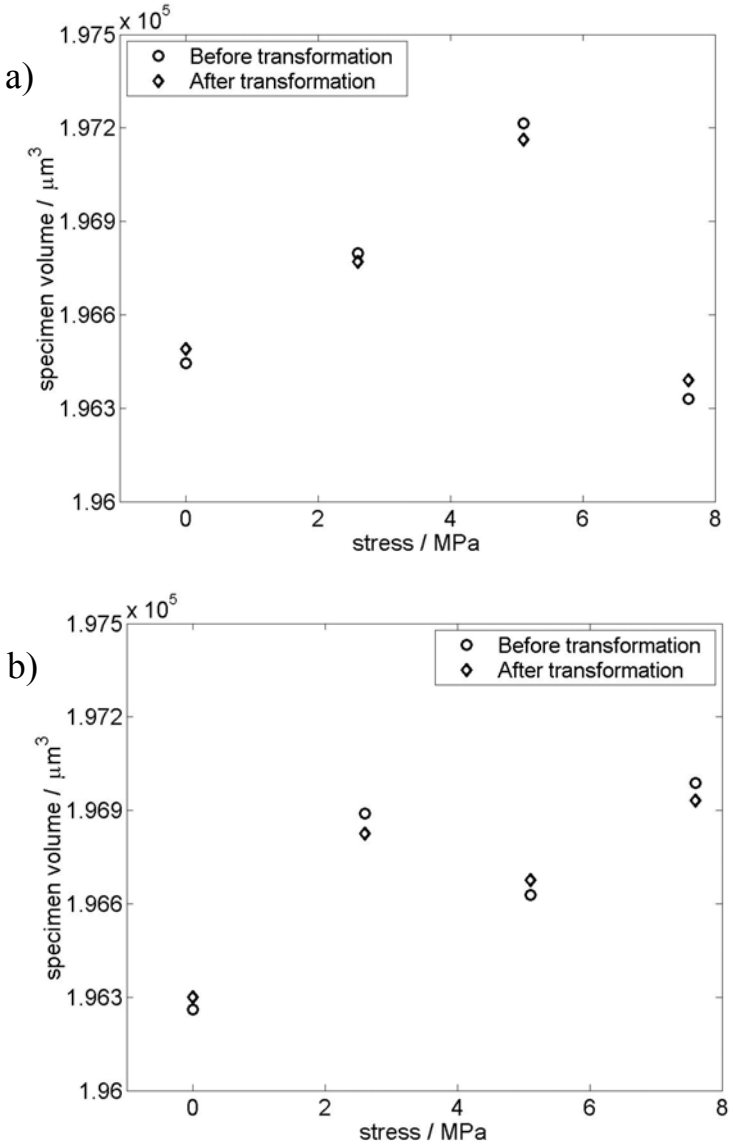

Fig. 4.9. The measured specimen volume before and after one complete transformation cycle as a function of applied compressive stress for (a) Fe-2.96at.%Ni and (b) Fe-5.93at.%Ni.

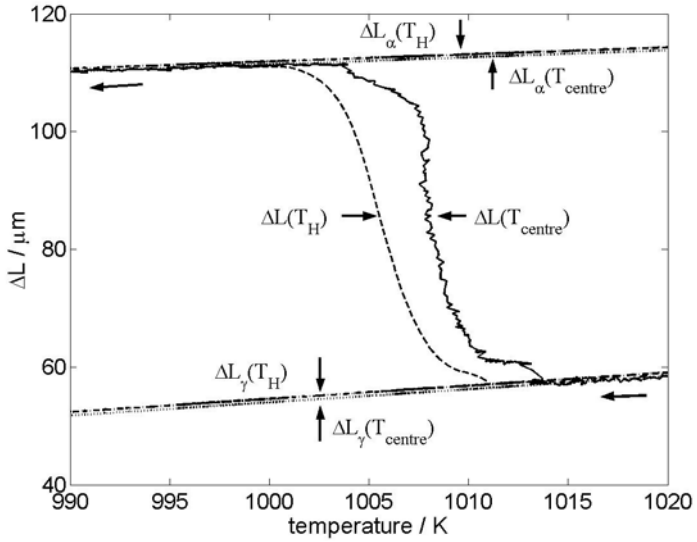

Fig. 4.10. The calibrated, $\Delta L\left(T_{centre}\right)$, calibrated and corrected, $\Delta L\left(T_H\right)$, dilations of the transforming specimen ($\gamma \rightarrow \alpha$ transformation) of Fe-2.96at.%Ni for the applied cooling rate of 20 $Kmin^{-1}$ under an applied stress of 0.005 MPa along with the measured and corrected dilations of the pure austenite phase ($\Delta L_\gamma(T_{centre})$ and $\Delta L_\gamma(T_H)$) and the pure ferrite phase ($\Delta L_\alpha(T_{centre})$ and $\Delta L_\alpha(T_H)$) as function of temperature.

4.4.4. Grain size and grain-size distribution

The ferrite grain size of the dilatometer specimens after $\gamma \rightarrow \alpha$ transformation under different applied compressive stresses was determined according to the procedure described in section 4.3.5. Independent of the applied stress all specimens show a more or less lognormal grain-size distribution: see the ferrite grain-size distributions of the Fe-2.96at.%Ni and Fe-5.93at.%Ni specimens subjected to 2.6 MPa shown in Fig. 4.11. The values of the average ferrite grain size after one complete heat treatment cycle under various compressive stresses have been gathered in Tables 4.2 and 4.3 for the Fe-2.96at.%Ni alloy and the Fe-5.93at.%Ni alloy, respectively. An overall increase in average ferrite grain size was observed for the Fe-2.96at.%Ni and the Fe-5.93at.%Ni alloys with increasing applied compressive stress. The increase in ferrite grain size with increasing applied compressive stress may be interpreted as that the number of nuclei apparently decreases with increasing applied compressive stress.

Table 4.2 The average grain diameter (unit: μm) of Fe-2.96at.%Ni for two repeated sets of experiments determined by the line intercept method as a function of thermo-mechanical history for various *compressive* stresses.

heat treatment process	average grain diameter, μm
As cast, after annealing at 1423 K for 100 h	65.7±3
Heat treatment cycle with 0.005 MPa stress	67.6±3
Heat treatment cycle with 2.6 MPa stress	76.5±3
Heat treatment cycle with 5.1 MPa stress	74.4±3
Heat treatment cycle with 7.6 MPa stress	78.4±3

Table 4.3 The average grain diameter (unit: μm) of Fe-5.93at.%Ni for two repeated sets of experiments determined by the line intercept method as a function of thermo-mechanical history for various *compressive* stresses.

heat treatment process	average grain diameter, μm
As cast, after annealing at 1423 K for 100 h	49.0±3
Heat treatment cycle with 0.005 MPa stress	50.6±3
Heat treatment cycle with 2.6 MPa stress	54.4±3
Heat treatment cycle with 5.1 MPa stress	59.5±3
Heat treatment cycle with 7.6 MPa stress	64.1±3

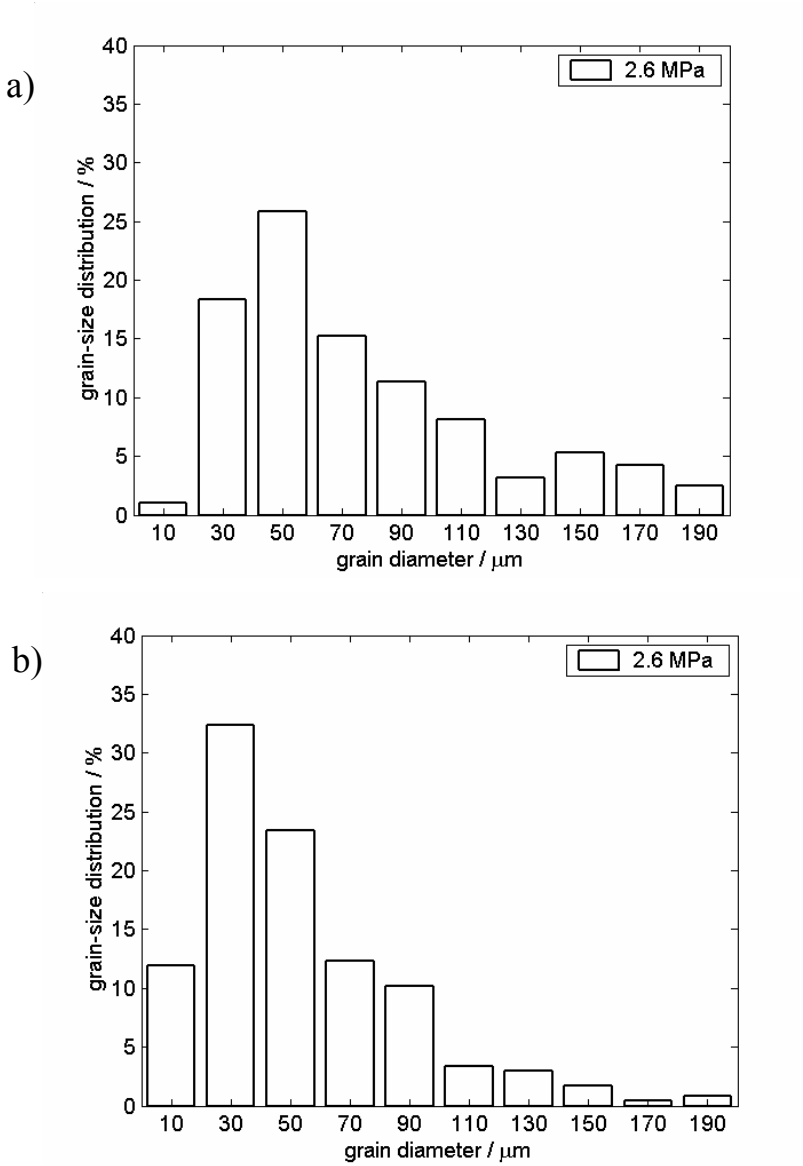

Fig. 4.11. Ferrite grain-size distribution of (a) Fe-2.96at.%Ni and (b) Fe-5.93at.%Ni after the $\gamma \rightarrow \alpha$ transformation at a cooling rate of 20 $Kmin^{-1}$ and at an applied uniaxial compressive stress of 2.6 MPa.

4.4.5. Temperature range of the $\gamma \rightarrow \alpha$ transformation

The start temperature of the $\gamma \rightarrow \alpha$ transformation was determined from the measured length change and the temperature T_{end} both as a function of time upon cooling; see Fig. 4.12. During the phase transformation, T_{centre} decreases about linearly with time (Fig. 4.12) because thermocouple1 (measures the temperature, T_{centre}, Fig. 4.2) controls the applied temperature program, whereas T_{end} decreases nonlinearly with time during the

phase transformation which is ascribed to the local recalescence effect caused by the phase transformation. Because $T_{end}<T_{centre}$, the $\gamma \rightarrow \alpha$ transformation upon cooling starts in the end regions of the specimen where T_{end} prevails. The first observable deviation of the length change from a tangent to the linear thermal dilation part of pure austenite during cooling (i.e. AB in Fig. 4.12) larger than the scatter of the data was taken as to identify the start of transformation (i.e. C in Fig. 4.12). The T_{end} temperature corresponding to the length change at point C (i.e. D in Fig. 4.12) then denotes the *measured* start temperature (T_{start}) of the $\gamma \rightarrow \alpha$ transformation.

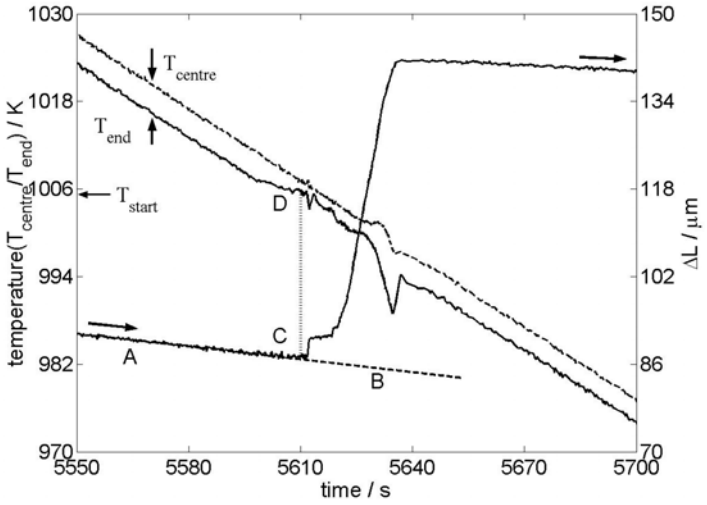

Fig. 4.12. The length change, ΔL and the temperatures, T_{centre} and T_{end}, as a function of time during the $\gamma \rightarrow \alpha$ transformation upon cooling from 1273 K at 20 $Kmin^{-1}$ of Fe-2.96 at.%Ni under the applied stress of 0.005 MPa. AB is the tangent to the linear shrinkage of the pure γ phase. The length change at point C corresponds to the first deviation of the linear shrinkage of the pure γ phase larger than the scatter of the data. The non-vertical arrows indicate the direction of length change during cooling. The non-linear behaviour of the measured T_{end} temperature during transformation is due to the (local) recalescence effect due to transformation.

The measured start temperatures of transformation determined for the Fe-2.96at.%Ni and Fe-5.93at.%Ni alloys are observed below the T_0 line (see Fig. 4.1 and begin of section 4.2). The start temperatures of transformation for both alloys increase slightly with increasing applied compressive stress (see Tables 4.4 and 4.5).It also follows from Tables 4.4 and 4.5 that the time of transformation depends on alloy

composition, but for each alloy is constant for all applied stresses within the limit of accuracy.

Table 4.4 The measured calibrated start temperature and time of transformation of Fe-2.96at.%Ni at a cooling rate of 20 $Kmin^{-1}$ under different applied uniaxial *compressive* stresses for repeated sets of experiments.

stress, MPa	start temperature, K	average start temperature, K	average time, s
0.005	1011.0 1010.0 1011.0 1011.0 1011.0 1011.0	1010.8±0.4	52±11
2.6	1012.0 1013.5 1013.0	1012.8±0.7	46±8
5.1	1014.5 1012.0 1013.5 1013.0 1012.5	1013.1±1.0	46±7
7.6	1014.5 1014.5 1014.0 1012.0	1013.8±1.2	44±16

Table 4.5 The measured calibrated start temperature and time of transformation of Fe-5.93at.%Ni at a cooling rate of 20 $Kmin^{-1}$ under different applied uniaxial *compressive* stresses for repeated sets of experiments.

stress, MPa	start temperature, K	average start temperature, K	average time, s
0.005	922.0 923.0 924.0	923.0±1.0	56±10
2.6	923.0 927.6 924.0 924.0 926.5	925.0±2.0	55±8
5.1	926.0 926.0 927.0 925.0	926.0±0.8	58±3
7.6	925.0 926.0 925.0	925.0±0.6	57±5

4.4.6. Transformed fraction and rate of transformation

The total length change determined for the $\gamma \rightarrow \alpha$ transformation depends on the applied compressive stress (see Fig. 4.7), but the volume of the specimen before and after one complete heat treatment cycle, involving a $\alpha \rightarrow \gamma$ and a $\gamma \rightarrow \alpha$ transformation, is constant (Fig. 4.9; see section 4.4.2). Thus, it is likely that the change (increase) in volume by the $\gamma \rightarrow \alpha$ transformation is also constant, i.e. independent of applied compressive stress. Hence, it is reasonable to suppose that the increase in length in the longitudinal direction due to the $\gamma \rightarrow \alpha$ transformation is proportional to the increase in specimen diameter due to the $\gamma \rightarrow \alpha$ transformation. Hence, from the corrected and calibrated length change (see section 4.4.3), the transformed fraction, f_α, can be obtained using the conventional lever rule [17].

The thus obtained transformed fraction, f_α, as a function of homogeneous temperature is shown in Figs. 4.13 and 4.14 for various applied stresses for two sets of experiments for the Fe-2.96at.%Ni alloy and the Fe-5.93at.%Ni alloy, respectively. Beside the start temperature of transformation, $f_\alpha = 0$, (see Tables 4.4 and 4.5); the temperatures corresponding to $f_\alpha = 0.5$ and $f_\alpha = 0.8$ were determined for both Fe-2.96at.%Ni and Fe-5.93at.%Ni as function of applied stress (see Tables 4.6 and 4.7). For Fe-2.96at.%Ni, no systematic trend was observed for the temperatures corresponding to $f_\alpha = 0.5$ and 0.8, as a function of applied stress. For Fe-5.93at.%Ni, the temperatures corresponding to $f_\alpha = 0.5$ and $f_\alpha = 0.8$ increase slightly with increasing applied stress.

Table 4.6 The measured calibrated temperature at f_α=0.5 and at f_α=0.8 of Fe-2.96at.%Ni at a cooling rate of 20 $Kmin^{-1}$ under different applied uniaxial *compressive* stresses for two sets of experiments.

stress, MPa	f_α	temperature, K (set 1)	temperature, K (set 2)
0.005	0.5	1005.0	1007.0
	0.8	1003.0	1004.0
2.6	0.5	1005.0	1006.0
	0.8	1003.0	1004.0
5.1	0.5	1002.0	1004.0
	0.8	1000.0	1002.0
7.6	0.5	1006.5	1009.0
	0.8	1004.0	1007.0

Table 4.7 The measured calibrated temperature at f_α =0.5 and at f_α =0.8 of Fe-5.93at.%Ni at a cooling rate of 20 Kmin^{-1} under different applied uniaxial *compressive* stresses for two sets of experiments.

stress, MPa	f_α	temperature, K (set 1)	temperature, K (set 2)
0.005	0.5	916.0	916.0
	0.8	913.5	913.0
2.6	0.5	917.0	917.0
	0.8	914.0	915.0
5.1	0.5	919.0	920.0
	0.8	918.0	917.0
7.6	0.5	920.0	921.0
	0.8	917.0	918.0

The rate of transformation, df_α/dt, calculated from the transformed fraction, f_α, as a function of cooling time, is shown as a function of transformed fraction for Fe-2.96at.%Ni and Fe-5.93%at.%Ni in Figs. 4.15 and 4.16, respectively, for one representative set of experiments. The obtained behaviour for df_α/dt as a function of f_α is rather smooth, unlike the fluctuations observed in Refs. 17 and 18 for pure Fe and iron based alloys (Fe-2.26at.%Mn, Fe-1.79at%Co), which are of the order of around ±0.004 s^{-1} *. For comparison, the determined df_α/dt as a function of f_α 2.96at.%Ni is shown for an applied stress of 7.6 MPa in Fig. 4.17. This is illustrative for the observed stop and go mechanism of the interface during transformation as discussed in Refs. 18 and 19 and observed in Ref. [20]. The results for df_α/dt shown in Figs. 4.15 and 4.16 shows that the applied compressive stress has little influence on the variation of df_α/dt.values, respectively.

* The smoothening procedure adopted in the current work to extract the length change as a function of homogeneous temperature, T_H, from the measured length change as a function T_{centre} temperature (see Ref. [16]), contributes to the smoothness in the variation of df_α/dt as a function of f_α.

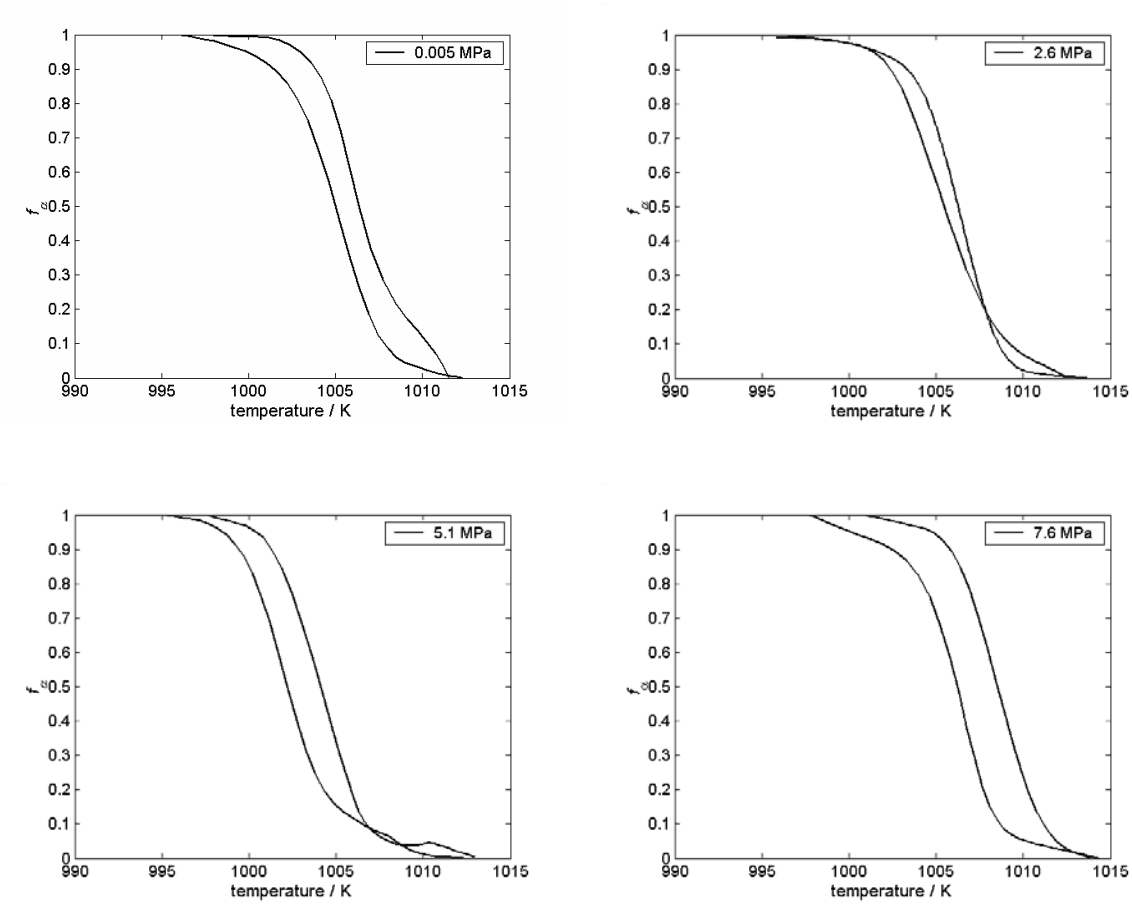

Fig. 4.13. The transformed fraction, f_α, as a function of homogeneous temperature, T_H, as determined from the length change, $\Delta L(T_H)$, of Fe-2.96at.%Ni at a cooling rate of 20 $Kmin^{-1}$ under various indicated applied uniaxial compressive stress for two repeated sets of experiments.

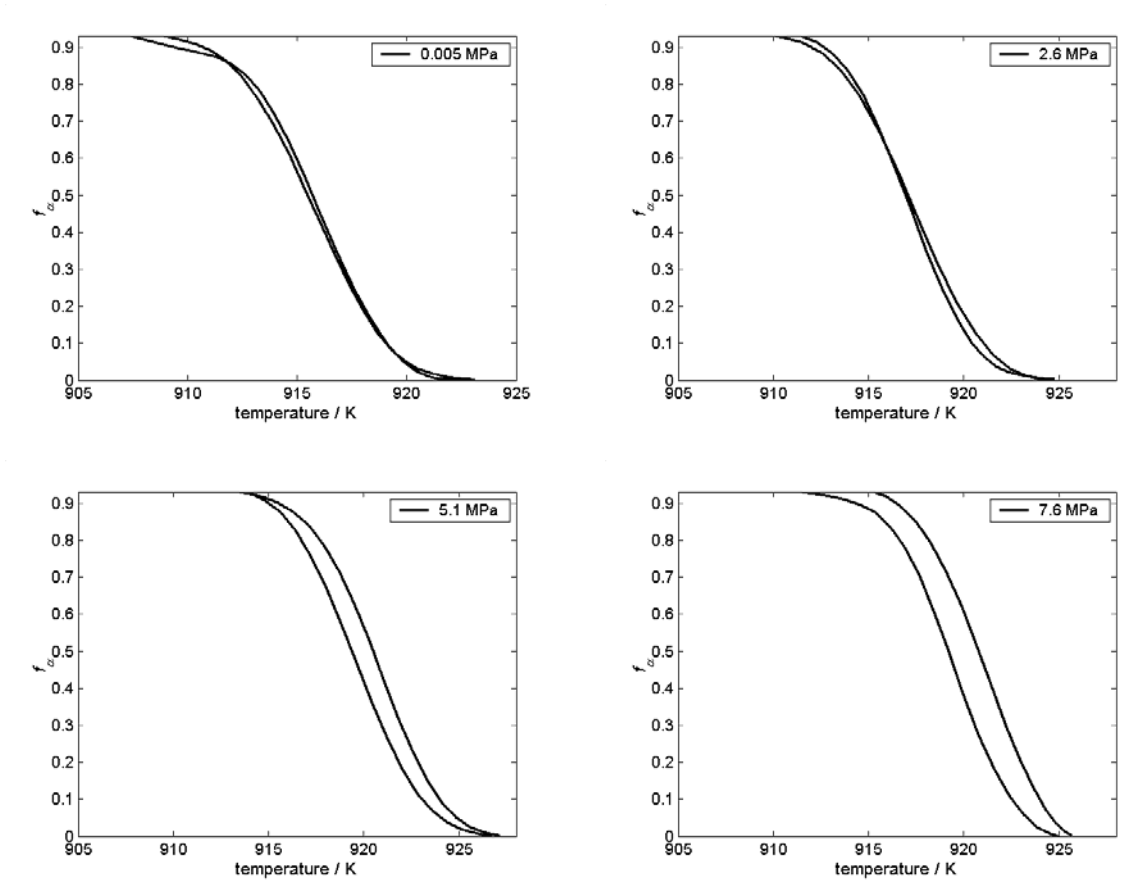

Fig. 4.14. The transformed fraction, f_α, as a function of homogeneous temperature, T_H as determined from the length change, $\Delta L(T_H)$, of Fe-5.93at.%Ni at a cooling rate of 20 $Kmin^{-1}$ under various indicated applied uniaxial compressive stress for two repeated sets of experiments.

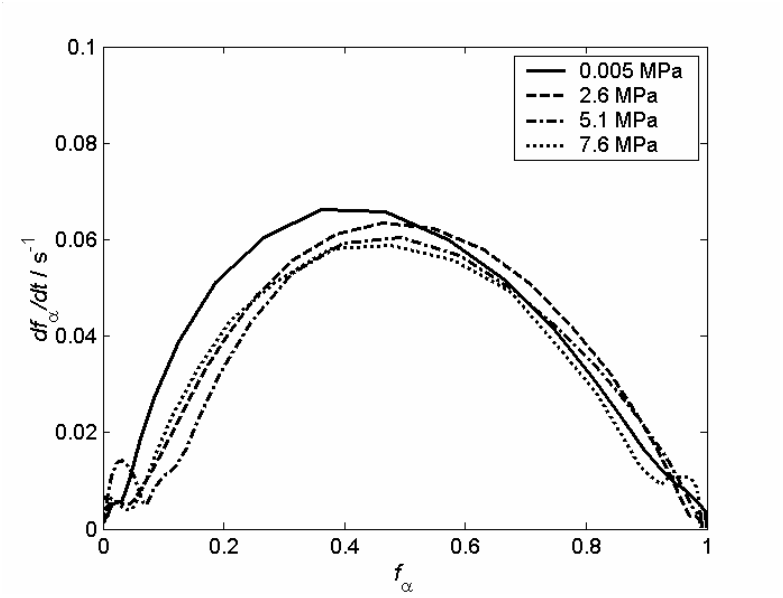

Fig. 4.15. The rate of transformation, df_α/dt, as a function of transformed fraction, f_α, of Fe-2.96at.%Ni at a cooling rate of 20 Kmin^{-1} under various indicated applied uniaxial compressive stresses.

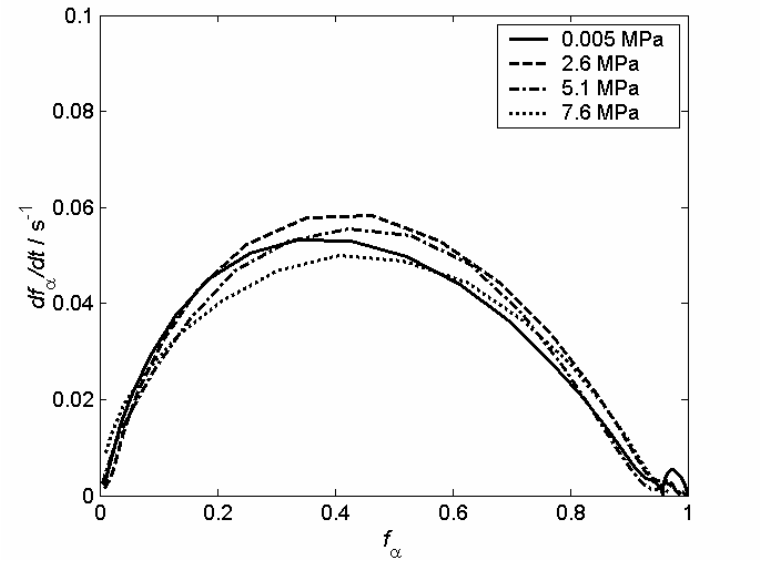

Fig. 4.16. The rate of transformation, df_α/dt, as a function of transformed fraction, f_α, of Fe-5.93at.%Ni at a cooling rate of 20 Kmin^{-1} under various indicated applied uniaxial compressive stresses.

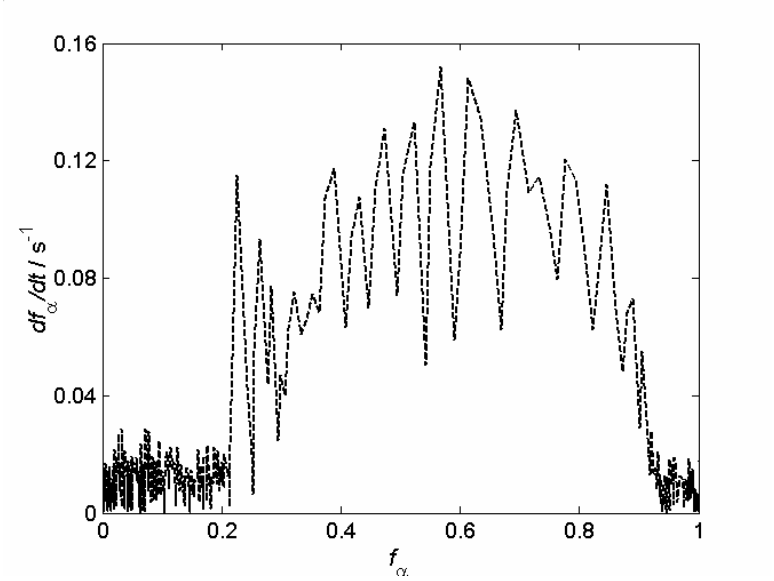

Fig. 4.17. The rate of transformation, df_α/dt, as a function of transformed fraction, f_α, as determined from the original measured length change (see section 4.4.6) for Fe-2.96at.%Ni at a cooling rate of 20 Kmin^{-1} under an applied uniaxial compressive stress of 7.6 MPa.

4.4.7. Interface velocity

From the experimentally determined parameters, (1) the transformed fraction, f_α, (2) the rate of transformation, df_α/dt, and (3) the average grain diameter after one complete heat treatment cycle, the γ/α interface velocity can be calculated according to Eq. (4.5). The obtained values for the interface velocity are shown in Figs. 4.18 and 4.19 for Fe-2.96at.%Ni and Fe-5.93at.%Ni, respectively (the interface velocity result for $f_\alpha < 0.1$ and $f_\alpha < 0.9$ are not reliable because in these boundary ranges of f_α the left hand and right hand sides of Eq. (4.5) both approach zero, independent of the values of interface velocity). The interface velocity averaged over the entire transformation for both Fe-2.96at.%Ni and Fe-5.93at.%Ni is about $1\pm0.5\times10^{-6}$ ms^{-1}. So, the obtained average interface velocity is of the same order of magnitude as obtained for pure Fe [18], Fe-2.26at.%Mn and Fe-1.79at%Co [19], which have been determined as $4\pm0.5\times10^{-6}$ ms^{-1}, $1.5\pm0.5\times10^{-6}$ ms^{-1} and $3\pm1\times10^{-6}$ ms^{-1}, respectively, in the absence of applied stress.

It can be concluded that the average interface velocity is almost constant during the transformation and does not change with applied compressive stress in the elastic

regime. Because the Fe-2.96at.%Ni and Fe-5.93at.%Ni alloys have average grain sizes of around 50 to 80 μm so called abnormal $\gamma \rightarrow \alpha$ transformation behaviour as observed for pure Fe [18] is not observed: only one maximum in df_α/dt as function of f_α was observed for (normal transformation) average grain size smaller than about 300 μm.

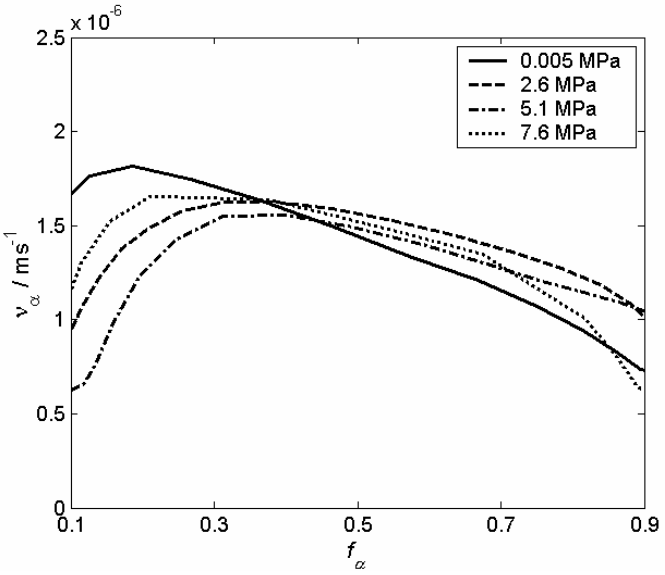

Fig. 4.18. The average γ/α interface velocity as determined for various indicated applied compressive stresses for Fe-2.96at.%Ni at a cooling rate of 20 Kmin^{-1}.

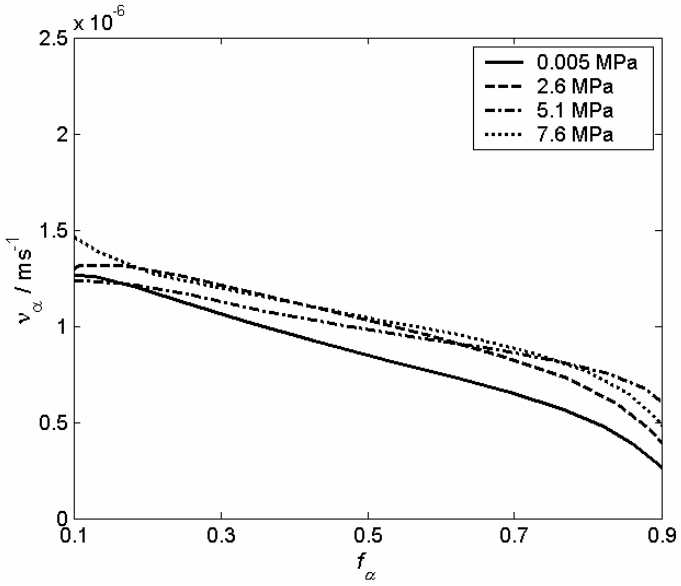

Fig. 4.19. The average γ/α interface velocity as determined for various indicated applied compressive stresses for Fe-5.93at.%Ni at a cooling rate of 20 Kmin^{-1}.

4.4.8. Driving force for $\gamma \rightarrow \alpha$ transformation

4.4.8.1. $\Delta G_{\alpha\gamma}^{chem}(T)$

The chemical Gibbs energy, $\Delta G_{\alpha\gamma}^{chem}$, driving the $\gamma \rightarrow \alpha$ transformation of Fe-2.96at.%Ni and Fe-5.93at.%Ni, was determined using the CALPHAD assessment of the Fe-Ni system [21]. The obtained $\Delta G_{\alpha\gamma}^{chem}$ for Fe-2.96at.%Ni and Fe-5.93at.%Ni is presented as a function of temperature in Fig. 4.20. The absolute value of $\Delta G_{\alpha\gamma}^{chem}$ increases with decreasing temperature.

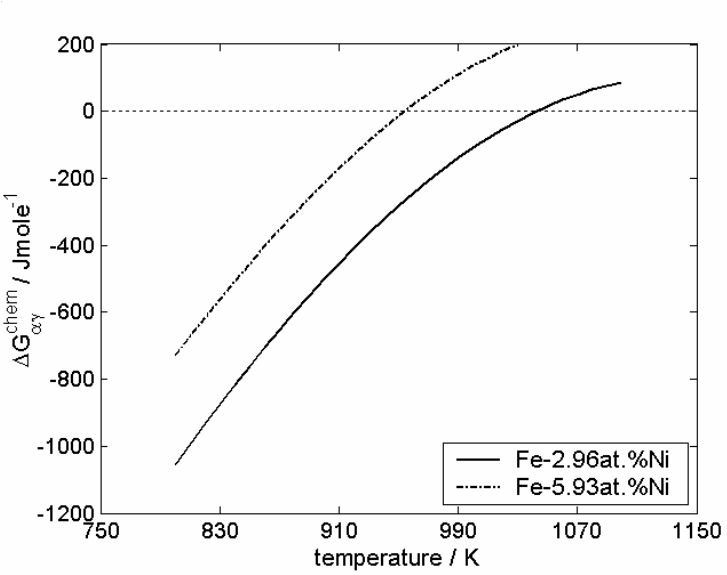

Fig. 4.20. The chemical Gibbs energy, $-\Delta G_{\alpha\gamma}^{chem}$, as a function of temperature for the $\gamma \rightarrow \alpha$ transformation for the alloys indicated.

4.4.8.2. $\Delta G_{\alpha\gamma}^{def}(f_\alpha) + \Delta G_{\alpha\gamma}^{int}(f_\alpha)$

The driving force ($\Delta G_{\alpha\gamma}$; cf. Eq. (4.2a)) can be determined from Eq. (4.2a) using the data of the interface-migration velocity (see Figs. 4.18 and 4.19) and the interface-mobility data of pure iron given in Section 4.2.1. The $\Delta G_{\alpha\gamma}^{def}(f_\alpha) + \Delta G_{\alpha\gamma}^{int}(f_\alpha)$ can be

determined using Eq. (4.3). Again (see discussion of Figs. 4.15 and 4.16) the results for f_α<0.1 and f_α>0.9 have not been considered due to mathematical instability of Eq. (4.5) upon approaching f_α=0 or f_α=1. Further, in an advanced stage of transformation the results for the interface velocity become rather sensitive to the type of impingement correction chosen. This leads to a (systematic) uncertainty in the results of $\Delta G_{\alpha\gamma}$ for large values of transformed fraction.

A comparison of values obtained as described above for the chemical Gibbs energy, $\Delta G_{\alpha\gamma}^{chem}$ (see section 4.4.8.1), the driving force, $\Delta G_{\alpha\gamma}$, (using Eq. (4.2a)) and the sum of crystalline misfit accommodation energy and interfacial energy, $\Delta G_{\alpha\gamma}^{def} + \Delta G_{\alpha\gamma}^{int}$, (using Eq. (4.3)) is provided by Figs. 4.22 and 4.23 for both alloys. The $-\Delta G_{\alpha\gamma}^{chem}$ for the $\gamma \rightarrow \alpha$ transformation is smaller for Fe-2.96at.%Ni than for Fe-5.93at.%Ni. The determined value of the driving force ($-\Delta G_{\alpha\gamma}$) is very small as compared to $-\Delta G_{\alpha\gamma}^{chem}$. The sum of deformation and interfacial energy ($\Delta G_{\alpha\gamma}^{def} + \Delta G_{\alpha\gamma}^{int}$,) is of the same order of magnitude as the negative of the chemical Gibbs energy, $-\Delta G_{\alpha\gamma}^{chem}$. The determined value of driving force, $-\Delta G_{\alpha\gamma}$, is almost constant for Fe–2.96at.%Ni alloy during the entire $\gamma \rightarrow \alpha$ transformation. However, the $-\Delta G_{\alpha\gamma}$ for Fe-5.93at.%Ni starts at a larger value than that of Fe–2.96at.%Ni and subsequently shows a gradually decreasing value as the transformation proceeds. This could be ascribed to the fact that although the time of transformation is same for both alloys (see, Tables 4.4 and 4.5) within the limit of accuracy, the transformation temperature for Fe-5.93at.%Ni alloy is around 90 K lower than that of Fe–2.96at.%Ni. Hence, the (temperature dependent) relaxation of misfit accommodation energy during $\gamma \rightarrow \alpha$ transformation is smaller for Fe-5.93at.%Ni than that of Fe–2.96at.%Ni. This results in an ever decreasing driving force, ($-\Delta G_{\alpha\gamma}$) (see, Eq. (4.3)), for the $\gamma \rightarrow \alpha$ transformation in Fe-5.93at.%Ni alloy with respect to Fe–2.96at.%Ni alloy.

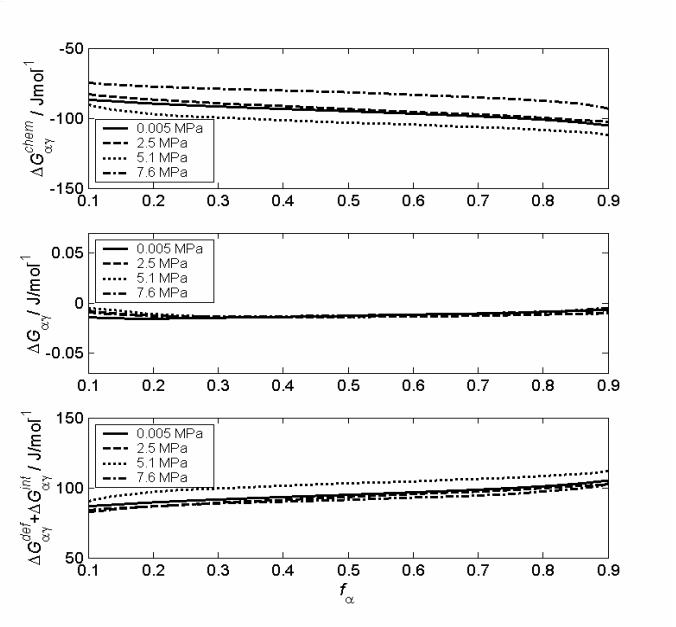

Fig. 4.21. The chemical Gibbs energy, $-\Delta G^{chem}_{\alpha\gamma}$,(a), $\Delta G_{\alpha\gamma}$, (b) and the sum of misfit-accommodation energy and interface energy, $\Delta G^{def}_{\alpha\gamma} + \Delta G^{int}_{\alpha\gamma}$, (c) as a function of transformed fraction, f_α, for the $\gamma \rightarrow \alpha$ transformation of Fe-2.96at.%Ni for various applied tensile stresses as indicated.

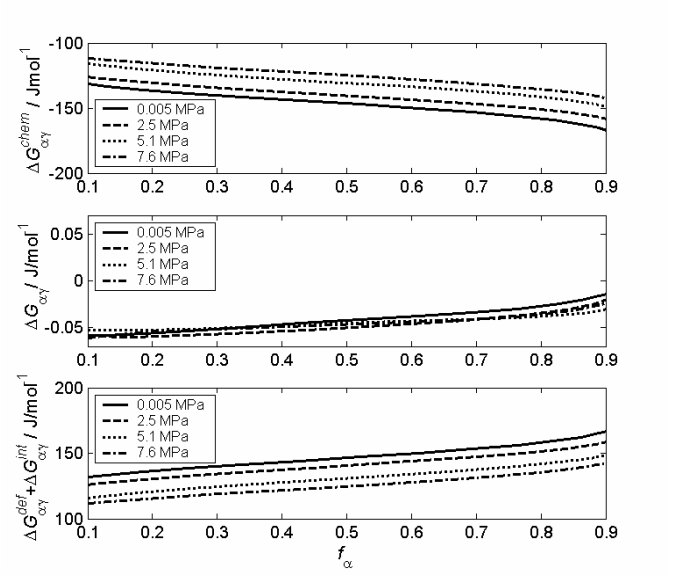

Fig. 4.22. The chemical Gibbs energy, $-\Delta G^{chem}_{\alpha\gamma}$, (a), $\Delta G_{\alpha\gamma}$, (b) and the sum of misfit-accommodation energy and interface energy, $\Delta G^{def}_{\alpha\gamma} + \Delta G^{int}_{\alpha\gamma}$, (c) as a function of transformed fraction, f_α, for the $\gamma \rightarrow \alpha$ transformation of Fe-5.93at.%Ni for various applied tensile stresses as indicated.

4.5. Conclusions

1. The imposition of uniaxial applied *compressive* stress within the elastic regime slightly increases the start temperature of the $\gamma \rightarrow \alpha$ transformation for Fe-2.96at.%Ni and 5.93at.%Ni alloys.
2. Increase in applied compressive stress results in increase of ferrite grain size after the $\gamma \rightarrow \alpha$ transformation: the number of nuclei is reduced upon applying a compressive stress.
3. The total length change pertaining to the $\gamma \rightarrow \alpha$ transformation for Fe-2.96at.%Ni and Fe-5.93at.%Ni decreases slightly with increasing applied compressive stress. Lack of evidence of local plastic deformation induced by transformation plasticity and proven constancy of volume after complete heat treatment cycle suggest that the volume change due to transformation preferentially occurs in the radial direction of the specimen.
4. An applied compressive stress within the elastic regime during $\gamma \rightarrow \alpha$ transformation of Fe-2.96at.%Ni and Fe-5.93at.%Ni alloys has little influence on the rate of transformation. The obtained average interface velocity is about $1 \pm 0.5 \times 10^{-6}$ ms^{-1} which is of the same order of magnitude as obtained for pure Fe [18], Fe-2.26at.%Mn and Fe-1.79at%Co [19].
5. The determined net driving force ($-\Delta G_{\alpha\gamma}$) is almost constant for both alloys during the entire transformation range.

References

[1] G. E. Dieter, Mechanical Metallurgy, SI Metric Edition, McGraw-Hill Book Company, London, 1988.

[2] W. D. Swanson, J. Gordon Parr: J. Iron Steel Inst. 1964; 202: 687.

[3] T. B. Massalski, J. H. Perepezko, J. Jaklovsky, Mat Sci Engg. 1975; 18: 193.

[4] M. Hillert Met. Trans. A 1975; 6A: 5.

[5] A. Borgenstam, M. Hillert, Acta Mater. 2000 ; 48: 2765

[6] A. D. Romig, J. I. Goldstein, Metall. Trans., 1980; 11: 1151.

[7] F. W Jones, W.I Pumphrey J. Iron steel Inst. 1949; 163: 121.

[8] A. T. W. Kempen, F. Sommer, E. J. Mittemeijer, Acta Mater 2002; 50: 3545.

[9] E. J. Mittemeijer, F. Sommer, Z Metallkd 2002; 93: 352

[10] J. W. Christian, The Theory of Transformation in Metals and Alloys, Part 1, Equilibrium and General Kinetic Theory, Pergamon Press, Oxford, 1981.

[11] Y. C. Liu, F. Sommer, E. J. Mittemeijer, Thermochimica Acta 2004; 413: 215

[12] S. V. Zemskiy, V. S. L'vov, L. S. Makashova, Phys. Met. Metallogr. 1976, 41 (4), 85.

[13] G. Mohapatra, F. Sommer, E. J. Mittemeijer, submitted for publication (chapter 1).

[14] ASTME112, Annual Book of ASTM Standard 1988; 03.01: 297.

[15] T. A. Kop, J. Sietsma, S. Ven der Zwaag, J. Mat. Sci. 2001; 36: 519.

[16] G. Mohapatra, F. Sommer, E. J. Mittemeijer, submitted for publication (chapter 2).

[17] Y. C. Liu, F. Sommer, E. J. Mittemeijer, Acta. Mater 2003; 51: 507.

[18] Y. C. Liu, F. Sommer, E. J. Mittemeijer, Philosophical Magazine 2004; 84: 1853.

[19] Y. C. Liu, F. Sommer, E. J. Mittemeijer, Acta. Mater 2004; 52: 2549.

[20] M. Onink, F. D. Tichelaar, C. M. Brakman, E. J. Mittemeijer, S. Ven der Zwaag, J Mater Sci 1995; 30: 209.

[21] S. X. Zhong, D. D. Gohil, A. T. Dinsdale, T. G. Chart, Natn. Phys. Lab., DMA(a) 103, London, 1985.

5. The austenite to ferrite transformation of Fe-Ni under the influence of a uniaxially applied tensile stress

G. Mohapatra, F. Sommer, E.J. Mittemeijer

Abstract

Differential dilatometry has been employed to study the austenite (γ)-ferrite (α) massive phase transformation of Fe-3.1at.%Ni upon cooling under the influence of an applied, constant uniaxial tensile stress. The applied stress level was chosen below the yield stress of the alloy. It was found that an extra length change of the specimens occurs during the transformation as a result of transformation induced plasticity. The local plastic deformation induced by transformation plasticity results in anisotropic volume change of the specimen in longitudinal direction. A phase transformation model, involving site saturation, interface-controlled continuous growth and an appropriate impingement correction, has been employed to extract the interface velocity of the γ/α interface. The observed scatter in the interface velocity decreases with increasing applied stress due to relaxation of misfit deformation energy by transformation induced inhomogeneous plastic deformation. The interface velocity remains almost constant during the whole transformation.

5.1. Introduction

The austenite (γ) to ferrite (α) phase transformation in iron-based alloys (steels) is of great importance from both a fundamental and a technological point of view [1]. Understanding of the $\gamma \rightarrow \alpha$ transformation behaviour is essential to control the final microstructure of the α phase. The microstructure of a material is decisive for its mechanical properties. Research has been carried out on the influence of uniaxial stress on (the kinetics of) the austenite to pearlite transformation [e.g. 2], the austenite to bainite transformation [e.g. 3] and the austenite to martensite transformation [e.g. 4]. However, according to the present authors' knowledge, no publication exists on the influence of applied uniaxial tensile stress, in the elastic range, on the massive austenite to ferrite transformation.

This paper reports on the quantitative influence of an applied uniaxial tensile stress, below the yield stress of the alloy, on the start temperature, length (and volume) change evolution, interface velocity and driving force of the austenite to ferrite, massive transformation in Fe-3.1at.%Ni alloy.

5.2. Phase transformation kinetics

The Fe-Ni partial equilibrium phase diagram relevant to the present study is shown in Fig. 5.1 [5]. This phase diagram was determined employing very long annealing times (days) in order to assure that equilibrium was reached [e.g. 6]. The investigated Fe-3.1at.%Ni alloy reaches the single phase region upon cooling (at 20 $Kmin^{-1}$) at about 960 K (see the dashed line in Fig. 5.1). The T_0 curve, indicating the temperature where the Gibbs energies of the product (α) and parent (γ) phases of the same composition are equal, has been shown as function of Ni content in Fig. 5.1 as well.

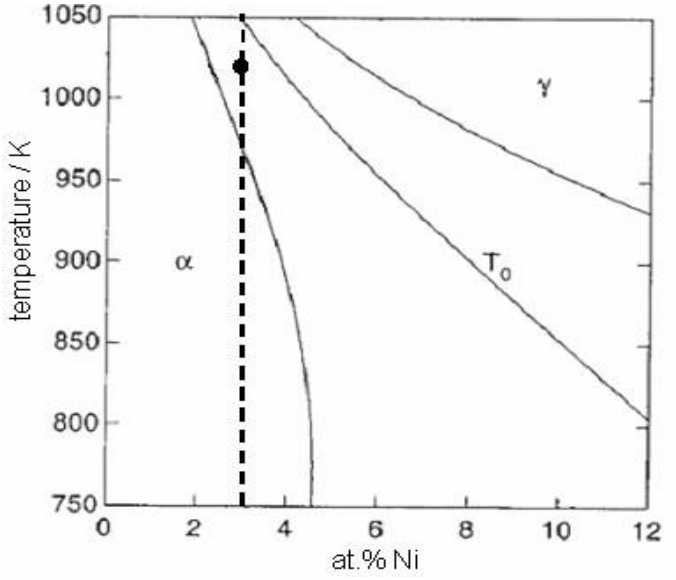

Fig. 5.1. Partial equilibrium phase diagram for Fe-Ni showing the T_0 line (temperature corresponding to equal Gibbs energies of the metastable product and parent phases). The dashed line represents the alloy composition of Fe-3.1at.%Ni. The measured start temperature of transformation of $\gamma \rightarrow \alpha$ transformation under an applied stress of 0.005 MPa is given by the circular point.

5.2.1. Transformation model

A general procedure for the simulation of phase transformation kinetics on the basis of nucleation, growth and impingement mechanisms has been given in Refs. [7, 8]. The first step of this procedure involves the calculation of the volume of all growing particles, assuming that the grains never stop growing and that new grains hypothetically nucleate also in the transformed material (i.e. at this stage, 'hard impingement' is ignored). This volume is called the extended volume (V_e), and the extended volume divided by the total specimen volume (V_0) is called the extended transformed fraction x_e. V_e is given by

$$V_e = g\left(\int v(T,f)\,dt\right)^3 \tag{5.1}$$

where g is a geometrical factor (which is 1 for cubical growth and $4\pi/3$ for spherical growth), v is the interface velocity which depends on the temperature, T, and the transformed fraction, f, which has to be integrated over time, t. The interface velocity is

considered to be proportional with the product of the interface mobility (M) and the driving force ($-\Delta G_{\alpha\gamma}$) [9]:

$$v_\alpha = M(T)\left[-\Delta G_{\alpha\gamma}(T, f_\alpha)\right] \tag{5.2a}$$

The interface mobility exhibits an Arrhenious- like temperature dependence

$$M(T) = M_0 exp(-Q/RT) \tag{5.2b}$$

where M_0 is the pre-exponential factor, Q is the activation energy.

Data for the interface mobility are experimentally hardly available. With known driving forces, the interface mobility can be calculated from the observed interface migration velocity. In this work experimental mobility data on the recrystallization of pure iron ferrite have been used as reported in Ref. [10] with M_0=4.9×10^3 ms^{-1}molJ^{-1}, and Q=1.47×10^5 Jmol^{-1} [10]. The driving force ($-\Delta G_{\alpha\gamma}$) in Eq. (5.2a) is given by

$$\Delta G_{\alpha\gamma}(T, f_\alpha) = \Delta G_{\alpha\gamma}^{chem}(T) + \left[\Delta G_{\alpha\gamma}^{def}(f_\alpha) + \Delta G_{\alpha\gamma}^{int}(f_\alpha)\right] \tag{5.3}$$

where $\Delta G_{\alpha\gamma}^{chem}$ is the molar chemical Gibbs energy difference between ferrite and austenite which depends on temperature, T. $\Delta G_{\alpha\gamma}^{int}$ is the molar Gibbs energy of the γ/α interface, and $\Delta G_{\alpha\gamma}^{def}$ is the summation of elastic and plastic molar accommodation energies resulting from the misfit between the ferrite and austenite phases. The driving force, $-\Delta G_{\alpha\gamma}$, consists of a negative term, $\Delta G_{\alpha\gamma}^{chem}$, which favours the transformation, and two positive terms ($\Delta G_{\alpha\gamma}^{def}$ and $\Delta G_{\alpha\gamma}^{int}$) which obstruct the transformation. The chemical driving force depends on temperature, and not on the fraction transformed, because the transformation is partitionless. Both $\Delta G_{\alpha\gamma}^{int}$ and $\Delta G_{\alpha\gamma}^{def}$ depend primarily on the fraction transformed, f_α (and not directly on temperature).

In a next step, the extended transformed fraction is corrected for 'hard impingement' of the growing particles. The impingement correction adopted here corresponds to an intermediate case of ideally periodically and ideally randomly dispersed growing particles [11]:

$$f = tanh(x_e) \tag{5.4}$$

with $x_e = V_e/V_0$ as the extended fraction. Thus, the kinetic model is characterised by the specific models adopted for (1) the nucleation process, (2) the growth process, and (3) the (hard) impingement. With a low cooling rate of 20 Kmin^{-1} all nuclei can be supposed to be present at the very start of growth i.e. 'site saturation' at t=0 can be adopted. Further, since the transformation is partitionless, interface-controlled growth can be adopted. The interface velocity then can be derived from the rate of transformation, df_α/dt, the transformed fraction, f_α, and the grain size ($2\overline{r}_\alpha$) of the fully transformed ferrite phase:

$$df_\alpha/dt = 3(1 - f_\alpha^2)\operatorname{arctanh}^{\frac{2}{3}}(f_\alpha)\overline{r}_\alpha^{-1}v_\alpha(T,f) \tag{5.5}$$

5.3. Experimental details

5.3.1. Specimen preparation

Bulk high purity Fe (99.98 wt. %) and Ni (99.99 wt. %) were used for the preparation of alloys. The purity of both Fe and Ni has been indicated by the composition data (determined by Inductive Coupled Plasma-Optical Emission Spectrometry (ICP-OES)) in Table 5.1. Melting of appropriate amounts of Fe and Ni was carried out in a vacuum-melting furnace, and the molten alloy was cast in a copper mould. The as-cast ingots of 100 mm length and 10 mm diameter were hammered down to rods of 9.5 mm diameter. In order to achieve a homogeneous microstructure, the rods/castings were sealed in a quartz container filled with argon gas at 2×10^4 Pa. The specimens were heated from room temperature to 1423 K at 5 Kmin^{-1} followed by annealing at 1423 K for 100 h and subsequently furnace cooled to room temperature. The composition of the Fe-Ni rods was found to be Fe-3.1at.%Ni (determined by Inductive Coupled Plasma-Optical Emission spectrometry (ICP-OES)). Finally, the rods were machined to dilatometry specimens with an inner dimension of 10 mm in length and 5mm in diameter (see also Fig. 5.2).

Table 5.1 Chemical composition of the iron and nickel used. Unit: ppm in mass

element	Fe	Ni
C	8	16
Si	10	0.23
Cu	1	0.17
Ti	0.6	1.3

5.3.2. Dilatometric measurements and temperature program

A dilatometer DIL-805 A/D (Baehr-Thermoanalysis GmbH) (see Fig. 5.2), employing inductive heating/cooling was used to measure the thermal dilation of the alloys as a function of temperature/time during the heat treatment cycles. For all the specimens undergoing heat treatment cycles two thermocouples were spot welded on the specimen surface as shown in Fig. 5.2 to measure the temperature difference between the centre and the end of the specimen along the longitudinal direction. The experiments were performed under vacuum (6×10^{-6} mbar) to avoid oxidation of the specimen. The applied heat treatment cycle in the dilatometer experiments was as follows: the as received machined specimens of Fe-3.1at.%Ni (exhibiting average grain diameter of 98.7±4 μm) were heated from room temperature up to 1273 K at a rate of 20 $Kmin^{-1}$ and kept at this temperature for thirty minutes [12]. Then all the specimens were cooled down to room temperature at 20 $Kmin^{-1}$ and simultaneously subjected to various uniaxial constant tensile stresses of 0.005, 5.1 and 12.7 MPa during the $\gamma \rightarrow \alpha$ transformation.

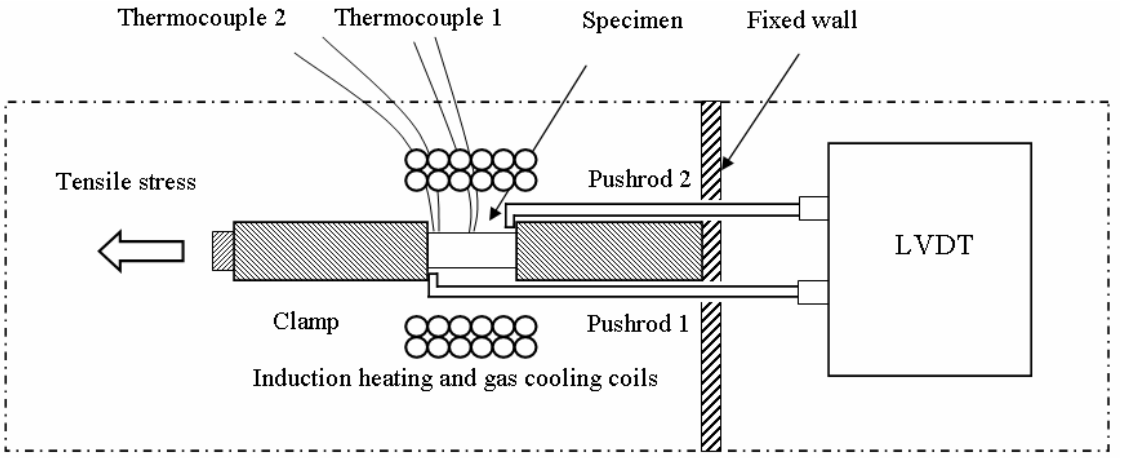

Fig. 5.2. Schematic (top view cross sectional) diagram showing the arrangement for the dilatometer DIL-805 A/D in tensile mode. The length change is measured by a linear variable differential transformer (LVDT).

5.3.3. Yield stress measurement for austenite and ferrite phases

The yield stress of the austenite phase of Fe-3.1at.%Ni was taken from Ref. [13] as determined under compressive stress at a temperature of 1073 K. The yield stress at 1000 K of the ferrite phase of Fe-3.1at.%Ni was measured in this study using the procedure given in Ref. [13]. The yield stress for the austenite phase at 1073 K is about 23 MPa (see point A in Fig. 5.3) and the yield stress of the ferrite phase at 1000K is about 18 MPa (see point B in Fig. 5.3). All phase transformation experiments were performed at an applied tensile stress which was maximally 12.7 MPa, which is well below the elastic limit of both phases of the alloy.

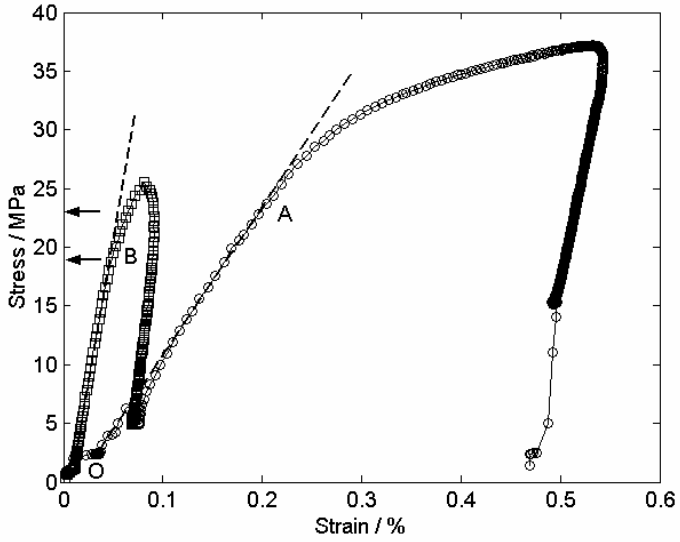

Fig. 5.3. The compressive stress-strain curves of the austenite phase (γ) (circular data points) and the ferrite phase (α) (square data points) at 1073 K and at 1000 K, respectively, for Fe-3.1at.%Ni. Points A and B indicate the corresponding transitions from elastic to plastic behaviour.

5.3.4. Temperature calibration

The temperature calibration during heating and cooling was done on the basis of the Curie temperature, T_C, (ferro- to paramagnetic transition) [14]. For Fe-3.1at.% Ni alloys a self calibration was used from the observed Curie temperature during heating. The T_C could not be observed upon cooling because the T_C of Fe-3.1at.% Ni is larger than the start temperature of the $\gamma \rightarrow \alpha$ transformation. The T_C during cooling was taken equal to the T_C value upon heating corrected for the measured hysteresis of the Curie temperature of 1 K as observed for heating and cooling of pure Fe [14].

5.3.5. Length change calibration

The length change calibration was done for the pure α and γ phases as well as during $\alpha \rightarrow \gamma$ and $\gamma \rightarrow \alpha$ transformations. For the pure α and γ phases the calibration was performed according to the procedure developed in Ref. [14]. The length change calibration during $\gamma \rightarrow \alpha$ transformation was done as follows: first the transformed fraction f_α was determined from the measured length change adopting the lever rule [15].

Secondly, taking into account the f_α and extrapolated calibration length changes for the pure α and γ phases in the $\gamma \rightarrow \alpha$ transformation range, the length change calibration during $\gamma \rightarrow \alpha$ transformation is given by:

$$\left(\Delta L\right)_{cal,\ \gamma\rightarrow\alpha} = f_\alpha \left(\Delta L\right)_{cal,\ \alpha} + \left(1 - f_\alpha\right)\left(\Delta L\right)_{cal,\ \gamma} \tag{5.6}$$

where $\left(\Delta L\right)_{cal,\ \alpha}$ and $\left(\Delta L\right)_{cal,\ \gamma}$ are the calibrated length changes for the pure α and γ phases, respectively (see Fig. 5.6). A similar expression can also be given for length change calibration during $\alpha \rightarrow \gamma$ transformation.

5.3.6. Grain size determination

The fully transformed ($\gamma \rightarrow \alpha$) dilatometric specimens were sectioned at room temperature along the longitudinal direction. The grain boundaries were exposed by etching with a 2.5 vol.% Nital solution and subsequently analyzed by light optical microscopy. The line intercept method [16] was employed in three different directions in order to determine the grain size. The line-intercept method results in a grain size value which underestimates the true grain size. The true average of all grain diameters of the ferrite, $2\overline{r}_\alpha$, was thus assessed by multiplying the obtained intercept length by a factor of 1.5 [16]. The grain-size distribution was obtained by dividing the number of grains in a certain range of the true average grain diameter by the total number of measured grains.

5.4. Results and discussion

5.4.1. Length change due to $\gamma \rightarrow \alpha$ transformation

In all the experiments performed the temperature gradient, i.e. T_{centre}-T_{end} (see Fig. 5.2), was only about 1.0 K just before the start of $\gamma \rightarrow \alpha$ transformation. Hence, the length change correction due to a temperature gradient in the specimen as developed in Ref. [17] was not necessary. The small value of the temperature gradient in the specimens is due to the geometry: the heated clamps on both sides of the specimen (see Fig. 5.2) prevent heat loss from the specimen (for the experiments performed in Ref. [13] in

compressive mode the heat loss from the specimen was larger because of no such heated clamps were applied). With such a small temperature gradient of about 1 K the calibrated temperature T_{centre} (see section 5.3.4) can be and was taken as the specimen temperature.

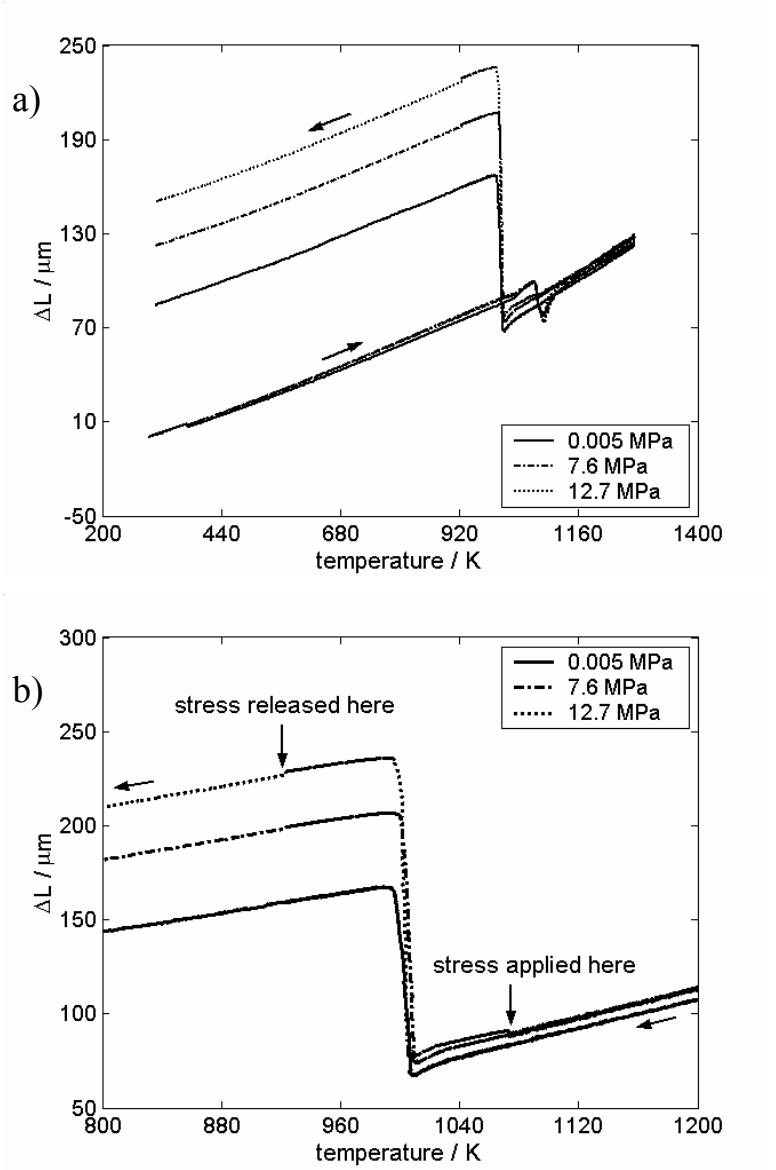

Fig. 5.4. (a) The calibrated length change as a function of temperature with a heating and cooling rate of 20 $Kmin^{-1}$ for Fe-3.1at.%Ni subjected to various applied tensile stresses as indicated (starting with fresh specimens with the same initial average grain size). The up-arrow and down-arrow indicate the heating and cooling cycle, respectively. (b) Enlargement around the $\gamma \rightarrow \alpha$ transformation indicating the temperatures at which the stress was applied and where it was released.

The length change during heating and cooling of a fresh Fe-3.1at.%Ni specimen, after incorporating the temperature and length change calibrations (see sections 5.3.4 and 3.5), is shown in Fig. 5.4(a). The up-and down arrows indicate the heating and cooling parts of the heat treatment cycle, respectively. Enlarged portions of the measured length change of the $\gamma \rightarrow \alpha$ transformation are shown in Fig. 5.4(b) for all applied stress values. The small increase in length (see vertical arrow) before the start of transformation corresponds to the application of stress and the small decrease in length (see vertical arrow) after the completion of transformation corresponds to the release of stress.

The measured length change, ΔL, as function of temperature, T_{centre}, as well as function of time around the $\gamma \rightarrow \alpha$ transformation is shown in Fig. 5.5. Evidently, ΔL as a function of time is smooth, whereas ΔL as a function of temperature exhibits some scatter, which is due to a scatter in the measured T_{centre}.

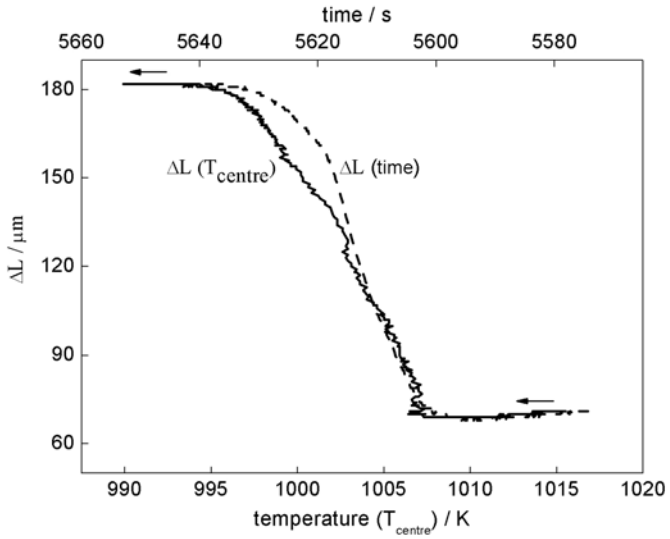

Fig. 5.5. The measured length change, ΔL, as a function of temperature (T_{centre}) (solid line) and time (dashed line) upon $\gamma \rightarrow \alpha$ transformation at a cooling rate of 20 $Kmin^{-1}$ of Fe-3.1at.%Ni under an applied stress of 0.005 MPa. The arrows indicate the direction of progress of transformation.

The total length change measured at a temperature corresponding to 50% transformed fraction (see EF Fig. 5.6) of the $\gamma \rightarrow \alpha$ transformation for repeated sets of experiments is shown in Fig. 5.7 as a function of applied tensile stress for Fe-3.1at.%Ni.

The measured total length change increases from about 90 μm to about 150 μm with increase in applied tensile stress from 0.005 MPa to 12.7 MPa.

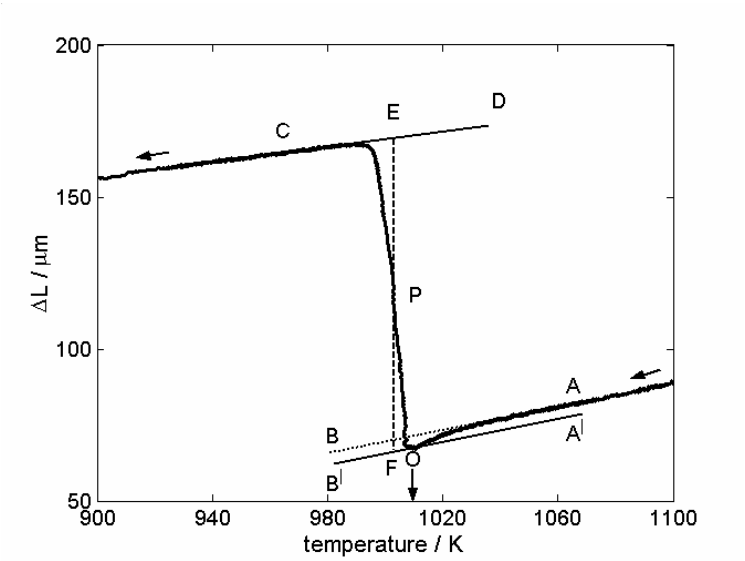

Fig. 5.6. The calibrated length change as a function of temperature upon $\gamma \rightarrow \alpha$ transformation at a cooling rate of 20 $Kmin^{-1}$ of Fe-3.1at.%Ni under 0.005 MPa applied stress. AB and CD are the extrapolated linear thermal dilations of the pure γ phase and the pure α phase, respectively. AB has been shifted vertically to $A'B'$ so that $A'B'$ passes through O the minimum in the length change measurement. The temperature corresponding to O, shown by arrow, is the start temperature of transformation. EF, corresponding to the 50% length change at P, is the total length change during transformation (at the temperature corresponding to EF).

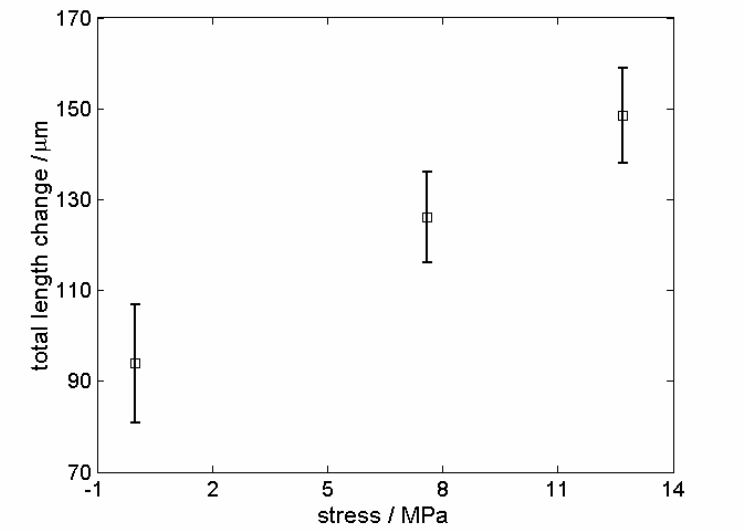

Fig. 5.7. The total length change pertaining to the $\gamma \rightarrow \alpha$ transformation as a function of applied tensile stress for Fe-3.1at.%Ni for repeated set of experiments performed at a cooling rate of 20 $Kmin^{-1}$.

The SEM micrograph taken from the surface of the dilatometric specimen after completed $\gamma \rightarrow \alpha$ transformation, upon cooling under an applied stress of 7.6 MPa, is presented in Fig. 5.8. The micrograph shows inhomogeneous appearance of slip bands (not observed in all grains) as indicated by the arrows. For an applied stress of 0.005 MPa no slip bands were observed.

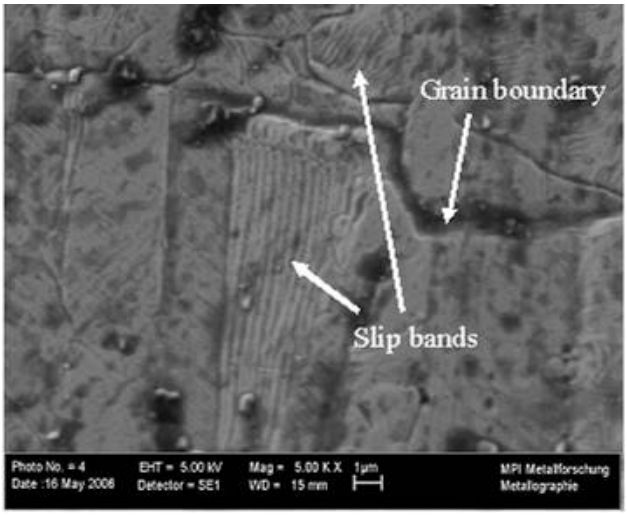

Fig. 5.8. SEM micrograph showing inhomogeneous occurrence of slip bands in the ferrite phase, as observed for Fe-3.1at.%Ni at room temperature, after $\gamma \rightarrow \alpha$ transformation under an applied stress of 7.6 MPa at a cooling rate of 20 $Kmin^{-1}$.

Further evidence of local plastic deformation upon $\gamma \rightarrow \alpha$ transformation at 7.6 MPa was obtained by application of a scanning electron microscope (LEO 438VP) equipped with a device for electron back-scatter diffraction and software for the analysis of Kikuchi Patterns (EBSD) (TLS, OIM 2.6 for data acquisition and evaluation). The thus obtained orientation image maps for two specimens subjected to 0.005 MPa and 7.6 MPa applied stress during transformation, are shown in Figs. 5.9(a) and 5.9(b). It follows that the specimen transformed at 0.005 MPa shows a small number of subgrains (see the red and blue lines), whereas the specimen transformed at 7.6 MPa shows a significantly larger number of subgrains (see the red and blue lines). The occurrence of a large number of

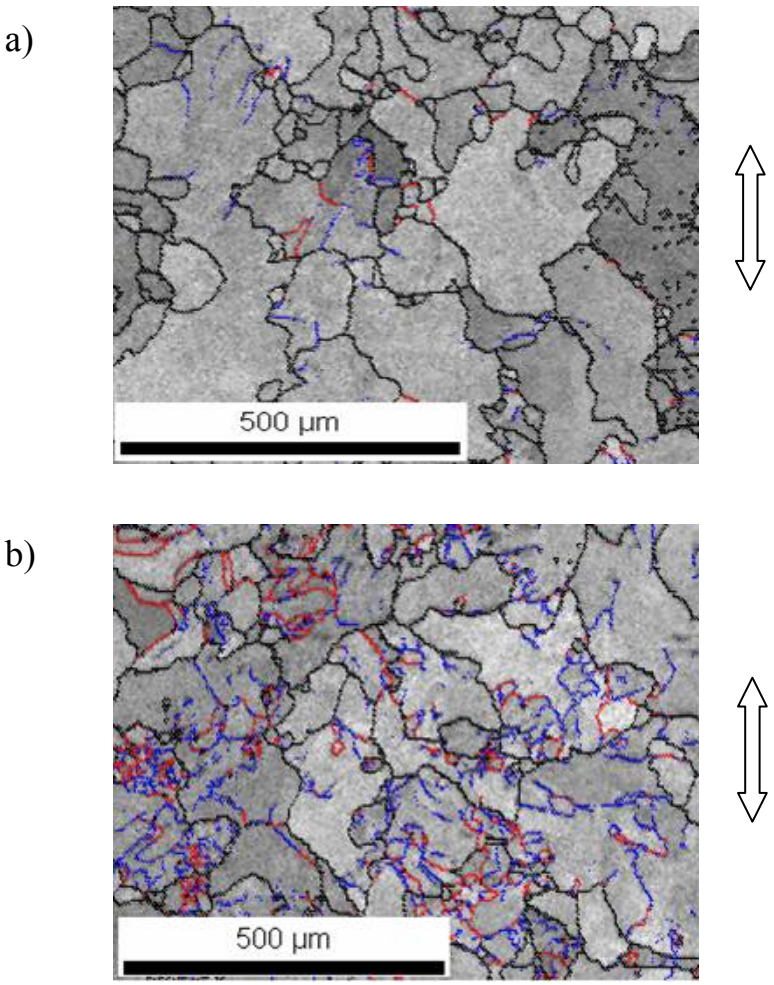

Fig. 5.9. Orientation image maps (obtained from EBSD measurements) of the Fe-3.1at.%Ni after $\gamma \rightarrow \alpha$ transformation showing high angle grain boundaries (black: boundary rotation angle (BRA) > 15^0) and low angle grain boundaries (red: 5^0<BRA>15^0 ; blue: BRA<5^0) for the Fe-3.1at.%Ni alloy with applied stress of (a) 0.005 MPa and of (b) 7.6 MPa stress, respectively. The arrows indicate the direction of the applied stress.

subgrains upon transformation at 7.6 MPa can be understood as follows: with the larger applied stress (7.6 MPa) the specimen experiences local, inhomogeneous plastic deformation (see Fig. 5.8) because the sum of the internal (misfit) stress generated by the transformation and the externally applied tensile stress exceeds locally the yield stress of the α phase (α is a softer phase than γ; see Fig. 5.3). Since the transformation temperature is high (around 1000 K) stored strain energy due to plastic deformation can be (partly) released by regrouping (edge) dislocations into dislocation walls low-angle boundaries; *polygonization* [18]. It is concluded that the observed significant increase in $\gamma \rightarrow \alpha$ transformation length change for the applied tensile stresses of 7.6 MPa and 12.7 MPa (see Figs. 5.4 and 5.7) can be ascribed to transformation induced plasticity [e.g. 19-22]. This can be quantitatively verified as follows. The transformation plasticity depends on the change in specific volume ($\Delta V/V$) upon transformation, the yield stress (E) of the 'weaker phase', the applied stress (σ) and the transformed fraction (f_α) [22]. The strain due to transformation plasticity is given by

$$\varepsilon^{pt} = \frac{3}{4}\frac{\sigma}{E}\frac{\Delta V}{V}\left(f_\alpha - \frac{2}{3}f_\alpha^{3/2}\right) \qquad (5.7)$$

The plastic strain (ε^{pt}) contribution to the length change was calculated using Eq. (5.7). The measured length change after subtraction of the contribution of transformation plasticity according to Eq. (5.7) is shown in Fig. 5.10 for experiments with various applied stresses. It follows that the length change due to only the phase transformation is about the same, irrespective of the applied stress. Thereby the above assertion that the increase in length change during transformation with an increasing applied tensile stress is due to the transformation induced plasticity, has been validated.

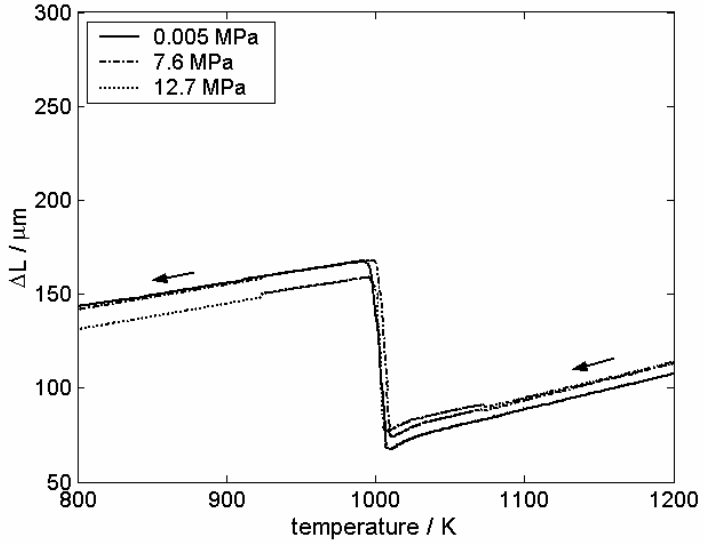

Fig. 5.10. The calibrated length change as a function of temperature upon $\gamma \rightarrow \alpha$ transformation, after removing the length change due to transformation plasticity (from the length change as shown in Fig. 5.4). Results pertaining to Fe-3.1at.%Ni upon cooling at 20 $Kmin^{-1}$ for the applied stresses indicated.

The diameter of the specimens was measured before and after one complete heat treatment cycle for the various applied stresses. The results shown in Fig. 5.11 indicate a decrease of the diameter of the specimen that increases with increasing applied stress. The volume of the specimen measured before and after one complete heat treatment cycle, involving a $\alpha \rightarrow \gamma$ and a $\gamma \rightarrow \alpha$ transformation, was found to be constant, irrespective of value of applied tensile stress.

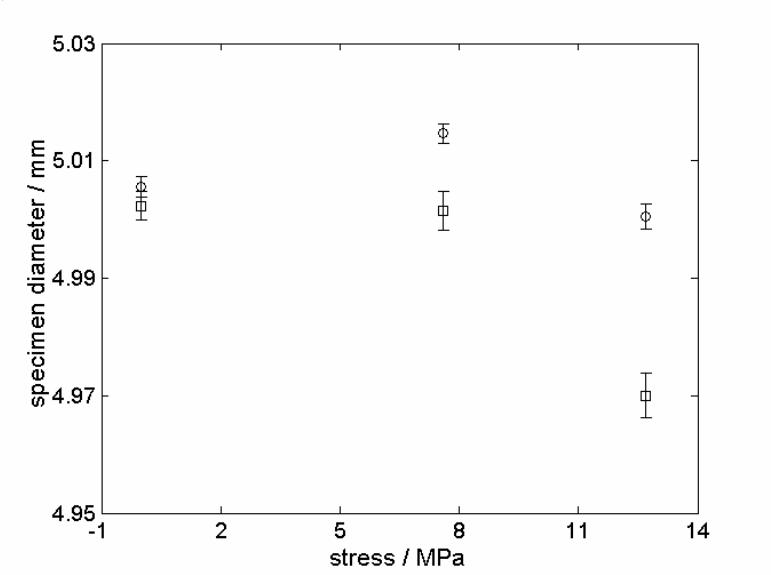

Fig. 5.11. The measured diameter of the specimen at the beginning of heat treatment cycle (circular data points) and after one complete heat treatment cycle (square data points), as a function of applied tensile stress (starting with fresh specimens with the same initial average grain size) for two sets of experiments of Fe-3.1at.%Ni cooled at 20 $Kmin^{-1}$.

5.4.2. Temperature range of $\gamma \rightarrow \alpha$ transformation

The procedure to determine the start temperature of the $\gamma \rightarrow \alpha$ transformation in tensile mode is as follows (see Fig. 5.6): The tangent AB to the linear thermal dilation of pure austenite phase upon cooling is drawn. AB is shifted vertically to $A'B'$ so that $A'B'$ passes through 'O', the minimum observed in the length change measurement (the occurrence such a minimum in length change, at the onset of the $\gamma \rightarrow \alpha$ transformation during tensile loading has been discussed in Ref. [14]). The temperature corresponding to 'O' (arrow in Fig. 5.6) is taken as the start temperature of the transformation.

The values for the thus determined start temperature of transformation, the average temperature during transformation and the average time of transformation for Fe-3.1at.%Ni have been gathered in Table 5.2 for repeated sets of experiments. The start temperature of the $\gamma \rightarrow \alpha$ transformation decreases with increasing applied tensile stress. The effect of applied stress (tensile (this work) and compressive [13]) on the start temperature of the $\gamma \rightarrow \alpha$ transformation of Fe-3.1at.%Ni is shown in Fig. 5.12.

Table 5.2 The start temperature and the time of $\gamma \rightarrow \alpha$ transformation of Fe-3.1at.%Ni at a cooling rate of 20 $Kmin^{-1}$ under different applied uniaxial *tensile* stresses.

stress, MPa	start temperature, K	average start temperature, K	average time of transformation, s
0.005	1012.0 1015.0 1011.0 1010.0	1012.0±2.1	49±15
7.6	1006.0 1012.5 1014.5 1009.0	1010.5±3.7	47±9
12.7	1008.0 1004.5 1000.5	1004.3±3.7	50±10

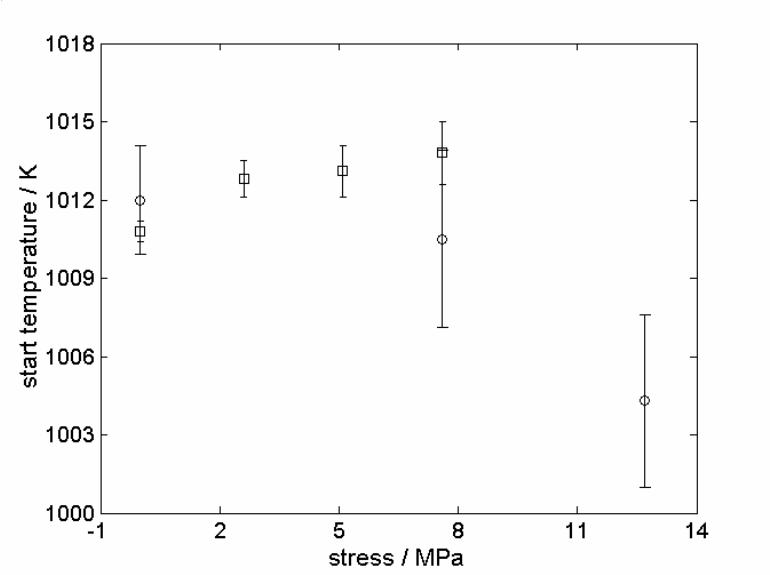

Fig. 5.12. The influence of tensile (circular data points for Fe-3.1at%Ni) and compressive (square data points for Fe-2.96at%Ni) stress [14] on the start temperature of the $\gamma \rightarrow \alpha$ transformation.

5.4.3. Grain size and grain-size distribution

The ferrite grain size of the dilatometer specimens transformed under different applied tensile stresses was determined according to the procedure described in section 5.3.6. All specimens show a typical lognormal grain-size distribution. As an example the ferrite grain-size distribution of the specimen subjected to an applied stress of 7.6 MPa is shown in Fig. 5.13.

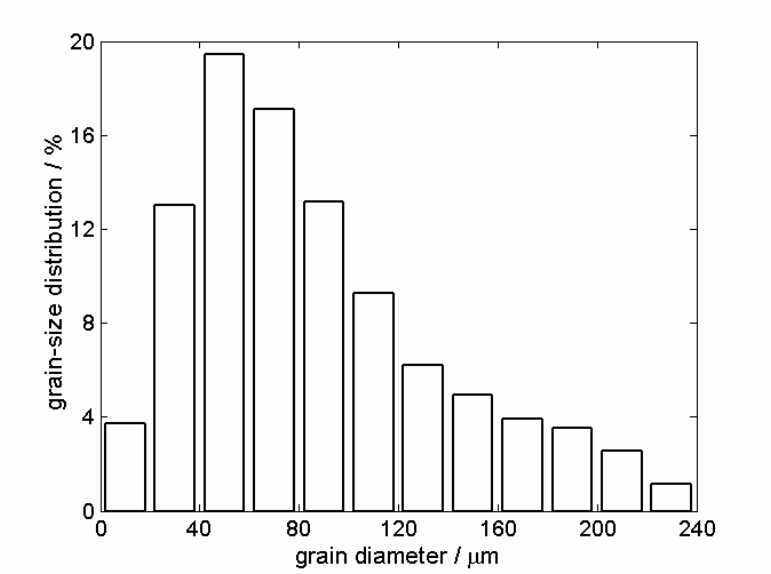

Fig. 5.13. Ferrite grain-size distribution of Fe-3.1at.%Ni after $\gamma \rightarrow \alpha$ transformation at an applied uniaxial tensile stress of 7.6 MPa and at a cooling rate of 20 $Kmin^{-1}$.

The results obtained for the average grain size as given in Table 5.3 show a decrease in average grain size from about 94 μm to 55 μm with increasing applied tensile stress from 0.005 to 12.7 MPa. The decrease in average grain size suggests an enhanced nucleation upon increasing applied tensile stress, which could have been induced by the local plastic deformation (see section 5.4.1).

Table 5.3 The average grain diameter (unit: μm) of Fe-3.1at.%Ni for two repeated sets of experiments determined by the line intercept method, as cast and as after transformation under various *tensile* stresses.

heat treatment	average grain diameter, μm
As cast, after annealing at 1423 K for 100 h	98.7+4
Heat treatment cycle with 0.005 MPa stress	94.5+3
Heat treatment cycle with 7.6 MPa stress	65.4+4
Heat treatment cycle with 12.7 MPa stress	55.3+4

5.4.4 Transformed fraction and rate of transformation

The total length change determined for the $\gamma \rightarrow \alpha$ transformation depends on the applied tensile stress (see Fig. 5.7), but the volume of the specimen before and after one complete heat treatment cycle, involving a $\alpha \rightarrow \gamma$ and a $\gamma \rightarrow \alpha$ transformation, is constant (see section 5.4.1). Thus, it is likely that the change (increase) in volume by the $\gamma \rightarrow \alpha$ transformation is also constant, i.e. independent of applied tensile stress. Then it is reasonable to suppose that the increase in length in the longitudinal direction due to the $\gamma \rightarrow \alpha$ transformation is proportional to the increase in specimen diameter due to the $\gamma \rightarrow \alpha$ transformation: $\Delta L_{\text{longitudinal}}(\gamma \rightarrow \alpha) \sim \Delta L_{\text{radial}}(\gamma \rightarrow \alpha)$. Hence, from the calibrated length change (see section 5.4.1), the transformed fraction, f_α, can be obtained using the conventional lever rule [15].

The obtained f_α as a function of temperature is shown in Fig. 5.14 for different applied stresses for two repeated sets of experiments. The variations in f_α are due to the measured variations in the local temperature, T_{centre} (see section 5.4.1). The corresponding values for df_α/dt as a function of f_α for different applied stresses are shown in Fig. 5.15

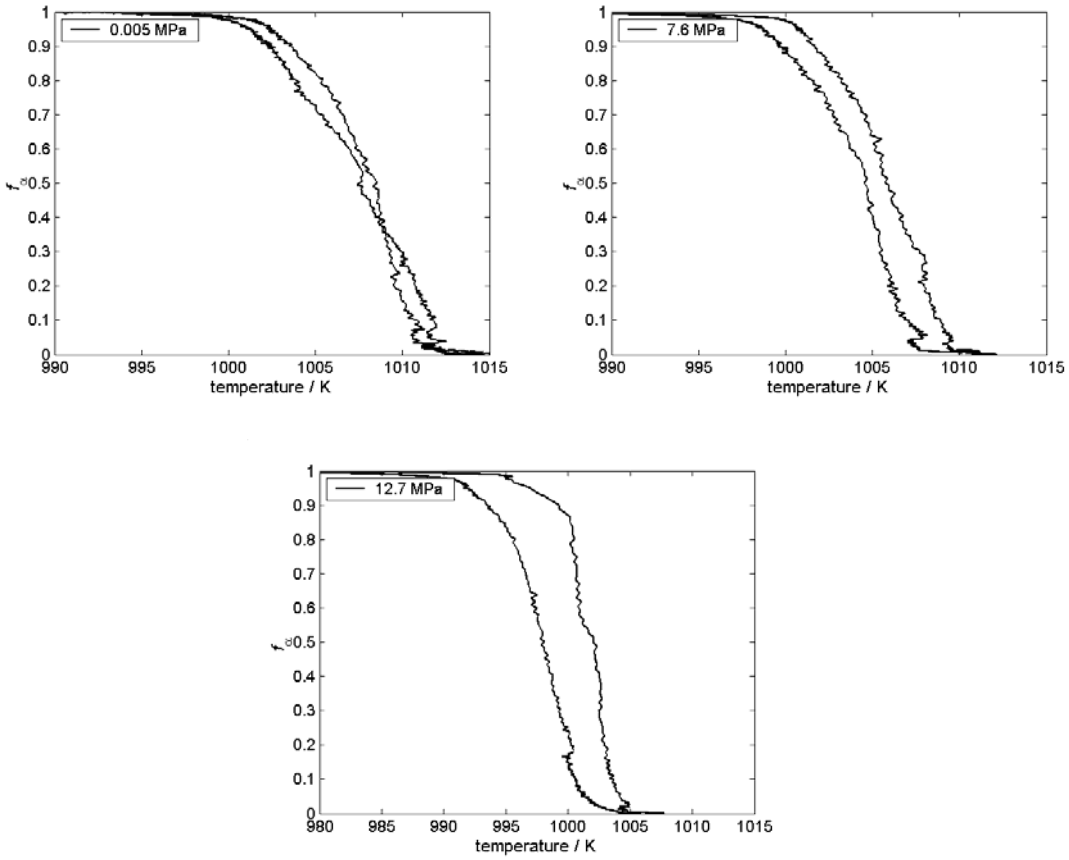

Fig. 5.14. The transformed fraction, f_α, as a function of temperature, as determined from the calibrated length change as a function of temperature of Fe-3.16at.%Ni at a cooling rate of 20 Kmin^{-1} under indicated applied uniaxial tensile stresses (starting with fresh specimens with the same initial average grain size) for two repeated sets of experiments.

for the same sets of experiments. The rate of transformation df_α/dt is not influenced significantly by the applied stress. However, the scatter in df_α/dt observed for in particular 0.005 MPa applied stress is significant (compare with the results for the applied stresses of 7.6 and 12.7 MPa); see also discussion in section 5.5. This large scatter in df_α/dt observed for the applied stress of 0.005 MPa is not an instrumental effect. The accuracy of the measured length change for the applied dilatometer is about ±50 nm, which causes a relative error of $\pm 5\times10^{-4}$ in the value determined for the ferrite fraction. This error in f_α introduces the same relative error in df_α/dt i.e. $\pm 5\times10^{-4}$, which is very

much smaller than the observed scatters (±0.7) in df_α/dt (see further discussion in section 5.5).

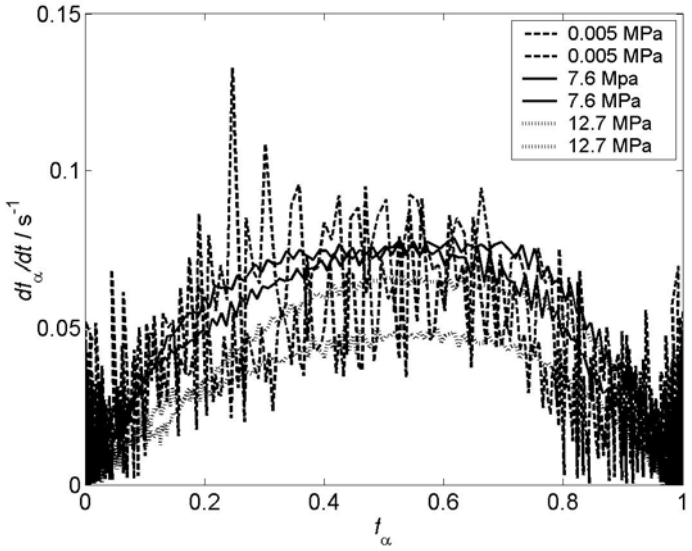

Fig. 5.15. The rate of transformation, df_α/dt, as a function of transformed fraction, f_α, for Fe-3.1at.%Ni upon cooling at 20 Kmin^{-1} under indicated applied uniaxial tensile stresses for two sets of experiments.

5.5. Interface velocity

From the experimentally determined parameters, (1) the transformed fraction, f_α, (2) the rate of transformation, df_α/dt, and the average grain diameter after one complete heat treatment cycle, the interface velocity, v_α, can be calculated applying to Eq. (5.5). The results v_α for $f_\alpha < 0.1$ and $f_\alpha < 0.9$ are not reliable because at theses values of f_α the left hand and the right hand side of Eq. (5.5) become vanishingly small, independent of the value of interface velocity, v_α. The obtained values for v_α are shown in Fig. 5.16 for various applied tensile stresses for one set of experiments of Fe-3.1at.%Ni. The interface velocity v_α (an average for the entire specimen) is almost constant over the whole range of transformed fraction for the applied tensile stresses from 0.005 to 12.7 MPa. A larger scatter on the v_α data can be observed for 0.005 MPa

applied stress. This scatter is induced by the scatter in df_α/dt, which is larger than the experimental accuracy (see end of section 5.4.4). This phenomenon was also observed for Fe-2.26at.%Mn, Fe-1.79at%Co [23] and pure Fe [24] specimens cooled at 20 Kmin^{-1} without any applied stress. The observed fluctuation in v_α (see Fig. 5.16) might correspond to a succession of periods of acceleration and deceleration (stop and go) in the interface migration process, in correspondence with the observation by *in-situ* transmission electron microscopy analysis [25]. This stop and go mechanism is due to a build up of misfit deformation energy and subsequent relaxation.

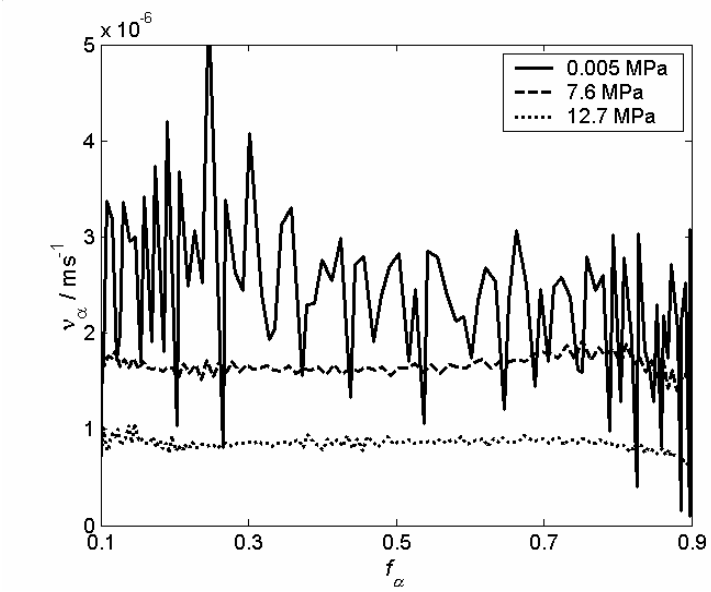

Fig. 5.16. The γ / α interface velocity as determined for indicated applied tensile stresses for Fe-3.1at.%Ni at a cooling rate of 20 Kmin^{-1}.

The interface velocity was found to be smooth (relative scatter: ±0.04) for the applied stress of 7.6 MPa and 12.7 MPa, which is almost within the experimental accuracy (±0.02). As compared to the result obtained at the applied stress of 0.005 MPa, the significantly smaller scatter in both df_α/dt (section 5.4.4) and v_α for the applied stresses of 7.6 MPa and 12.7 MPa is ascribed to (the above discussion (section 5.4.1)) inhomogeneous plastic deformation due to transformation plasticity which may relax directly the misfit deformation energy build up during the $\gamma \rightarrow \alpha$ transformation.

5.6. Driving force for $\gamma \rightarrow \alpha$ transformation

5.6.1. $\Delta G_{\alpha\gamma}^{chem}(T)$

The chemical Gibbs energy, $\Delta G_{\alpha\gamma}^{chem}$, driving the $\gamma \rightarrow \alpha$ transformation of Fe-3.1at.%Ni was determined using the CALPHAD assessment of the Fe-Ni system [26]. The obtained $\Delta G_{\alpha\gamma}^{chem}$ for Fe-3.1at.%Ni is presented as a function of temperature in Fig. 5.17. The absolute value of $\Delta G_{\alpha\gamma}^{chem}$ increases with decreasing temperature.

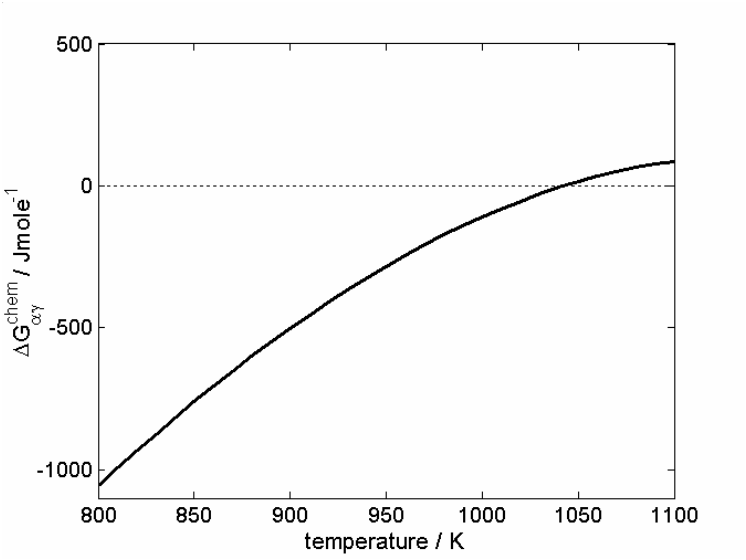

Fig. 5.17. The chemical driving force, $\Delta G_{\alpha\gamma}^{chem}$, as a function of temperature for the $\gamma \rightarrow \alpha$ transformation of Fe-3.1at.%Ni.

5.6.2. $\Delta G_{\alpha\gamma}^{def}(f_\alpha) + \Delta G_{\alpha\gamma}^{int}(f_\alpha)$

The driving force ($-\Delta G_{\alpha\gamma}$; c.f. Eq. (5.3)) can now be determined from Eq. (5.2a) using the data of interface-migration velocity (see Fig. 5.16) and of interface mobility of pure iron (see section 5.2.1). Again (see discussion of Fig. 5.16) the results for f_α<0.1 and f_α>0.9 have not been given due to mathematical instability of Eq. (5.5) at f_α=0 and f_α=1. Further, in an advanced stage of transformation the results for the interface

velocity become rather sensitive to the type of impingement correction chosen. This leads to a (systematic) uncertainty in the results (of $\Delta G_{\alpha\gamma}$) for large values of f_α.

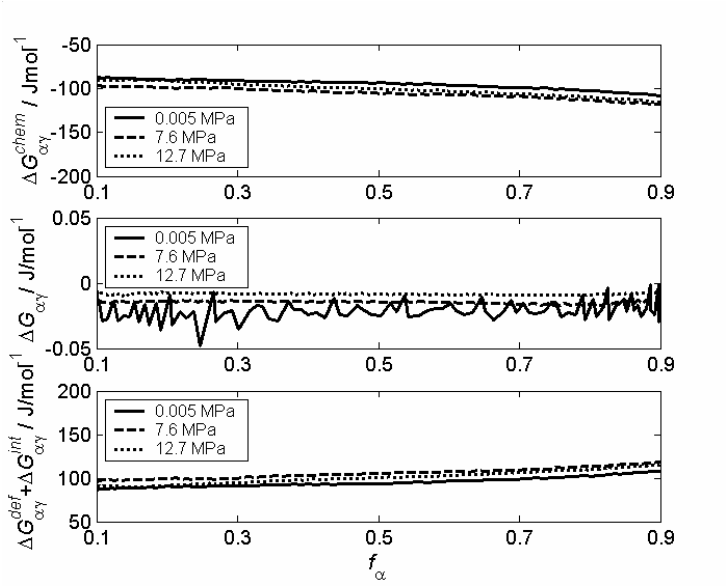

Fig. 5.18. The chemical Gibbs energy, $\Delta G^{chem}_{\alpha\gamma}$, (a) the driving force, $-\Delta G_{\alpha\gamma}$, (b) and the sum of misfit-accommodation energy and interface energy, $\Delta G^{def}_{\alpha\gamma} + \Delta G^{int}_{\alpha\gamma}$, (c) as a function of transformed fraction, f_α, for the $\gamma \rightarrow \alpha$ transformation of Fe-3.1at.%Ni for applied tensile stresses as indicated.

A comparison of values obtained as described above for the chemical Gibbs energy, $\Delta G^{chem}_{\alpha\gamma}$, the driving force, $-\Delta G_{\alpha\gamma}$, and (using Eq. (5.3)) the sum of crystalline misfit accommodation energy and interfacial energy, $\Delta G^{def}_{\alpha\gamma} + \Delta G^{int}_{\alpha\gamma}$, is provided by Fig. 18. The determined value of the driving force, $-\Delta G_{\alpha\gamma}$, of Fe-3.1at.%Ni is very small in comparison to $-\Delta G^{chem}_{\alpha\gamma}$, as most of the $\Delta G^{chem}_{\alpha\gamma}$ is dissipated by misfit deformation energy. The driving force determined for Fe-2.96 at.%Ni in compressive mode [13] is almost the same as the driving force obtained here for Fe-3.1at.%Ni in tensile mode because respective v_α are similar.

5.7. Conclusions

6. Application of applied tensile stress far below the yield limits of both ferrite (α, 18 MPa at 1000 K) and austenite (γ, 23 MPa at 1073 K) yet leads to distinct transformation plasticity upon the $\gamma \rightarrow \alpha$ transformation at 7.6 MPa in Fe-3.1at.%Ni.
7. After correction of the observed length change for the length increase due to transformation plasticity on the basis of a simple model (Eq. (5.5)), the observed length change upon transformation becomes practically independent of the applied stress.
8. The rate of transformation (as a function of the degree of transformation) is practically the same for all applied tensile stresses. The start temperature of the $\gamma \rightarrow \alpha$ transformation decreases upon increasing applied stress.
9. The interface velocity is almost constant over the entire range of transformation. The scatter in both the rate of transformation and the interface velocity for an applied tensile stress of 0.005 MPa is much larger than the experimental inaccuracy. This observed fluctuation can correspond to a succession of periods of acceleration and deceleration (stop and go) in the interface migration process. This stop and go mechanism is due to a build up of misfit deformation energy and subsequent relaxation. With increase in applied stress (7.6 and 12.7 MPa) the scatter in both the rate of transformation and the interface velocity decrease significantly, which is ascribed to transformation plasticity which relaxes the misfit deformation energy due to the $\gamma \rightarrow \alpha$ transformation.
10. The driving force for the $\gamma \rightarrow \alpha$ transformation for Fe-3.1at.%Ni is very small as compared to the chemical Gibbs energy change: most of the chemical Gibbs energy released is dissipated by the misfit deformation energy due to the $\gamma \rightarrow \alpha$ transformation.

References

[1] H. I. Aaronson, Metall. Mater. Trans. A 2002; 33: 2285

[2] G. Nocke, E. Jansch, P. Lenk Neue. Hutte. 1976; 21: 468

[3] M. D Jepson, F. C. Thompson J. Iron Steel Inst. 1949; 187: 49

[4] J. R. Patel, M. Cohen, Acta Metall. 1962; 10: 531

[5] A. Borgenstam, M. Hillert, Acta Mater. 2000 ; 48: 2765

[6] A. D. Romig, J. I. Goldstein, Metall. Trans. 1980; 11: 1151.

[7] T. B. Massalski, J. H. Perepezko, J. Jaklovsky, Mat Sci Engg. 1975; 18: 193.

[8] E. J. Mittemeijer, F. Sommer, Z Metallkd 2002; 93: 352.

[9] J. W. Christian, The Theory of Transformation in Metals and Alloys, Part 1, Equilibrium and General Kinetic Theory, Pergamon Press, Oxford, 1981.

[10] M. Hillert, Met. Trans. A 1975; 6A: 5.

[11] A. T. W. Kempen, , F. Sommer, E. J. Mittemeijer, Acta Mater 2002; 50: 3545

[12] Y. C. Liu, F. Sommer, E. J. Mittemeijer, Thermochimica Acta 2004; 413: 215

[13] G. Mohapatra, F. Sommer, E. J. Mittemeijer, submitted for publication (chapter 4).

[14] G. Mohapatra, F. Sommer, E. J. Mittemeijer, submitted for publication (chapter 2).

[15] Y. C. Liu, F. Sommer, E. J. Mittemeijer, Acta. Mater 2003; 51:507.

[16] ASTME112, Annual Book of ASTM Standard 1988; 03.01: 297.

[17] G. Mohapatra, F. Sommer, E. J. Mittemeijer, submitted for publication (chapter 3).

[18] R. E. Reed-Hill, Physical Metallurgy Principle, Second Edition, Van Nostrand Reinhold Company, New York, 1972

[19] G. W. Greenwood, R. H. Johnson, Proc. R. Soc. Lond. 1965; 283A: 403.

[20] P. Zwigl, D. C. Dunand, Metall. Trans., 1998, 29A, 565.

[21] S. Denis, E. Gautier, A Simon, G. Beck, Met. Techol. 1985; 1: 805.

[22] F. Abrassart: PhD thesis, Universite de Nancy I, 1972.

[23] Y. C. Liu, F. Sommer, E. J. Mittemeijer, Acta. Mater 2004; 52: 2549.

[24] Y. C. Liu, F. Sommer, E. J. Mittemeijer, Philosophical Magazine 2004; 84: 1853.

[25] M. Onink, F. D. Tichelaar, C. M. Brakman, E. J. Mittemeijer, S. Ven der Zwaag, J Mater Sci 1995; 30: 209.

[26] S. X. Zhong, D. D. Gohil, A. T. Dinsdale, T. G. Chart, Natn. Phys. Lab., DMA(a) 103, London, 1985.

6. Summary: Phase Transformation Kinetics; the Role of Stress

6.1. Introduction

Austenite (γ, f.c.c.) to ferrite (α, b.c.c.) transformation under uniaxial compressive and tensile stress within elastic limit of the Fe-Ni alloys has been studied in the current thesis work. Attention has been paid to investigate the influence of applied stress on start temperature, length-change evolution and γ/α interface velocity during $\gamma \rightarrow \alpha$ transformation.

The temperature calibration of the applied dilatometric was done on the basis of the Curie temperature of pure Fe for Fe-5.91at.%Ni and Fe-5.93at.%Ni and an *in situ* calibration for Fe-2.96at.%Ni and Fe-3.1at.%Ni. The length change calibration was done with the known length change for pure Pt or pure Fe.

A distinct temperature gradient was observed during heating and cooling of an inductively heated solid cylindrical dilatometric specimen. To overcome the temperature gradient in the specimen, a temperature correction procedure has been proposed to recalculate the length-change of the specimen as a function of homogeneous temperature during the $\gamma \rightarrow \alpha$ transformation.

Applying the above methods (calibration (temperature and length-change) and temperature inhomogeneity correction), to the measured temperature and length change during $\gamma \rightarrow \alpha$ transformation under applied compressive and tensile stresses, the start temperature and the subsequent transformation kinetics have been determined.

6.2. Experimental

Bulk high purity Fe (99.99 wt. %) and Ni (99.99 wt. %) were used for the preparation of alloys. Melting of appropriate amounts of Fe and Ni was carried out in a vacuum-melting furnace, and the molten alloy was cast in a copper mould. The composition of the Fe-Ni rods were found to be Fe-2.96at.%Ni, Fe-3.1at.%Ni, Fe-5.91at.%Ni and Fe-5.93at.%Ni.

A dilatometer, employing inductive heating/cooling (DIL-805 A/D; Baehr-Thermoanalysis GmbH) was used to measure the thermal dilation of the alloys as a function of temperature/time during applied heat treatment cycles. Two thermocouples were spot welded on the surface of the dilatometric specimen to measure the temperature difference between the centre (T_{centre}) and the end (T_{end}) of the specimen in its longitudinal direction. The experiments were performed under vacuum (6×10^{-6} mbar) to avoid oxidation of the specimen.

The applied thermal treatment cycle was as follows: the specimens were heated from room temperature up to 1273 K at a rate of 20 $Kmin^{-1}$ and kept at this temperature for thirty minutes. Then all the specimens were cooled down to room temperature at 20 $Kmin^{-1}$ and simultaneously subjected to various uniaxial constant (compressive and tensile) stresses.

6.3. Results and discussion

6.3.1. Length-change and temperature calibration

The length-change calibration has to be performed for heating and cooling separately. The length-change calibration for the normal (see Fig. 6.1) and compressive modes is possible applying a Pt reference specimen and for the tensile mode applying pure iron as reference material with known thermal dilation data. The temperature calibration for both heating and cooling can be performed for all modes utilizing the hysteresis-free Curie temperature of pure Fe. Temperature calibration was performed *in situ* for Fe-2.96at.%Ni (compressive specimen) and Fe-3.1at.%Ni (tensile specimen) exhibiting a ferro-magnetic transition. The calibration methods developed in this work were applied successfully to determine the linear thermal expansion coefficient for both the ferrite phase and the austenite phase of Fe-2.96at.%Ni and Fe-5.93at.%Ni.

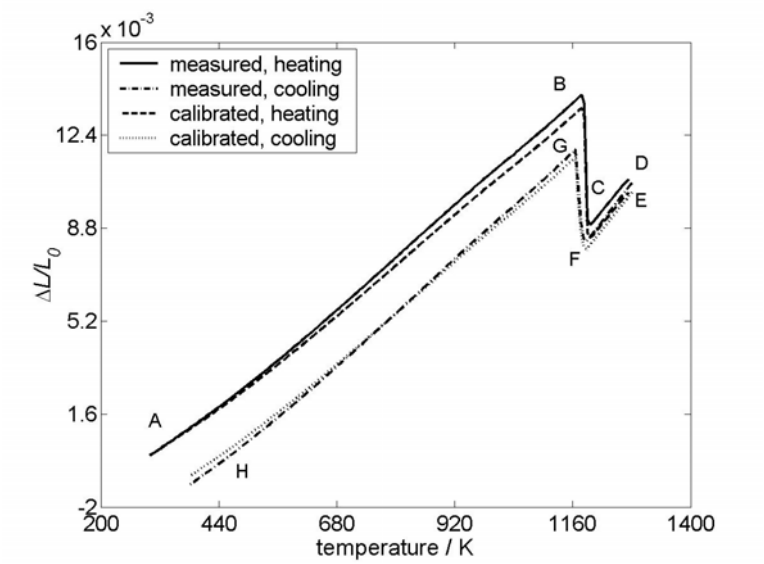

Fig. 6.1. Comparison of the measured relative length-change as a function of temperature and calibrated relative length-changes of pure iron (normal mode) (calibration is performed by a Pt specimen) made during continuous heating (20 K min^{-1}) from room temperature to 1273 K and subsequent continuous cooling (20 K min^{-1}), interrupted by an isothermal annealing at 1227 K for 30 min.

6.3.2. Correction procedure for temperature inhomogeneity

The temperature correction procedure to correct for the temperature inhomogeneity in the longitudinal direction of the dilatometric specimen is based on hypothetical segmentation of the specimen into a number of small segments in the longitudinal direction so that each segment can be supposed to have a homogeneous temperature and such that the temperature difference between adjacent segments in a particular temperature step and the temperature difference of successive temperature steps is identical. The dilation contribution from one segment, during transformation, is calculated from the difference in dilation for the whole specimen between two successive temperature steps. This leads to a recursive procedure to calculate the relative change of length during the transformation. The obtained dilation for one segment can then be used to calculate the dilation for the full specimen. The aforementioned procedure was adopted to recalculate the $\gamma \rightarrow \alpha$ transformation length-change (see Fig. 6.2) as a function of homogeneous temperature for Fe-5.91at.%Ni for the applied cooling rate of 20 $Kmin^{-1}$

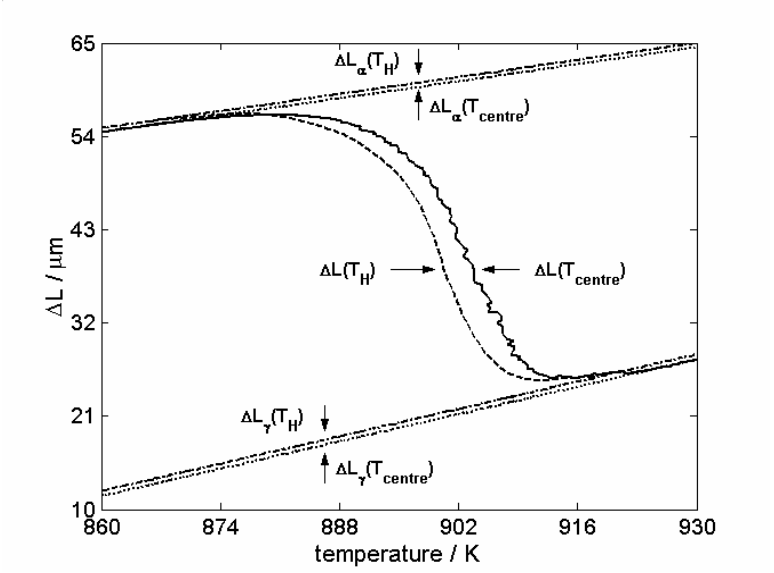

Fig. 6.2. The measured, $\Delta L(T_{centre})$, and corrected, $\Delta L(T_H)$, dilations of the transforming specimen ($\gamma \rightarrow \alpha$ transformation of Fe-5.91at.%Ni for the applied cooling rate of 20 $Kmin^{-1}$) along with the measured and corrected dilations of the pure austenite phase and the pure ferrite phase, ΔL_γ and ΔL_α, as a function of temperature.

6.3.3. $\gamma \rightarrow \alpha$ transformation under applied uniaxial compressive stress

Compressive stress measurements were performed (see Fig. 6.3) with applied stresses of 0.005, 2.6, 5.1 and 7.6 MPa (well below the elastic limits of both the α and γ phases of the alloys) during $\gamma \rightarrow \alpha$ transformation for Fe-2.96at.%Ni and Fe-5.93at.%Ni specimens. The imposition of uniaxial applied *compressive* stress slightly increases the start temperature of the $\gamma \rightarrow \alpha$ transformation for both alloys. Increase in applied compressive stress results in an increase of ferrite grain size after the $\gamma \rightarrow \alpha$ transformation: the number of nuclei is reduced upon applying a compressive stress.

The total length change pertaining to the $\gamma \rightarrow \alpha$ transformation for Fe-2.96at.%Ni and Fe-5.93at.%Ni decreases (see Fig. 6.4) slightly with increasing applied compressive stress, which suggests a preferential growth of product phase in the radial directions of the specimen. Compressive stress within the elastic regime during $\gamma \rightarrow \alpha$ transformation of Fe-2.96at.%Ni and Fe-5.93at.%Ni alloys has little influence on the rate of transformation.

The γ/α interface velocity was determined using a model incorporating nucleation (site saturation), interface controlled growth and an appropriate impingement mechanism. The average interface velocity remains almost constant and is independent of applied stress for both alloys (see Fig. 6.5). The determined net driving force ($-\Delta G_{\alpha\gamma}$) is almost constant for both alloys during the entire transformation range.

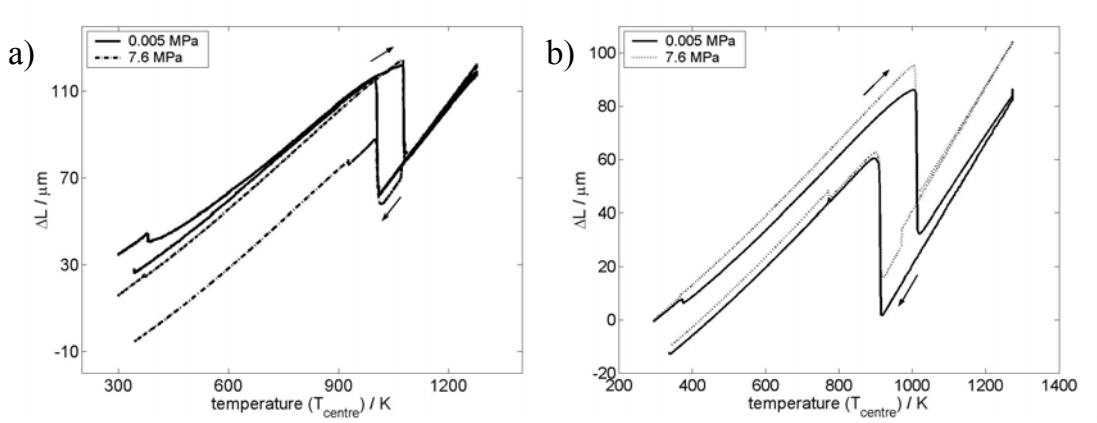

Fig. 6.3. The measured length change (for minimum:0.005 MPa and maximum:7.6 MPa applied uniaxial compressive stresses) as a function of temperature, T_{centre}, with a heating and cooling rate of 20 $Kmin^{-1}$ of (a) Fe-2.96at.%Ni and (b) Fe-5.93at.%Ni. The up-arrow and down-arrow indicate the heating and cooling parts of the heat treatment cycle, respectively.

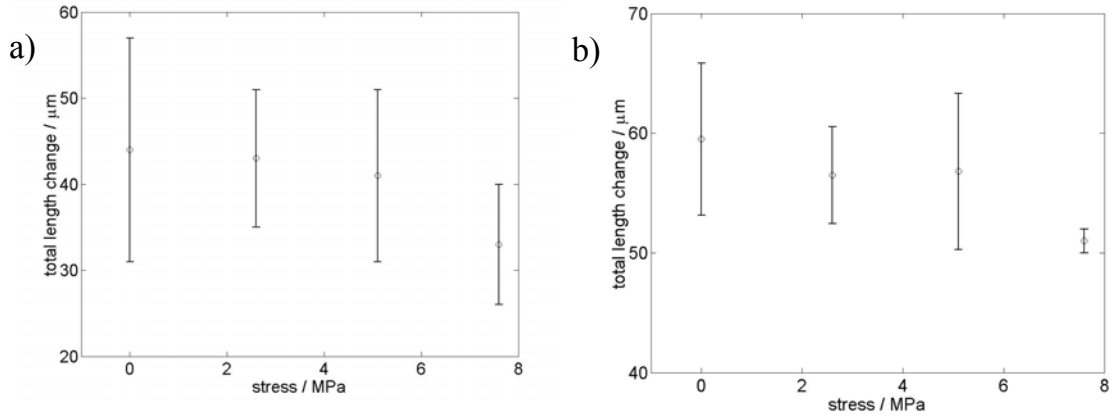

Fig. 6.4. The total length change pertaining to the $\gamma \rightarrow \alpha$ transformation as a function of applied compressive stress for (a) Fe-2.96at.%Ni and for (b) Fe-5.93at.%Ni. The error bars correspond to the standard deviations for repeated sets of experiments.

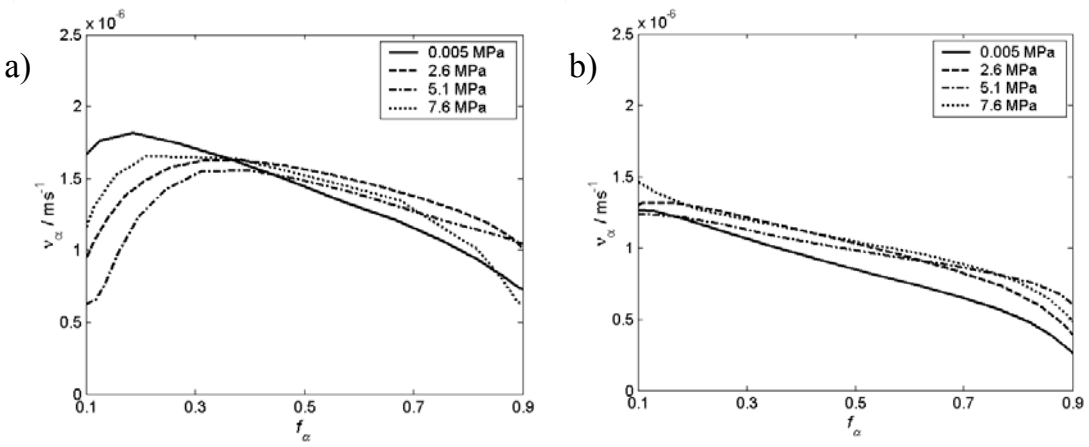

Fig. 6.5. The average γ/α interface velocity as determined for indicated applied compressive stresses for (a) Fe-2.96at.%Ni and (b) Fe-5.93at.%Ni at a cooling rate of 20 $Kmin^{-1}$.

6.3.4. $\gamma \rightarrow \alpha$ transformation under applied uniaxial tensile stress

Tensile stress measurements were performed (see Fig. 6.6) with applied stresses of 0.005, 7.6 and 12.7 MPa (yield limits of both ferrite (α, 18 MPa) and austenite (γ, 23 MPa) of Fe-3.1at.%Ni) during $\gamma \rightarrow \alpha$ transformation for Fe-3.1at.%Ni. The start temperature of the $\gamma \rightarrow \alpha$ transformation decreases upon increasing applied stress. Increase in applied tensile stress results in a decrease of ferrite grain size after the $\gamma \rightarrow \alpha$ transformation. The decrease in average grain size suggests an enhanced nucleation upon increasing applied tensile stress, which could have been induced by the local plastic deformation.

Applied tensile stress leads to significant increase in $\gamma \rightarrow \alpha$ transformation length-change with increase in applied tensile stress which is related to local plastic deformation induced by transformation plasticity.

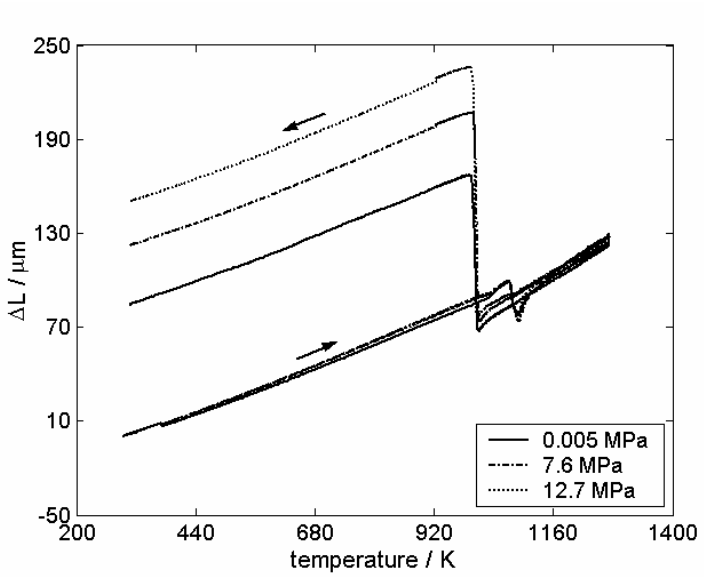

Fig. 6.6. The calibrated length change as a function of temperature with a heating and cooling rate of 20 $Kmin^{-1}$ for Fe-3.1at.%Ni subjected to various applied tensile stresses as indicated (starting with fresh specimens with the same initial average grain size). The up-arrow and down-arrow indicate the heating and cooling cycle, respectively.

The rate of transformation (as a function of the degree of transformation) is practically the same for all applied tensile stresses (see Fig. 6.7). The γ/α interface velocity was determined using a model incorporating nucleation (site saturation), interface controlled growth and an appropriate impingement mechanism. The interface velocity is almost constant over the entire range of transformation (see Fig. 6.8). The scatter in both the rate of transformation and the interface velocity for an applied tensile stress of 0.005 MPa is much larger than the experimental inaccuracy. This observed fluctuation can correspond to a succession of periods of acceleration and deceleration (stop and go) in the interface migration process. This stop and go mechanism is due to a build up of misfit deformation energy and subsequent relaxation.

With increase in applied stress (7.6 and 12.7 MPa) the scatter in both the rate of transformation and the interface velocity decrease significantly, which is ascribed to transformation plasticity which relaxes the misfit deformation energy due to the $\gamma \rightarrow \alpha$ transformation.

The driving force for the $\gamma \rightarrow \alpha$ transformation for Fe-3.1at.%Ni is very small as compared to the chemical Gibbs energy change: most of the chemical Gibbs energy released is dissipated by the misfit deformation energy due to the $\gamma \rightarrow \alpha$ transformation.

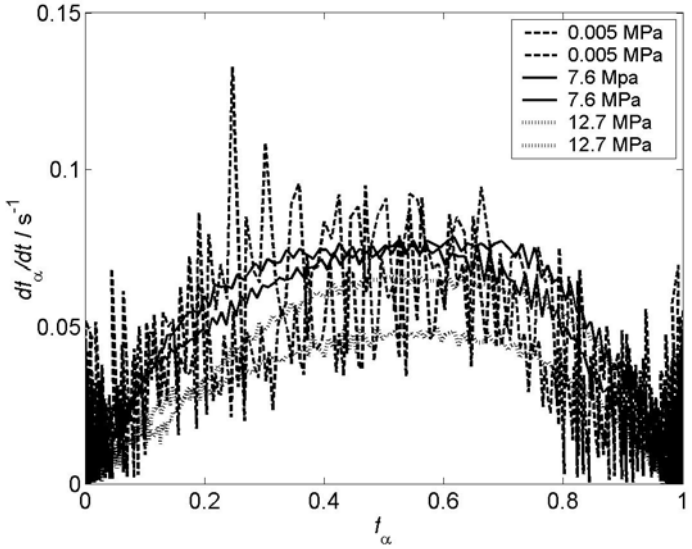

Fig. 6.7. The rate of transformation, df_α/dt, as a function of transformed fraction, f_α, for Fe-3.1at.%Ni upon cooling at 20 Kmin^{-1} under indicated applied uniaxial tensile stresses for two sets of experiments.

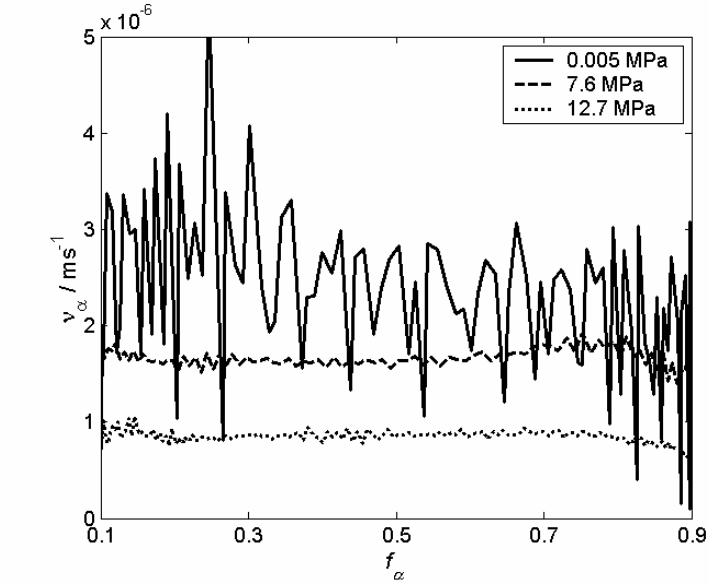

Fig. 6.8. The γ/α interface velocity as determined for indicated applied tensile stresses for Fe-3.1at.%Ni at a cooling rate of 20 Kmin^{-1}.

7. Zusammenfassung: Kinetik von Phasenumwandlungen; der Einfluss von Spannung

7.1. Einführung

Die Austenit (γ, f.c.c) in Ferrit (α, b.c.c.) Umwandlung in Fe-Ni Legierungen wurde in dieser Arbeit unter einachsiger Druck- und Zugspannung im elastischen Bereich untersucht. Insbesondere wurde der Einfluss der angelegten Spannung auf die Starttemperatur, die Änderung der Länge und die γ/α Grenzflächengeschwindigkeit während der $\gamma \rightarrow \alpha$ Umwandlung untersucht.

Die Eichung der Temperatur für das verwendete Dilatometer wurde auf Basis der Curie-Temperatur von reinem Eisen und von Fe-5.91 At.% Ni und Fe-5.93 At.% Ni sowie mit einer in situ Eichung für Fe-2.96 At.% Ni und Fe-3.1 At% Ni durchgeführt. Die Eichung der Änderung der Länge wurde mit Hilfe der bekannten Änderung der Länge von reinem Platin oder Eisen durchgeführt.

In der induktiv geheizten zylindrischen Probe wurde bei dilatometrischen Messungen beim Aufheizen und Abkühlen ein Temperaturgradient beobachtet. Es wurde ein Verfahren zur Korrektur des Temperaturgradienten entwickelt um die Änderung der Länge der Probe in Abhängigkeit von einer homogenen Temperatur während der $\gamma \rightarrow \alpha$ Umwandlung zu erhalten.

Mit Hilfe der Kalibrierung von Temperatur und Änderung der Länge sowie der Korrektur des Temperaturgradienten für die gemessene Änderung der Länge während der Änderung der Länge unter angelegter Druck- und Zugspannung wurde die Starttemperatur und die Umwandlungskinetik ermittelt.

7.2. Experimentelles

Zur Herstellung der Legierungen wurde hochreines Eisen (99,99 Gew.%) und Nickel (99.99 Gew. %) verwendet. In einem Vakuum-Ofen wurden die Legierungskomponenten aufgeschmolzen und in eine Kupferkokille abgegossen. Die Zusammensetzung der

Zylinder aus Fe-Ni-Legierungen beträgt, Fe-2.96 At% Ni, Fe-3.1 At% Ni, Fe-5.91 At% Ni und Fe-5.93 At.% Ni.

Die thermische Ausdehnung der Legierungen in Abhängigkeit von Temperatur und Zeit während der gewählten Wärmebehandlung wurde mit einem Dilatometer mit induktiver Heizung und Kühlung (DIL-805 A/D; Bähr-Thermoanalyse GmbH) gemessen. Zwei Thermoelemente wurden auf die Oberfläche der Probe aufgeschweisst um den Unterschied in der Temperatur zwischen der Mitte (T_{centre}) und dem Ende der Probe (T_{end}) in Längsrichtung zu messen. Die Untersuchungen wurden unter Vakuum (6×10^{-6} mbar) durchgeführt um eine Oxidation der Probe zu vermeiden.

Die angewandte Wärmebehandlung verläuft folgendermaßen: die Proben werden von Raumtemperatur mit einer Aufheizrate von 20 $Kmin^{-1}$ auf 1273 K aufgeheizt und bei dieser Temperatur für 30 Minuten gehalten. Dann werden alle Proben mit 20 $Kmin^{-1}$ auf Raumtemperatur abgekühlt und gleichzeitig mit unterschiedlichen Druck- und Zugspannungen belastet.

7.3. Resultate und Diskussion

7.3.1 Änderung der Länge und Temperatureichung

Die Eichung der Änderung der Länge muss für den Aufheiz- und Abkühlvorgang getrennt durchgeführt werden. Die Eichung der Änderung der Länge ohne Belastung (siehe Fig. 7.1) und für Druckspannung wird mit einer Referenzprobe aus Platin durchgeführt und für die Zugspannung wird eine Referenzprobe aus Eisen verwendet wobei die Werte für die thermische Ausdehnung bekannt sind. Die Eichung der Temperatur erfolgte sowohl für das Aufheizen wie auch für das Abkühlen für alle Messungen mit der Curie-Temperatur von reinem Eisen. In situ Eichungen wurden für Fe-2.96 At.% Ni (unter Druckspannung) und Fe-3.1 At% Ni (unter Zugspannung) durchgeführt, da diese Legierungen einen ferromagnetischen Übergang zeigen. Die entwickelten Methoden zur Eichung wurden erfolgreich eingesetzt um den linearen Ausdehnungskoeffizienten für die Ferrit- und Austenit-Phase für Fe-2.96 At% Ni und Fe-5.93 At.% Ni zu bestimmen.

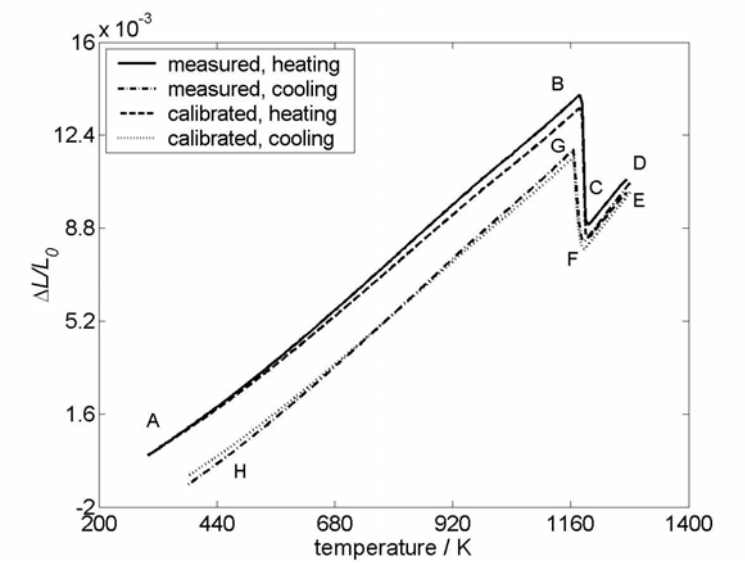

Fig. 7.1. Vergleich der gemessenen und geeichten relativen Änderung der Länge in Abhängigkeit von der Temperatur für reines Eisen (ohne angelegte Spannung, die Eichung erfolgte mit eine Probe aus Platin) während kontinuierlicher Aufheizung (20 $Kmin^{-1}$) von Raumtemperatur auf 1273 K und anschließender Abkühlung (20 $Kmin^{-1}$), unterbrochen von einer Wärmebehandlung bei 1273 K für 30 min.

7.3.2 Methode zur Korrektur eines Temperaturgradienten

Die Methode zur Korrektur von Inhomogenitäten in der Temperatur in Längsrichtung der dilatometrischen Probe basiert auf einer hypothetischen Unterteilung der Probe in kleine Segmente in Längsrichtung, so dass für jedes Segment eine konstante Temperatur angenommen werden kann und so dass die Differenz in der Temperatur zwischen benachbarten Segmenten für eine bestimmten Temperaturschritt und die Differenz in der Temperatur von den Temperaturschritten gleich ist. Der Beitrag zur Ausdehnung von einem Segment während der Umwandlung wird aus der Differenz der Ausdehnung für die gesamte Probe zwischen zwei aufeinander folgenden Schritten berechnet. Dies führt zu einer rekursiven Methode um die relative Änderung der Länge während der Phasenumwandlung zu berechnen. Aus der erhaltenen Ausdehnung für ein Segment kann die Ausdehnung der gesamten Probe berechnet werden. Mit dieser Methode wurde die Änderung der Länge für die $\gamma \rightarrow \alpha$ Umwandlung in Abhängigkeit von der homogenen Temperatur für Fe-5.91 At.% Ni bei einer Kühlrate von 20 $Kmin^{-1}$ berechnet.

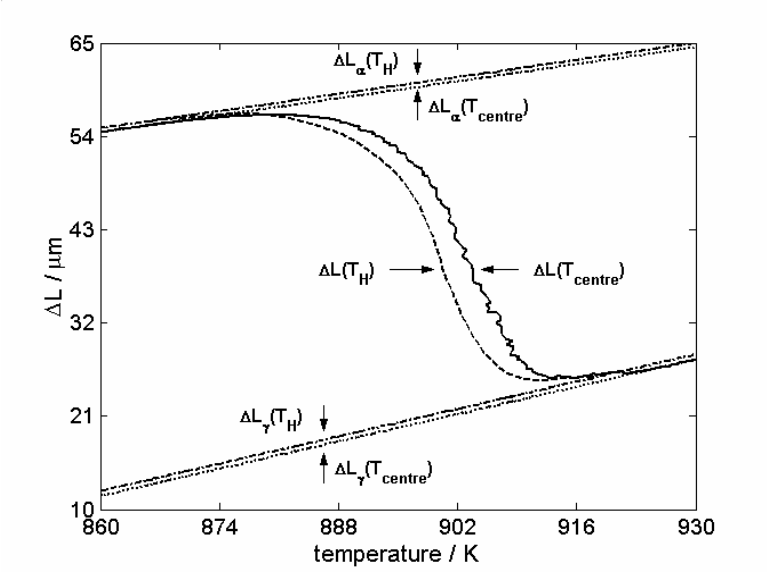

Fig. 7.2. Die gemessenen, $\Delta L(T_{centre})$, und berichtigten, $\Delta L(T_H)$, Ausdehnungen der sich umwandelnden Probe ($\gamma \rightarrow \alpha$ Umwandlung für Fe-5.91 At.% Ni bei einer Kühlrate von 20 $Kmin^{-1}$) zusammen mit den gemessenen und berichtigten Ausdehnungen der Austenit- und Ferrit-Phase, ΔL_γ und ΔL_α, in Abhängigkeit von der Temperatur.

7.3.3. $\gamma \rightarrow \alpha$ Umwandlung unter einachsiger Druckspannung

Messungen unter Druckspannung wurden mit Spannungen von 0.005, 2.6, 5.1 und 7.6 MPa (weit unterhalb der Elastizitätsgrenze sowohl der α als auch der γ Phase der Legierungen) während der $\gamma \rightarrow \alpha$ Umwandlung für Fe-2.96 At.% Ni und Fe-3.1 At% Ni Proben durchgeführt (siehe Fig. 7.3). Die Anwendung einachsiger Druckspannung ergibt eine geringe Erhöhung der Starttemperatur der $\gamma \rightarrow \alpha$ Umwandlung für beide Legierungen. Die Erhöhung der Druckspannung verursacht eine Vergrößerung der Korngröße von Ferrit nach der der $\gamma \rightarrow \alpha$ Umwandlung: die Zahl der Keime wird mit angelegter Druckspannung erniedrigt.

Die gesamte Änderung der Länge während der $\gamma \rightarrow \alpha$ Umwandlung für Fe-2.96 At.% Ni und Fe-3.1 At% Ni (siehe Fig. 7.4) erniedrigt sich gering mit Erhöhung der Druckspannung. Dies legt ein bevorzugtes Wachstum in radialer Richtung der Probe nahe. Die Druckspannung im elastischen Bereich hat während der $\gamma \rightarrow \alpha$

Umwandlung für Fe-2.96 At.% Ni und Fe-At% Ni kaum einen Einfluss auf die Umwandlungsrate.

Die γ / α Grenzflächengeschwindigkeit wurde mit einem Model beschrieben das die Keimbildung (präformierte Keime), grenzflächen-kontrolliertes Wachstum und ein geeignetes „impingement" Model berücksichtigt. Die mittlere Grenzflächengeschwindigkeit ist für beide Legierungen nahezu konstant und hängt nicht von der angelegten Spannung ab (siehe Fig. 7.5). Die berechnete Triebkraft ($-\Delta G_{\alpha\gamma}$) ist für beide Legierungen im gesamten Umwandlungsbereich nahezu konstant.

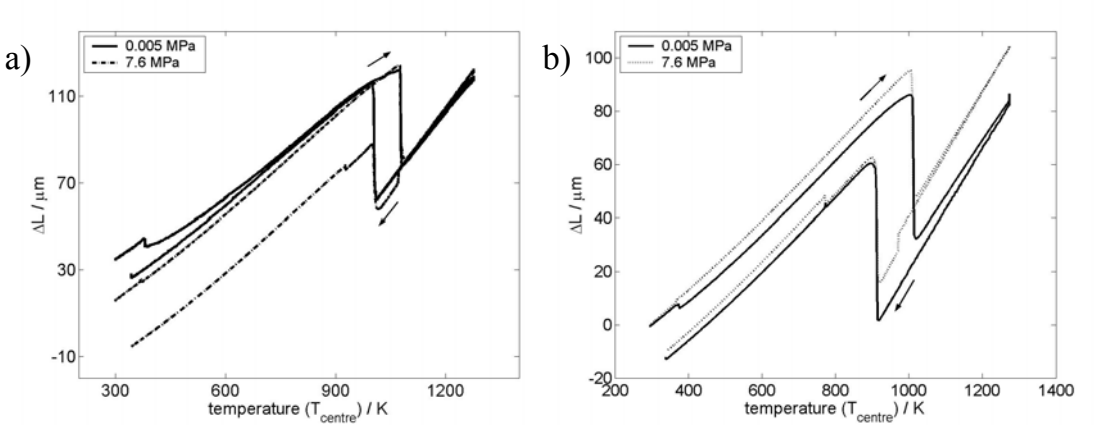

Fig. 7.3. Die gemessene Änderung der Länge (für 0.005 MPa und 7.6 MPa, jeweils die minimale und maximale einachsige Druckspannung) in Abhängigkeit von, T_{centre}, bei einer Aufheiz- und Abkühlrate von 20 $Kmin^{-1}$ für (a) Fe-2.96 At.% Ni und (b) Fe-5.93 At.% Ni. Die beiden Pfeile bezeichnen den Aufheiz- und Abkühlteil der Wärmebehandlung.

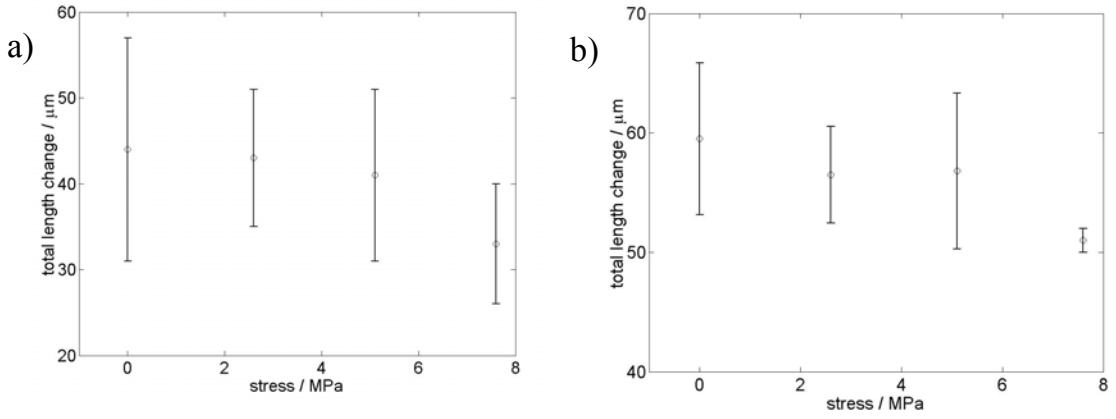

Fig. 7.4. Die gesamte Änderung der Länge während der $\gamma \rightarrow \alpha$ Umwandlung in Abhängigkeit von der angelegten Druckspannung für (a) Fe-2.96 At.% Ni und für (b) Fe-5.93 At.% Ni. Die Fehlerbalken entsprechen den Standardabweichungen für wiederholte Experimente.

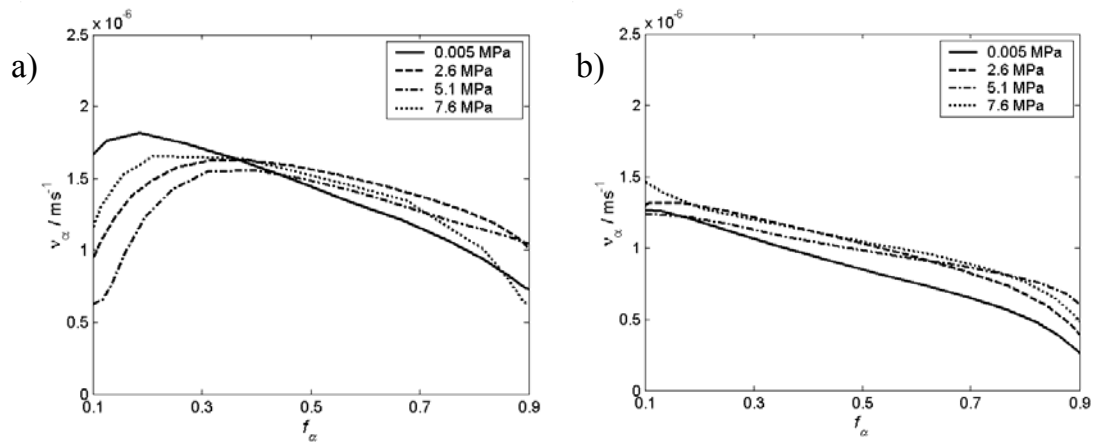

Fig. 7.5. Die berechnete mittlere γ / α Grenzflächengeschwindigkeit für die angegebenen Druckspannungen für (a) Fe-2.96 At.% Ni und (b) Fe-5.93 At.% Ni bei einer Kühlrate von 20 $Kmin^{-1}$.

7.3.4. $\gamma \rightarrow \alpha$ Umwandlung unter einachsiger Zugspannung

Messungen mit Zugspannungen von 0.005, 7.6. und 12.7 MPa (Fliessgrenze beider Ferrite (α, 18 MPa) und für Austenit (γ, 23 MPa) von Fe-3.1 At% Ni) wurden während der $\gamma \rightarrow \alpha$ Umwandlung für Fe-3.1 At% Ni durchgeführt (siehe Fig. 7.6). Die Starttemperatur während der $\gamma \rightarrow \alpha$ Umwandlung nimmt mit steigender Zugspannung

ab. Die Zunahme der angelegten Zugspannung verursacht eine Abnahme der Korngröße des Ferrits nach der $\gamma \rightarrow \alpha$ Umwandlung. Die Abnahme der mittleren Korngröße weist auf eine erhöhte Keimbildung mit zunehmender Zugspannung hin, die durch lokale plastische Verformung hervorgerufen sein kann.

Die angelegte Zugspannung verursacht eine deutliche Vergrößerung der mit der $\gamma \rightarrow \alpha$ Umwandlung verbundenen Änderung der Länge, die mit der lokalen plastischen Verformung, hervorgerufen durch die Umwandlungsplastizitä, verbunden ist.

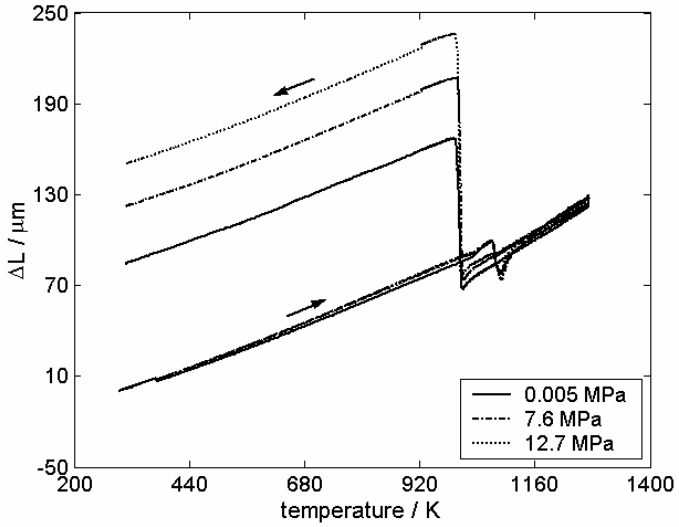

Fig. 7.6. Geeichte Änderungen der Länge in Abhängigkeit von der Temperatur für eine Heiz- und Kühlrate von 20 $Kmin^{-1}$ für Fe-3.1 At% Ni, die für verschiedene Zugspannungen gemessen wurden (es wurden jeweils neue Proben mit der gleichen Ausgangskorngröße verwendet). Die beiden Pfeile bezeichnen den Aufheiz- und Abkühlteil der Wärmebehandlung.

Die Umwandlungsrate (in Abhängigkeit vom Grad der Umwandlung) ist nahezu gleich für alle angelegten Zugspannungen (siehe Fig. 7.7). Die γ / α Grenzflächengeschwindigkeit wurde mit einem Model beschrieben das die Keimbildung (präformierte Keime), grenzflächen-kontrolliertes Wachstum und ein geeignetes „impingement" Model berücksichtigt. Die mittlere Grenzflächengeschwindigkeit ist nahezu konstant im gesamten Umwandlungsbereich (siehe Fig. 7.8). Die Streuung sowohl in der Umwandlungsrate wie auch in der Grezflächengeschwindigkeit für eine

angelegte Zugspannung von 0.005 MPa ist viel größer als die experimentelle Ungenauigkeit. Die beobachteten Streuungen hängen mit einer Folge von Perioden mit Beschleunigung und Verlangsammung („stop und go“) des Prozesses des Grenzflächenwachstums zusammen. Dieser „stop and go“ Mechanismus wird durch den Aufbau von Verformungsenergie durch Fehlpassung und nachfolgender Erholung verursacht.

Mit der Erhöhung der angelegten Spannung (7.6 und 12.7 MPa) erniedrigt sich die Streuung in der Umwandlungsrate wie auch in der Grezflächengeschwindigkeit deutlich. Dies wird durch die Umwandlungsplastizität verursacht, die Verformungsenergie durch Fehlpassung bei der $\gamma \rightarrow \alpha$ Umwandlung durch Erholungsprozesse kompensiert.

Die Triebkraft für die $\gamma \rightarrow \alpha$ Umwandlung für Fe-3.1 At% Ni ist sehr klein im Vergleich zu der Änderung in der chemischen Gibb´schen Energie: der größte Teil der Gibb´schen Energie wird durch die Verformungsenergie durch Fehlpassung bei der $\gamma \rightarrow \alpha$ Umwandlung verbraucht.

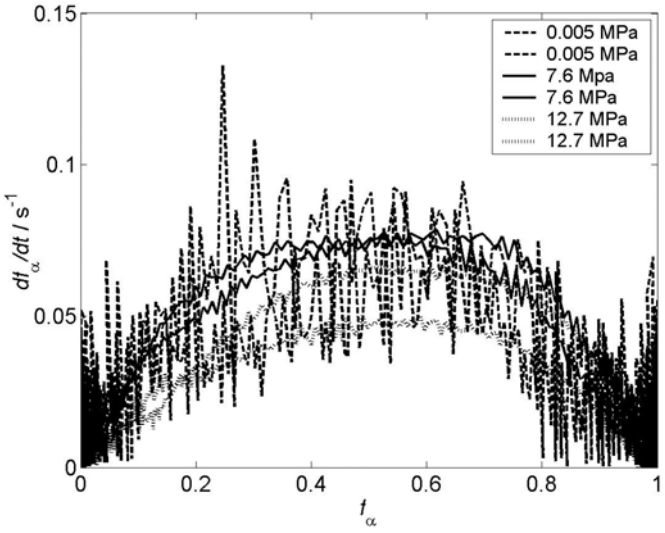

Fig. 7.7. Die Umwandlungsrate, df_α / dt, in Abhängigkeit des umgewandelten Anteils, f_α, für Fe-3.1 At% Ni bei einer Kühlrate von 20 $Kmin^{-1}$ und bei angelegten einachsigen Zugspannungen für zwei Sätze von Experimenten.

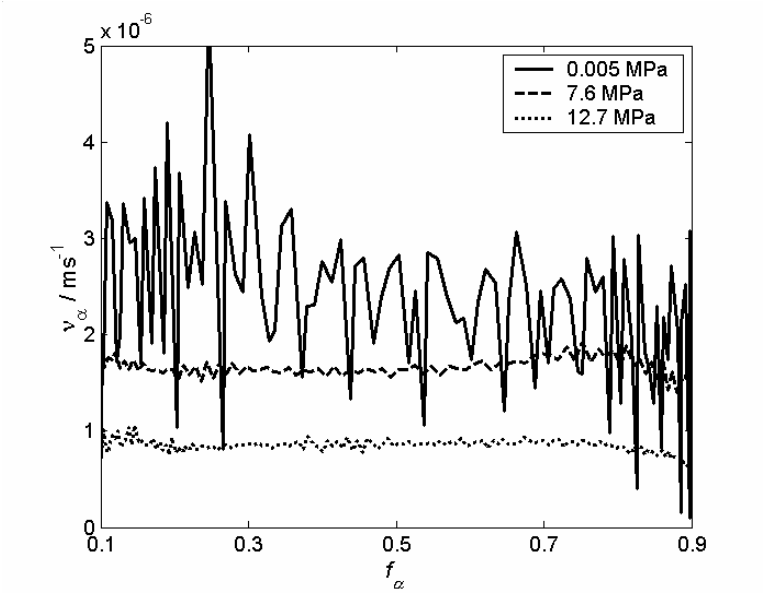

Fig. 7.8. Die berechnete γ / α Grenzflächengeschwindigkeit für die angegebenen angelegten Zugspannungen für Fe-3.1 At% Ni bei einer Kühlrate von 20 $Kmin^{-1}$.

Curriculum Vitae

Name	Goutam Mohapatra
Date of birth	29.05.1975
Place of birth	Rourkela (Orissa, India)
Nationality	Indian
School	1987-1990 Board of Secondary Education, Orissa, India 1990-1992 Council of Higher Secondary Education, Orissa, India
Higher Education	1994-1998 B.Eng., Indira Gandhi Institute of Technology, Talcher, Orissa (Utkal University) 1998-2000 MTech., Metallurgical and Materials Engineering Indian Institute of Technology, Kharagpur, India Since 2003 PhD Student in the department of Prof. Mittemeijer at the Max Planck Institute for Metals Research and at the Institute for Physical Metallurgy of the University of Stuttgart
Professional experience	2000-2002 Software Engineer in Frontier Information Tech Ltd, Hyderabad (India)

Acknowledgements

This thesis would not have been possible without the support of many people. First and foremost I thank my promoter Prof. Dr. Ir. E. J. Mittemeijer. He was always there to listen, discuss and motivate which has considerably contributed to the completion of this dissertation.

A special thank goes to my daily supervisor Prof. F. Sommer for many advices, the constant supervision and the numerous scientific discussions. He taught me how to be persistent to accomplish my goal.

I also thank all the colleagues in the Department Mittemeijer and the Max Planck Institute for the cooperation, their help with respect to many technical problems and the constructive and pleasant working atmosphere.

This Ph. D. project was made possible by a grant from the International Max Planck Research School for Advanced Materials (IMPRS-AM).

Finally, I acknowledge the continuous support and the encouragement provided by my family and friends.